

Diss
ELE
264

STUDY OF HIGH FREQUENCY FIELDS IN TWO
DIMENSIONAL CASSEGRAIN AND GREGORIAN
FOCUSSING SYSTEMS



Abdul Aziz


In Partial Fulfilment of the Requirements
for the Degree of
Doctor of Philosophy

Department of Electronics
Quaid-i-Azam University
Islamabad, Pakistan

2010


Certificate

It is certified that Mr. Abdul Aziz has carried out the work contained in this dissertation under my supervision.



Dr. Qaisar Abbas Naqvi
Associate Professor
Department of Electronics
Quaid-i-Azam University
Islamabad, Pakistan

Submitted through



Dr. Qaisar Abbas Naqvi
Chairman
Department of Electronics
Quaid-i-Azam University
Islamabad, Pakistan

Abstract

Focused electromagnetic waves have applications in many areas, such as microwave antennas and integrated optical systems etc. Asymptotic ray theory (ART) or the geometrical optics (GO) approximation is a powerful tool for evaluating high frequency fields in homogeneous and inhomogeneous medium but it fails in the vicinity of caustic. Maslov's method combines the simplicity of asymptotic ray theory and generality of Fourier transform method. This is achieved by representing the geometrical optics fields in terms of mixed coordinates consisting of space coordinates and wave vector coordinates. High frequency field expressions valid around focal regions of two dimensional Cassegrain and Gregorian dual reflector microwave antennas are derived using Maslov's method. The reflectors materials composed of perfect electric conductor (PEC), perfect electromagnetic conductor (PEMC) and chiral nihility coated PEMC are chosen for the study of field behavior around caustic region of these systems. Numerical computations are used to evaluate field patterns around the caustic of dual reflector microwave antennas. To establish validity of Maslov's method the results of cylindrical parabolic reflector based on Maslov's method are compared with the results obtained using Kirchhoff's approximation. The results are found in good agreement. The field reflected from both PEMC and chiral nihility backed by PEMC interface, contains both co-polarized and cross-polarized components. Dependence of co-polarized and cross-polarized field components for different values of admittance parameter of PEMC has been studied.

Contents

<i>Acknowledgements</i>	<i>iii</i>
<i>Dedication</i>	<i>iv</i>
<i>Abstract</i>	<i>v</i>
<i>List of publications</i>	<i>viii</i>
Chapter 1: Introduction	1
1.1. Formulation of GO Field	5
1.2. Field Formulation Using Maslov's Method	9
Chapter 2: PEC Arbitrary Cylindrical Reflector	18
2.1. Formulation of Geometrical Optics Field	18
2.1.1. Determination of Amplitude	21
2.2. Determination of Field Around Caustic	22
2.2.1. Evaluation of Phase Function	22
2.2.2. Evaluation of Amplitude Function	23
2.3. Validity of Maslov's Method	25
2.4. Special Case–Parabolic Cylindrical Reflector	26
2.5. Comparison with Huygens–Kirchhoff's Principle	28
2.6. Results and Discussion	29
Chapter 3: The PEC Dual Reflector Systems	33
3.1. Cassegrain Dual Reflector System	33
3.1.1. Formulation of Geometrical Parameters	34
3.1.2. Derivation of GO Field	36
3.1.3. Evaluation of Jacobian	38
3.2. Derivation of Field near Caustic	40
3.2.1. Results and Discussion	42

3.3. Gregorian Dual Reflector System	48
3.3.1. GO Field Formulation	49
3.3.2. Field Determination Around Caustic	51
3.4. Results and Discussion	53
Chapter 4: The PEMC Dual Reflector Systems	59
4.1. Plane Wave Reflection from PEMC Plane Surface	59
4.2. PEMC Gregorian Dual Reflector Antenna	61
4.2.1. Determination of Surface Field	63
4.2.2. Derivation of Caustic Field Expression	64
4.2.3. Result and Discussion	65
4.3. PEMC Cassegrain Dual Reflector Antenna	71
4.3.1. Evaluation of Surface Field	72
4.3.2. Results and Discussion	75
4.4. PEMC Backed Chiral Nihility Dual Reflector Systems	80
4.4.1 PEMC Backed Chiral Nihility Slab	80
4.4.2. PEMC Backed Chiral Nihility Parabolic Cylinder	84
4.4.3. Gregorian Dual Reflector System	85
4.4.4. Field Formulation at Caustic	86
4.4.5. Results and Discussion	88
4.5. Cassegrain Dual Reflector System	95
4.5.1. GO Field	95
4.5.2. Field Computation Near Caustic	96
4.5.3. Results and Discussion	98
Chapter 5: Summary and Conclusions	105
Appendices	108
References	117

List of Publications

The work in the thesis is based on the following published papers.

- [1] Aziz, A., Q. A. Naqvi and K. Hongo, Analysis of the fields in two dimensional Cassegrain system, Progress In Electromagnetics Research, PIER 71, 227–241, 2007.
- [2] Aziz, A., A. Ghaffar, Q. A. Naqvi and K. Hongo, Analysis of the fields in two dimensional Gregorian system, Journal of Electromagnetic Waves and Applications, 22, no.1, 85–97, 2008.
- [3] Fiaz, M. A., A. Aziz, A. Ghaffar and Q. A. Naqvi, High frequency expressions for the field in the caustic region of a PEMC Gregorian system using Maslov's method, Progress In Electromagnetics Research, PIER 81, 135–148, 2008.

To Be Published

- [1] Aziz, A., A. Ghaffar and Q. A. Naqvi, Study of high frequency image field of PEMC Cassegrain dual reflector system,
- [2] Ahsan Illahi, A. Aziz, and Q. A. Naqvi, Computation of high frequency field near caustic of chiral nihility coated PEMC Gregorian system,

Chapter 1

Introduction

Asymptotic ray theory (ART) or geometrical optics (GO) approximation is frequently employed for the analysis of wave propagation both in homogenous and inhomogenous media [1,2]. It gives both qualitative and quantitative picture of the field and is widely used to study variety of problems in different areas of electromagnetics, acoustics, and seismology [2-4]. In fact, GO deals with relatively high frequency field problems with limitation to predict the field only in a region where cross-sectional area of ray tube does not become zero. However, in practical applications there are regions such as focal region of focussing systems where cross-sectional area of ray tube reduces to zero as shown in Fig. 1.1. and Fig. 1.2., GO fails to quantify the ray field at these points. Therefore, GO approximation is not suitable for field evaluation around caustic where it shows singularity [3-6]. The formation of caustics is a frequent feature in electromagnetics, acoustics, and seismology etc., and again these are often the points of great interest for their usefulness in practical applications. So in order to study the field behavior near caustics [1,5] or focal points, some different approach is required.

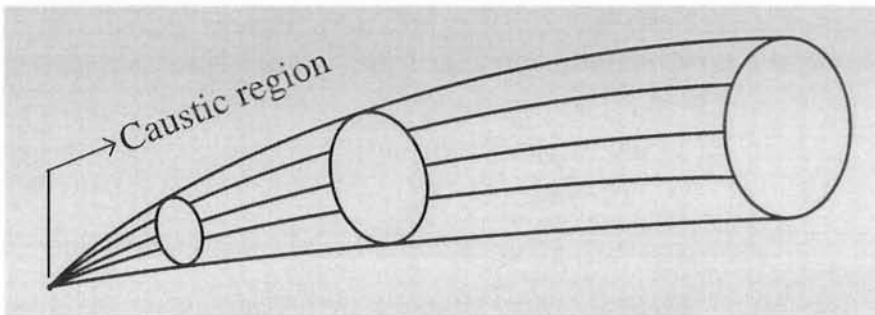


Fig. 1.1. *Transportation of electromagnetic energy in the form of a tube of geometrical rays*

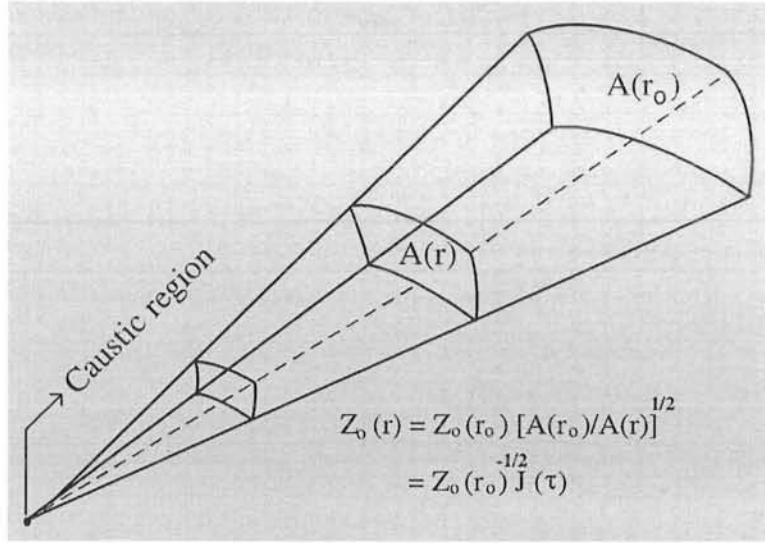


Fig. 1.2. The schematic diagram showing variation of field intensity of rectilinear rays as a function of area of field distribution

Maslov proposed an alternate method [8,9] to predict the field distribution around caustic region. Maslov's method is a systematic procedure which combines the simplicity of GO and generality of the Fourier transform which remedies the defects of GO field expression at caustic. The formulation of GO field around caustic may be done either in spatial domain or wave vector domain or in combination of both the domains known as phase space. Ray representation of the field in phase space along with their projections onto spatial domain and wave vector domain is shown in Fig. 1.3. The representation of GO field in wave vector domain is equivalent to Fourier transform of the wave field. The transformation removes the formation of ray singularity at caustic as shown in Fig. 1.3. Considering the problem of geometrical optics in physical space, mathematically there appears singularity around the caustic but in fact this singularity is not genuine. This is so, because the solution of electromagnetic wave equation is not singular. Maslov's method makes use of the fact that appearance of caustic/singularity is dependent on the choice of domain for field formulation. A caustic/singularity along the ray cannot appear both in its spatial and wave vector domain simultaneously as

shown in Fig. 1.3.

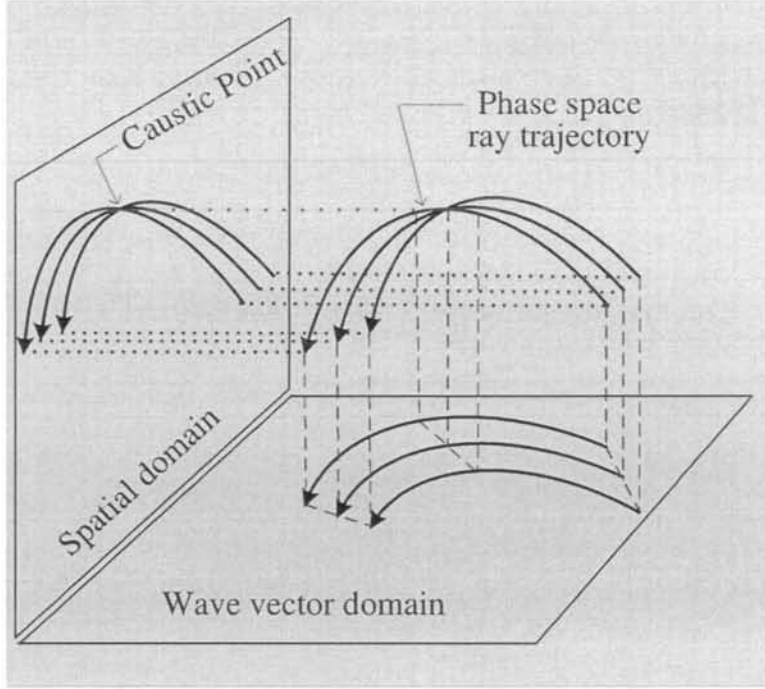


Fig. 1.3. The schematic diagram depicts the rectilinear rays as phase space trajectory along with their projections onto both spatial domain and wave vector domain. The singularity in spatial domain is removed in wave vector domain.

Rays never intersect in phase space, ray intersection and hence the caustic occurs only in spatial domain ray projection. Following properties of ray and wave constitute the basis of Maslov's method [8,9].

- (i) The trajectory of a ray in three dimensions is represented by the solution of Hamilton's canonical equations that is generally considered in spatial domain $\mathbf{r}(x, y, z)$. Again the ray trajectory can also be viewed in six dimensional phase space consisting of space co-ordinates $\mathbf{r}(x, y, z)$ and wave vector components $\mathbf{p}(p_x, p_y, p_z)$ as shown in Fig. 1.3. Furthermore, spatial domain and wave vector domain may then be taken as respective projections from six dimensional phase space. Other projections of phase space e.g., (x, p_y, p_z) , (p_x, p_y, z) called the mixed domain are

also possible. It implies that a ray can also be described in which a few components of space domain (x, y, z) are replaced by corresponding components of wave vector domain $\mathbf{p}(p_x, p_y, p_z)$, giving rise to a new domain (p_x, p_y, z) , referred as hybrid domain or mixed domain. The solution in mixed or hybrid domain is considered because in general, the singularities in different domains do not coincide. The ray shows singularity at caustic when one sees it in spatial domain (x, y, z) as in Fig. 1.3., but generally it is regular in the mixed domain as the singularity in each space is usually located at different locations.

- (ii) The solution of the Helmholtz equation may be represented as spectrum of superposition of plane wave. This is accomplished through Fourier transform representations of solution with unknown coefficients. The derivation of asymptotic ray expression in terms of unknown coefficients is obtained from Fourier integral by applying the stationary phase method of integration [6] to the integral. The ray expression thus obtained from plane wave spectrum may be compared with GO field expression derived using Hamilton's optics. This may lead to determine unknown coefficients of the integrand of Fourier integral. It may be pointed out that the integrand of integral transform is in mixed domain and predicts finite field at caustic.

In practical use, the field expression based on Maslov's method assumes the form of an integral representation of the solution which once again reduces to GO field expression in a region far away from the caustic when integral is solved by stationary phase method of integration. The integral which appears in the field expression can be evaluated either numerically or asymptotically to determine image field. Although Maslov's method has attracted attention of many investigators who frequently use the method to study the problems in acoustics and seismology [2-4], yet the literature related with the applications of the method to physical problems in electromagnetics is relatively few. The main objective of this research work is to encourage radio engineers

and scientists confronted with high frequency field problems to use Maslov's method for their solutions. In the next sections, mathematical formulation of field expression based on Maslov's method is carried out.

1.1. Formulation of GO Field

Consider two dimensional scalar Helmholtz equation

$$(\nabla^2 + k_0^2 n^2)U(\mathbf{r}) = 0 \quad (1.1.1)$$

where $\mathbf{r} = (x, z)$, $\nabla^2 = \frac{\partial^2}{\partial x^2} + \frac{\partial^2}{\partial z^2}$, and the field $U(\mathbf{r})$ is assumed to be uniform along y-axis, $k_0 = \frac{2\pi}{\lambda_0}$ is a wave number and λ_0 being the wave length in free space. Index of refraction of the medium is $n = \frac{k}{k_0}$ and assumed to be constant for homogenous and isotropic medium. For large values of parameter k , the asymptotic solution of the Helmholtz equation (1.1.1) is given as below

$$U(\mathbf{r}, k) = e^{-jkS(\mathbf{r})} A(\mathbf{r}, k) \quad (1.1.2)$$

where $S(\mathbf{r})$ is a slowly varying real-valued phase function and the amplitude $A(\mathbf{r}, k)$ is a slowly varying complex valued function. For large k , amplitude function can be expressed in terms of Luneberg-Kline asymptotic expansion as

$$A(\mathbf{r}, k) = \sum_{m=0}^{\infty} (-jk)^{-m} Z_m(\mathbf{r}) \quad (1.1.3)$$

Therefore the asymptotic solution of (1.1.1) may be written as

$$U(\mathbf{r}, k) = \exp[-jkS(\mathbf{r})] \sum_{m=0}^{\infty} \frac{Z_m(\mathbf{r})}{(-jk)^m} \quad (1.1.4)$$

For high frequency fields, k tends to become large and assumes infinite value so that retaining the leading term of the asymptotic series (1.1.4), gives

$$U(\mathbf{r}, k) = Z_0(\mathbf{r})e^{-jkS(\mathbf{r})} \quad (1.1.5)$$

Phase and amplitude functions may be determined by substituting (1.1.4) in (1.1.1) and setting the co-efficient of each powers of k equal to zero. Thus co-efficient of k^2 yields the equation for phase function $S(\mathbf{r})$, known as Eikonal equation [3]

$$[\nabla S(\mathbf{r})]^2 - n^2 = 0 \quad (1.1.6)$$

Similarly the co-efficient of k yields the amplitude equation

$$2\nabla Z_m(r)\nabla S + \nabla^2 S Z_m(r) = -\nabla^2 Z_{m-1}(r), \quad (m = 1, 2, 3, 4, \dots) \quad (1.1.7)$$

For $m = 0$, zeroth order transport equation [3] is obtained and is given by

$$2\nabla Z_0(r)\nabla S + \nabla^2 S(Z_0(r)) = 0 \quad (1.1.8)$$

This retains the leading term of asymptotic series (1.1.4). The equation (1.1.8) further reduces to

$$2\frac{\partial Z_0(r)}{\partial \tau} + (\nabla^2 S)Z_0(r) = 0 \quad (1.1.9)$$

where

$$\frac{\partial}{\partial \tau} = \frac{\partial \mathbf{r}}{\partial \tau} \cdot \frac{\partial}{\partial \mathbf{r}} = \nabla S \cdot \nabla \quad (1.1.10)$$

it may be noted that ∇S has a direction perpendicular to the surface $S(\mathbf{r}) = \text{constant}$, so that τ specifies position of a point on the curve perpendicular to this surface.

i-Phase Function

Phase function of a ray is given by the solution of Eikonal equation (1.1.6). Now, wave vector is defined as $\mathbf{p} = \nabla S$ and Hamiltonian as $H(\mathbf{r}, \mathbf{p}) = \frac{1}{2}(\mathbf{p} \cdot \mathbf{p} - n^2)$ so that Eikonal equation (1.1.6) becomes

$$H(\mathbf{r}, \mathbf{p}) = 0 \quad (1.1.11)$$

which describes the path of propagation of a ray. Eikonal equation can be converted to ordinary differential equations using the theory of characteristics which gives

$$\frac{d\mathbf{r}}{d\tau} = \nabla_p H = \mathbf{p} \quad (1.1.12)$$

$$\frac{d\mathbf{p}}{d\tau} = -\nabla_r H = \frac{1}{2} \frac{dn^2(\mathbf{r})}{dr} = 0 \quad (1.1.13)$$

where refractive index n remains constant for homogenous medium. Using $\mathbf{p} = \nabla S$ and (1.1.12), one can readily obtain

$$\frac{dS}{d\tau} = \frac{dS}{d\mathbf{r}} \cdot \frac{d\mathbf{r}}{d\tau} = \mathbf{p} \cdot \nabla_p H \quad (1.1.14)$$

where τ is the parameter along the ray. In (1.1.12) and (1.1.13), ∇_p and ∇_r are differential operators with respect to wave vector $\mathbf{p}(p_x, p_y, p_z)$ and space coordinates $\mathbf{r}(x, y, z)$ respectively.

Hamilton's equations in cartesian components are

$$\begin{aligned} \frac{dx}{d\tau} &= p_x, & \frac{dz}{d\tau} &= p_z \\ \frac{dp_x}{d\tau} &= 0, & \frac{dp_z}{d\tau} &= 0 \end{aligned} \quad (1.1.15)$$

Solution of Hamilton's equations is obtained below

$$\begin{aligned} x &= \xi + p_x \tau, & z &= \zeta + p_z \tau \\ p_x &= p_{x_0}, & p_z &= p_{z_0} \end{aligned} \quad (1.1.16)$$

where (ξ, ζ) and (p_{x_0}, p_{z_0}) are the initial value of (x, z) and (p_x, p_z) respectively. Integration of (1.1.14) yields

$$S(\tau) = S_0(\tau_0) + (\tau - \tau_0)n^2 \quad (1.1.17)$$

τ_0 is value of parameter at initial point. Parameter τ is related with the length of the ray σ and is given by

$$d\tau = \frac{d\sigma}{n} \quad (1.1.18)$$

ii-Amplitude Function

Amplitude of the ray is given by the solution of transport equation. Consider the zeroth order transport equation given by (1.1.9). Now, if $\frac{d\mathbf{r}}{d\tau} = \mathbf{F}(r)$ has the solution $\mathbf{r} = \mathbf{R}(\xi, \tau)$ then one can have the relation

$$\frac{d}{d\tau}[\ln J(\tau)] = \nabla_r \cdot \mathbf{F}, \quad J(\tau) = \frac{D(\tau)}{D(0)}, \quad D(\tau) = \frac{\partial(x, z)}{\partial(\xi, \tau)} \quad (1.1.19)$$

This relation can be shown by differentiation $J(\tau)$ directly and using the relation

$$\frac{d}{d\tau} \frac{\partial x_k}{\partial T} = \frac{\partial}{\partial T} \left(\frac{dx_k}{d\tau} \right) = \frac{\partial F_k}{\partial x_1} \frac{\partial x_1}{\partial T} + \frac{\partial F_k}{\partial x_2} \frac{\partial x_2}{\partial T} + \frac{\partial F_k}{\partial x_3} \frac{\partial x_3}{\partial T} \quad (1.1.20)$$

In the above equation $\mathbf{r} = (x_1, x_2, x_3)$ and T represents one of the variables (ξ, τ) . Hamilton's equation $\frac{d\mathbf{r}}{d\tau} = \mathbf{p}$ has the same form if one sets $\mathbf{F} = \mathbf{p}$, and $\nabla_r \cdot \mathbf{F} = \nabla_r \cdot \mathbf{p} = \nabla_r^2 S$ so that the solution may be expressed in the form

$$\frac{d}{d\tau}[\ln J(\tau)] = \nabla_r^2 S \quad (1.1.21)$$

The solution of the transport equation (1.1.9) is obtained in the form

$$\frac{d}{d\tau}[\ln Z_0^2(r)] = -\nabla_r^2 S \quad (1.1.22)$$

Comparison of (1.1.21) and (1.1.22) yields,

$$Z_0^2 = \frac{1}{J(\tau)}$$

or more explicitly

$$Z_0(r) = Z_0(r_0)J(\tau)^{-\frac{1}{2}}, \quad \text{where } J(\tau) = \frac{D(\tau)}{D(0)} \quad (1.1.23)$$

In order to explain the Jacobian physically and mathematically, please refer to Fig 1.2. which shows variation of field distribution area of rectilinear rays as a function of distance. It may be noted that cross-sectional area of paraxial ray $A(r)$ is proportional

to transformation $D(\tau)$ from ray co-ordinates (ξ, τ) to cartesian co-ordinates (x, y) so that $J(\tau) = \frac{A(r)}{A(r_0)} = \frac{D(\tau)}{D(0)}$ where $r_0 = (\xi, 0)$ and $J(\tau)$ is the normalized Jacobian. Now substituting the phase and amplitude given by (1.1.17) and (1.1.23) respectively in (1.1.5), yields the approximate solution of wave equation (1.1.1) known as GO solution [1]

$$U(r) = Z_0(\xi)[J(\tau)]^{-\frac{1}{2}} \exp[-jkS_0(\xi) - jkn^2(\tau - \tau_0)] \quad (1.1.24)$$

When several rays pass through a point (x, z) , the field $U(x, z)$ is described by a sum of components of the type (1.1.24). Note that the GO field expression (1.1.24) fails to explain the behavior of the field at caustic both in terms of its amplitude and phase. The phase function undergoes a characteristic $\frac{\pi}{2}$ phase shift as the ray continues through a caustic. The Jacobian $J(\tau) = 0$ at caustic because the tube of rays in which the intensity is being conserved has zero cross-section there. The GO field expression, therefore, yields an infinite field at caustic. The next section includes the detail of mathematical work involved in the use of Maslov's method to derive the field expression valid around caustic region. The GO field expression that has been established using Hamilton's equations, needs some remedial treatment. The remedy for GO field is accomplished by expressing both its amplitude and phase in mixed coordinates through Fourier transform [1,5].

1.2. Field Formulation Using Maslov's Method

The occurrence of a caustic in spatial domain can be avoided by mapping the rays from phase space to the wave vector domain as shown in Fig. 1.3. The mapping from phase space to wave vector domain, separates the rays that intersect at caustic in spatial domain. The Maslov's method uses the ray solution in one domain to correct the ray solution in other domain. Transformation from spatial domain to spectral domain or vice versa, can be realized through the use of Fourier transform and this constitutes

the basis of Maslov's method. Let $U(\mathbf{r})$ and $V(\mathbf{Y})$ be the two wave functions in spatial and wave vector domain respectively, defined by

$$U(\mathbf{r}) = U(x, z)$$

$$V(\mathbf{Y}) = V(x, p_z)$$

Their Fourier transform may be defined as

$$V(\mathbf{Y}) = \int_{-\infty}^{\infty} U(\mathbf{r}) \exp(jkzp_z) dz \quad (1.2.1)$$

and

$$U(\mathbf{r}) = \frac{1}{2\pi} \int_{-\infty}^{\infty} V(\mathbf{Y}) \exp(-jkzp_z) dp_z \quad (1.2.2)$$

Equation (1.2.2) provides an integral representation of U if V is known. The Maslov's method essentially entails the replacement of the function V in (1.2.2) by an approximation obtained using the stationary phase approximation to the integral in (1.2.1). Working in mixed domain may enable one to determine solution of Helmholtz equation that remains valid near caustic and it is the main feature of Maslov's method.

Consider Helmholtz equation given by (1.1.1) which may be written more explicitly as

$$\frac{\partial^2 U(\mathbf{r})}{\partial x^2} + \frac{\partial^2 U(\mathbf{r})}{\partial z^2} + k^2 U(\mathbf{r}) = 0 \quad (1.2.3)$$

Fourier transform of (1.2.3) for homogeneous medium gives

$$\frac{\partial^2 V(Y)}{\partial x^2} + k^2 [1 - p_z^2] V(Y) = 0 \quad (1.2.4)$$

Equation (1.2.4) is considered to be the wave equation in the mixed domain $Y(x, p_z)$ and its formal asymptotic solution may be assumed to have the form

$$\begin{aligned} V(Y) &= \sum_{m=0}^{\infty} B_m(Y) (-jk)^{-m} \exp[-jkT(Y)] \\ &= [B_0(Y) + (-jk)^{-1} B_1(Y) + (-jk)^{-2} B_2(Y) + \dots] \exp[-jkT(Y)] \end{aligned} \quad (1.2.5)$$

Considering high frequency field, $k \rightarrow \infty$ and selecting the leading term of the asymptotic series (1.2.5), gives

$$V(Y) = B_0(Y) \exp(-jkT(Y)) \quad (1.2.6)$$

Substituting (1.2.6) in (1.2.2) gives

$$U(x, z) = \frac{1}{2\pi} \int_{-\infty}^{\infty} B_0(Y) \exp[-jk\{T(Y) + p_z z\}] dp_z \quad (1.2.7)$$

The integral can be evaluated approximately by applying stationary phase method of integration [6]. This yields an asymptotic solution in terms of unknown variables of phase $T(Y)$ and amplitude $B_0(Y)$. The unknowns are determined in such a way that the solution should have the following characteristics.

- (i) The solution yields the finite field at caustic so that at points far away from caustic it gives the same result as produced by the GO field expression (1.1.24). It implies that both expressions coincide at stationary point $p_z = p_{z_s}$ and consequently the comparison of the two field expressions will lead to determine unknown variables in (1.2.7).
- (ii) The unknown variables $T(Y)$ and $B_0(Y)$ determined above, are substituted back in (1.2.7) and for this, it is assumed that the field expression (1.2.7) holds for all values of p_z .

The stationary point is determined from the phase function of (1.2.7) and is found to be located at

$$\left[\frac{\partial T(Y)}{\partial p_z} + z \right]_{p_z=p_{z_s}} = 0$$

which gives

$$\frac{\partial T(Y)}{\partial p_z} = -z_s$$

The second derivative of phase function as required by stationary phase method of integration is

$$\left[\frac{\partial^2}{\partial p_z^2} (T + p_z z) \right]_{p_z=p_{z_s}} = \left[\frac{\partial}{\partial p_z} \left(\frac{\partial T}{\partial p_z} \right) \right]_{p_z=p_{z_s}} - \frac{\partial z_s}{\partial p_z} \Big|_{p_z=p_{z_s}} \quad (1.2.8)$$

where z_s is the value of z at stationary point and must be expressed as $z_s = z_s(x, p_{z_s})$. Using these relations, stationary phase method of integration gives the approximate solution which remains valid in the region far away from caustic

$$U(x, z) = \left(\frac{j}{2\pi k} \right)^{\frac{1}{2}} B_0(x, y, p_{z_s}) \left[\frac{\partial z_s}{\partial p_z} \right]^{-\frac{1}{2}} \exp[-jk\{T(x, p_{z_s}) + p_{z_s} z_s\}] \quad (1.2.9)$$

Comparison of (1.2.9) with (1.1.24) in respect of amplitude and phase respectively, yields

$$B_0(x, p_{z_s}) = \left(\frac{2\pi k}{j} \right)^{\frac{1}{2}} Z_0(\xi, \zeta) J^{-1/2}(\tau) \left[\frac{\partial p_{z_s}}{\partial z_s} \right]^{-\frac{1}{2}} \quad (1.2.10)$$

and

$$T(x, p_{z_s}) = S_0(\xi, \zeta) + (\tau - \tau_0)n^2 - p_{z_s} z_s \quad (1.2.11)$$

where ξ, ζ, τ and z must be expressed in terms of mixed co-ordinates (x, p_z) . Although (1.2.9) agrees with GO solution only at the stationary points, yet it is assumed that the expression is valid for all values of p_z . Under this assumption explicit form of $B_0(x, p_z)$ in (1.2.10) and $T(x, p_z)$ in (1.2.11) have been determined. In this respect, the method resembles the equivalent current distribution method in high frequency technique of electromagnetic diffraction theory. On substitution of (1.2.10) and (1.2.11) in (1.2.7), the field expression assumes the form of

$$U(x, z) = \left(\frac{k}{2\pi j} \right)^{\frac{1}{2}} \int_{-\infty}^{\infty} Z_0(\xi, \zeta) \left[J \frac{\partial p_z}{\partial z} \right]^{-\frac{1}{2}} \times \exp[-jk\{s_0(\xi, \zeta) + (\tau - \tau_0)n^2 - z_s(x, p_z)p_z + zp_z\}] dp_z \quad (1.2.12)$$

In (1.2.12) $J \frac{\partial p_z}{\partial z}$ can be evaluated by using the following relations

$$D(\tau) = \frac{\partial(x, z)}{\partial(\xi, \tau)}$$

$$\begin{aligned}\frac{\partial p_z}{\partial z} &= \frac{\partial(x, p_z)}{\partial(x, z)} \\ D(\tau) \frac{\partial p_z}{\partial z} &= \frac{\partial(x, z)}{\partial(\xi, \tau)} \cdot \frac{\partial(x, p_z)}{\partial(x, z)} \\ D(\tau) \frac{\partial p_z}{\partial z} &= \frac{\partial(x, p_z)}{\partial(\xi, \tau)} \\ J \frac{\partial p_z}{\partial z} &= \frac{\partial(x, p_z)}{\partial(\xi, \tau)} \cdot \frac{1}{D(0)}\end{aligned}$$

The field expression (1.2.12) expression based on Maslov's method, remains valid at all points including caustic region. The solution of (1.2.12) is obtained through numerical computations, which yields the field distribution around the caustic region of focussing systems. Maslov's method takes into account both the field reflected from the surface of the reflector and the field diffracted from edge of the reflector which is reflected in the field plots as main-lobe and minor-lobes respectively. The problem of field evaluation in focal region has been undertaken by Kay and Keller [13] using the conventional Huygens-Kirchhoff's integral or physical optics approximation. The two field expressions agree completely around the caustic region but differ slightly in phase and amplitude elsewhere.

The basic work of Maslov is reported in Maslov, 1972 [8], a book written in Russian and translated into French and another more recent book by Maslov and Fedoriuk, 1981 [9]. Maslov's method was originally developed for the purpose of finding uniform asymptotic solution of partial differential equations, such as Schrodinger's wave equation. The method has subsequently been applied to propagation and radiation of waves in homogenous and non homogeneous medium [1,2]. The physical interpretation of mathematics of Maslov's method and its relation to other ART methods have been discussed by Ziolkowski and Dechamp [5]. Arnold [12] has provided further physical insight into this technique. The application of Maslov's method to inhomogeneous medium and continuation problems have been discussed by Kravstov and Gorman [1,15]. The method has been summarized by Kravtsov, Ziolkowski and

Dechamps [5,14] and applied to propagation and radiation of waves in homogeneous and inhomogeneous medium. Chapman and Drumond [4] used it to construct the seismograms, Gorman and his associates [6,15] showed how to construct the asymptotic solution for various kinds of differential equations. Hongo and co-workers applied Maslov's method to derive the high frequency solutions for field distribution by a phase transformer, a cylindrical reflector, spherical reflector antenna, a dielectric spherical lens, spherical dielectric interface and radiation characteristic of plano convex lens antenna [17-28]. Aziz et al. utilized the Maslov's method to study the field distribution around caustics of two dimensional Cassegrain and Gregorian dual reflector systems composed of perfect electric conductor (PEC) and perfect electromagnetic conductor (PEMC) reflectors [23,24,43]. Ghaffar et al extended the work to three dimensional Cassegrain and Gregorian systems, study of focussing of field refracted by a plano convex lens into uni-axial crystal, study of focussing of field refracted by an inhomogeneous slab were studied [25-30]. Hussain et al. used this method to study the radiation characteristics of wood lens [32]. Ashraf et al recently used the method to study the fields in the focal space of symmetrical hyperbolic focusing lens [31]. Fiaz et al. utilized the Maslov's method to study the fields distribution around caustics of two dimensional PEMC Gregorian system [42,43]. Faryad and Naqvi extended the Hongo's work by studying the high frequency field expressions in the caustic region of a parabolic cylinder placed in chiral medium [45]. Ahsan and Naqvi used Maslov's method to study the behavior of reflected field around caustic region of a PEMC parabolic cylinder when it is coated with chiral nihility medium [54]. The work in the thesis will show that the method can be applied to derive the field expressions for both single and dual reflector systems for field around their caustic regions. Cassegrain and Gregorian dual reflector systems are considered for the study of field behavior around their focal regions. The reflectors used are of different materials which include PEC, PEMC and PEMC backed chiral nihility.

Concept of PEMC has been introduced by Lindell and Sihvola [35, 36] as a generalization of Perfect electric conductor (PEC) and perfect magnetic conductor (PMC). PEMC is a new class of metamaterials [Appendix F] that exhibits exceptional properties not readily observed in nature. At PEMC interface certain linear combinations of electromagnetic fields are required to vanish and has been discussed [35, 36]. Using differential-form representation [10, 37] the corresponding medium has been characterized as being the simplest possible medium. PEMC medium is defined through one scalar parameter, the PEMC admittance M [35], whose zero and infinite limits give the PMC and PEC media, respectively. It has been demonstrated theoretically that a PEMC material acts as a Perfect reflector of electromagnetic wave but differs from PEC and PMC in that the reflected field has both co and cross-polarized (cr-polarized) field components. PEMC does not allow electromagnetic energy to enter, so it can serve as boundary material. Non-reciprocity of the PEMC boundary can be demonstrated by showing that the polarization of plane wave reflected from its surface is rotated, the sense and angle of rotation depend on M , the admittance parameter. Many authors have used the PEMC concept [35-43]. Chiral nihility [Appendix F] is a special kind of chiral medium, for which the real part of permittivity and permeability are simultaneously zero, in other words refractive index becomes zero at certain frequency known as chiral nihility frequency [49]. In chiral nihility, the two eigenwaves are still circularly polarized. But one of them is a backward wave whose phase velocity has an anti-parallel direction with corresponding Poynting vector. Chiral is a meta-material and field reflected from PEMC backed chiral nihility reflector contains both co and cross-polarized field components which finds potential use in military applications.

The electromagnetic waves radiated from a distant source will become a field of plane waves at receiving antenna. The field is focussed around caustic region. The knowledge of field distribution pattern around caustic is necessary as it is helpful in selecting receiver/transmitter to be placed in the caustic region. The field pattern

at caustic leads to development of practical antenna design. The work on Maslov's method applied two dimensional dual reflector systems having reflectors of different materials has been original as reported in this dissertation [23],[24] and [43]. The work has attracted attention of a large number of researchers who have made more than fifteen citations of the work in this dissertation while taking this work as basis for their further research work. The results of 2-D in the dissertation may be useful in the design of more practical 3-D systems to receive signals of high frequency field in communication.

A Chapter wise brief description of the work carried out in the thesis is given below: In Chapter 2, field expression based on Maslov's method is applied to an arbitrary cylindrical reflector (PEC) to derive a general form of field expression which should remain valid at all points including the caustic. The general form of field expression so derived, can be applied to different shapes of single reflector antenna such as parabolic, circular and elliptical cylinder etc. The high frequency field expression contains an integral form of solution near caustic and may be evaluated either analytically/numerically or with uniform asymptotic techniques. The validity of field expression is established by showing that integral form of solution reduces to GO field expression when the field point is considered far away from caustic region. As an application, the field expression is applied to parabolic cylinder widely used as microwave antenna. The high frequency field expression obtained for a parabolic microwave antenna closely matches with that obtained by Kay and Keller [13] using induced current method. The field patterns evaluated around caustic region of parabolic cylinder for oblique and normal incident plane wave [18] using both Maslov's method and Huygens-Kirchhoff's integral, are compared and the results are found in complete agreement.

In Chapter 3, the work on Maslov's method is extended to include the study of field behavior around caustic region of more complex systems which include PEC Cassegrain and Gregorian dual reflector systems. Both utilize a sub-reflector which is placed to

intercept the field reflected from main-reflector [23-25]. The dimensional parameters of main-reflector and sub-reflector are determined using near field focussing properties of aperture antennas. The diameter of main-reflector [Appendix D] is obtained so that sub-reflector is properly illuminated by the reflected field. The sub-reflector profile is determined using ray optics to maximize the efficiency of parabolic reflector. Maslov's method is applied to derive high frequency field expressions for both Cassegrain and Gregorian dual reflector antennas for normal incident plane wave. Field patterns around their caustic regions are evaluated through numerical computations. The results of both the focussing systems are then compared with the results obtained by applying Huygens-Kirchhoff's integral to their equivalent parabolic reflector. They are found in complete agreement, which yet again testifies the validity of Maslov's method. The parameters of focussing systems under study are varied to see the impact on the image quality of focussing fields. The field patterns corresponding to three different set of parameters of dual reflector systems, are obtained to study the quality of image fields around the caustic region.

In first part of Chapter 4, the present work is extended to include the study of field behavior around the caustic region of dual reflector focussing systems in which one or both the PEC reflectors are replaced with PEMC reflectors. For this purpose following two cases are considered,

- (i) PEMC Gregorian dual reflector microwave antenna in which main-reflector is PEMC while sub-reflector is PEC.
- (ii) PEMC Cassegrain dual reflector microwave antenna in which both the reflectors are PEMC.

Maslov's method is applied to both PEMC Cassegrain and Gregorian dual reflector antennas to derive high frequency field expressions. The field expressions obtained thereby, yield finite field value around caustic of these systems. The integral of field

expression is solved through numerical computations to determine field distribution around the caustics. A comparison study of amplitude variation of both co-polarized and cr-polarized field components has been carried out for different values of parameter M , the admittance of PEMC boundary. The results are shown schematically.

In second Part, both Gregorian and Cassegrain dual reflector antennas in which main-reflector is PEMC backed chiral nihility whereas sub-reflector is PEC, are considered for the study of field behavior around their caustic regions. Field expressions valid around the caustic of both dual reflector systems are derived using Maslov's method. Solutions of field expressions are obtained through numerical computations to evaluate the field patterns around the caustics. Dependence of co-polarized and cr-polarized field components for different values of admittance parameter M of PEMC has been studied. Interpretation of the results is given by taking into account following observation. How admittance parameter effects the co and cr-polarized field components?

Chapter 5 concludes the present discussion with the observations based on the results presented in the thesis that the method is straightforward and provides an alternate to the conventional induced current method or Huygens-Kirchhoff's integral for field evaluation around the caustic region of focussing systems. Both Maslov's method and Huygens-Kirchhoff's integral yield the results which completely agree around the caustic region but show slight difference in phase and amplitude elsewhere. The coating of PEMC and chiral nihility metamaterial on reflectors of Cassegrain and Gregorian systems gives rise to co and cr-polarized field components when plane wave is incident on this metamaterial interface. The generation of co and cr-polarized field components finds potential use in military applications

Chapter 2

PEC Arbitrary Cylindrical Reflector

Maslov's method is used to derive field expression that is valid around the caustic of an arbitrary cylindrical reflector. The field expression so obtained, is used to study the field distribution around the caustic region of various shapes of single reflector focusing system i.e., parabolic, circular and elliptical cylinder etc. But here only parabolic cylinder is considered for the study of field pattern around caustic region. Results obtained for parabolic reflector using Maslov's method are compared with the results obtained by applying Huygens-Kirchhoff's principle. It is assumed that cylindrical reflector is of PEC and source of excitation is a uniform electromagnetic plane wave. Medium surrounding the reflector is homogeneous, isotropic, lossless, linear, and non-dispersive.

2.1. Formulation of Geometrical Optics Field

Consider an arbitrarily shaped cylindrical reflector as shown in Fig. 2.1. whose contour is described by

$$\zeta = f(\xi) \quad (2.1.1)$$

where (ξ, ζ) are the Cartesian coordinates of a point on the reflector. The surface of arbitrary cylinder is excited by a linearly polarized plane wave with time dependency time harmonic $\exp(j\omega t)$. The field is obliquely incident and is given by

$$E^i = \exp(-j\mathbf{k} \cdot \mathbf{r})$$

where

$$\mathbf{k} = k_x \mathbf{i}_x + k_z \mathbf{i}_z, \quad \mathbf{r} = x \mathbf{i}_x + z \mathbf{i}_z$$

Therefore incident field may be written as

$$E^i = \exp[-j(k_x x + k_z z)] \quad (2.1.2)$$

where $k_x = k \sin \phi_0$, $k_z = k \cos \phi_0$, and ϕ_0 is the angle of incident with respect to the z-axis. It may be noted that throughout the research work it is assumed that $k = k_0 = \omega \sqrt{\mu_0 \epsilon_0}$.

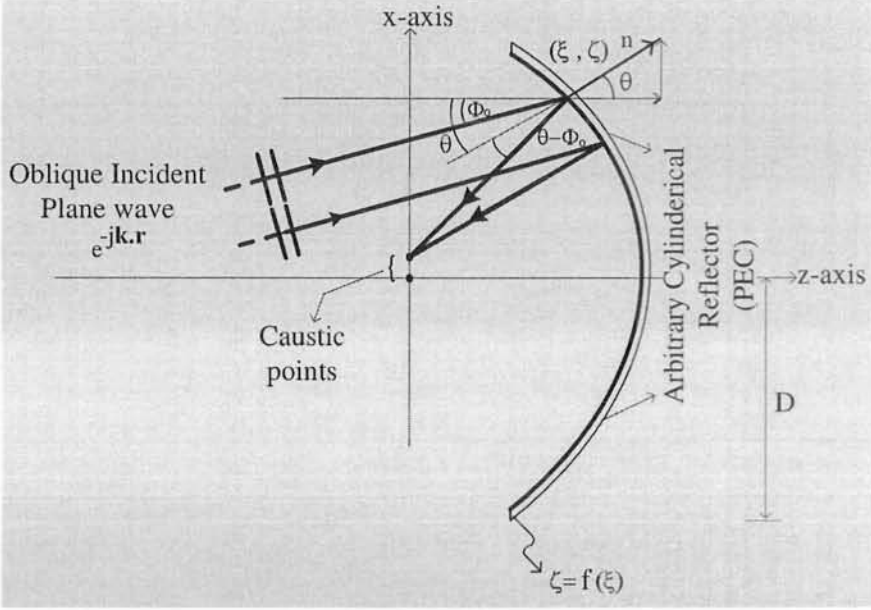


Fig. 2.1. An arbitrary cylindrical (PEC) reflector being excited by oblique incident plane electromagnetic wave .

The wave vector of the incident field is given by

$$\mathbf{p}^i = \sin \phi_0 \mathbf{i}_x + \cos \phi_0 \mathbf{i}_z \quad (2.1.3)$$

The wave vector of the reflected field may be obtained from the formula based on Snell's law as

$$\mathbf{p}^r = \mathbf{p}^i - 2(\mathbf{p}^i \cdot \mathbf{n})\mathbf{n} \quad (2.1.4)$$

where \mathbf{n} is unit normal at incident point (ξ, ζ) on the surface (2.1.1) and is defined by

$$\mathbf{n} = \sin \theta \mathbf{i}_x + \cos \theta \mathbf{i}_z \quad (2.1.5)$$

where

$$\sin \theta = \frac{-f'(\xi)}{\sqrt{1 + [f'(\xi)]^2}}, \quad \cos \theta = \frac{1}{\sqrt{1 + [f'(\xi)]^2}}, \quad \tan \theta = -f'(\xi) \quad (2.1.6)$$

where $f'(\xi)$ is the derivative of the function given by (2.1.1) with respect to ξ . Substituting (2.1.3) and (2.1.5) in (2.1.4) gives wave vector of the reflected field as

$$\begin{aligned} \mathbf{p}^r &= \left[\sin \phi_0 - 2 \sin \theta \cos(\theta - \phi_0) \right] \mathbf{i}_x + \left[\cos \phi_0 - 2 \cos \theta \cos(\theta - \phi_0) \right] \mathbf{i}_z \\ &= -\sin(2\theta - \phi_0) \mathbf{i}_x - \cos(2\theta - \phi_0) \mathbf{i}_z = p_x^r \mathbf{i}_x + p_z^r \mathbf{i}_z \end{aligned} \quad (2.1.7)$$

The coordinates of a point on the reflected ray are given by the solution of Hamilton's equation [19]

$$x = \xi + p_x^r \tau, \quad z = f(\xi) + p_z^r \tau \quad (2.1.8)$$

The GO field associated with the reflected ray at the point (x, z) is given by [8]

$$E^r(x, z) = A^r(x, z) \exp \left[-jkS(x, z) \right] \quad (2.1.9)$$

where amplitude $A^r(x, z)$ may be written as

$$A^r(x, z) = A_0^r(\xi) \left[\frac{D(\tau)}{D(0)} \right]^{-\frac{1}{2}} \quad (2.1.10)$$

and the phase function is given by

$$S(x, z) = \xi \sin \phi_0 + f(\xi) \cos \phi_0 + \tau = S_0 + \tau \quad (2.1.11)$$

$A_0^r(\xi)$ is the field amplitude on the reflector at point (ξ, ζ) and $A^r(x, z)$ is the field amplitude at observation point away from the reflector. $D(\tau)$ is the Jacobian of transformation from the ray coordinates (ξ, τ) to cartesian coordinates (x, z) . Quantity $S_0 = \xi \sin \phi_0 + f(\xi) \cos \phi_0$ is the initial value of the phase function at point (ξ, ζ) and τ represents the distance along the ray from a reference point (ξ, ζ) on the reflector.

Substituting (2.1.10) and (2.1.11) in (2.1.9), gives

$$\begin{aligned} E^r(x, z) &= A_0^r(\xi) \left[\frac{D(\tau)}{D(0)} \right]^{-\frac{1}{2}} \exp \left[-jk \left(\xi \sin \phi_0 + f(\xi) \cos \phi_0 + \tau \right) \right] \\ &= A_0^r(\xi) \left[\frac{D(\tau)}{D(0)} \right]^{-\frac{1}{2}} \exp \left[-jk \left(S_0 + \tau \right) \right] \end{aligned} \quad (2.1.12)$$

In the next section, Jacobian of transformation $J(\tau) = \frac{D(\tau)}{D(0)}$, is determined to evaluate the amplitude of the field reflected from the reflector.

2.1.1. Determination of Amplitude

The amplitude of the field associated with the ray reflected from the reflector is

$$A^r(x, z) = A_0^r(\xi) \left[\frac{D(\tau)}{D(0)} \right]^{-\frac{1}{2}} \quad (2.1.13)$$

where the Jacobian may be determined as

$$D(\tau) = \frac{\partial(x, z)}{\partial(\xi, \tau)} = \frac{\partial x}{\partial \xi} \cdot \frac{\partial z}{\partial \tau} - \frac{\partial z}{\partial \xi} \cdot \frac{\partial x}{\partial \tau} \quad (2.1.14)$$

Differentiating (2.1.8) with respect to ξ and τ , using (2.1.7) and substituting in (2.1.14) yields

$$D(\tau) = -\cos(2\theta - \phi_0) + f'(\xi) \sin(2\theta - \phi_0) + 2 \frac{\partial \theta}{\partial \xi} \tau$$

Referring to (2.1.6), gives $\tan \theta = -f'(\xi)$ and so $f''(\xi) = -\sec^2 \theta \frac{\partial \theta}{\partial \xi}$ and substituting in above relation gives

$$D(\tau) = -\frac{\cos(\theta - \phi_0)}{\cos \theta} - 2 \cos^2 \theta f''(\xi) \tau \quad (2.1.15)$$

so that

$$D(0) = -\frac{\cos(\theta - \phi_0)}{\cos \theta}$$

so that normalized Jacobian $J(\tau)$ may be written as

$$J(\tau) = \frac{D(\tau)}{D(0)} = 1 + \frac{2 \cos^3 \theta}{\cos(\theta - \phi_0)} f''(\xi) \tau \quad (2.1.16)$$

The location of caustic is given by the point satisfying $J(\tau) = 0$ so that

$$\tau = -\frac{\cos(\theta - \phi_0)}{2 \cos^3 \theta f''(\xi)} \quad (2.1.17)$$

Thus the coordinates of the caustic point (x_c, z_c) on the reflected ray are obtained by substituting (2.1.17) in (2.1.8)

$$\begin{aligned} x_c &= \xi + \frac{\sin(2\theta - \phi_0) \cos(\theta - \phi_0)}{2 \cos^3 \theta f''(\xi)} \\ z_c &= f(\xi) + \frac{\cos(2\theta - \phi_0) \cos(\theta - \phi_0)}{2 \cos^3 \theta f''(\xi)} \end{aligned} \quad (2.1.18)$$

GO expression for the field reflected from an arbitrary cylindrical reflector is obtained by substituting (2.1.16) in (2.1.12)

$$E^r(x, z) = A_0^r(\xi) \left[1 + \frac{2 \cos^3 \theta}{\cos(\theta - \phi_0)} f''(\xi) \tau \right]^{-\frac{1}{2}} \exp[-jk(S_0 + \tau)] \quad (2.1.19)$$

In above field expression, when $\tau = -\frac{\cos(\theta - \phi_0)}{2 \cos^3 \theta f''(\xi)}$, the field $E^r(x, z) = E^r(x_c, z_c)$ becomes infinite. This means that GO field expression (2.1.19) fails to predict the field around caustic region of an arbitrary cylindrical reflector. The objective is to derive field expression using Maslov's method that should yield the finite field value at all points including the caustic region. This is accomplished using Maslov's method.

2.2. Determination of Field Around Caustic

In order to obtain uniform field distribution around caustic, Maslov's method is used. According to Maslov's method, the field expression valid around caustic of arbitrary cylinder can be derived using the relation (1.2.12) as

$$E^r(x, z) = \sqrt{\frac{k}{j2\pi}} \int_{-\infty}^{\infty} A_0(\xi) \left[\frac{D(\tau)}{D(0)} \frac{\partial p_z^r}{\partial z} \right]^{-\frac{1}{2}} \times \exp \left\{ -jk \left[S_0 + \tau - z_s(x, p_z^r) p_z^r + p_z^r z \right] \right\} dp_z^r \quad (2.2.1)$$

where $S_0 = \xi \sin \phi_0 + f(\xi) \cos \phi_0$ is the initial phase of the field on the reflector. In above expression, $z_s(x, p_z^r)$ means that the coordinate z_s should be expressed in terms of mixed coordinates (x, p_z^r) using the solution of Hamilton's equations. The same is true for τ and it is given by $\tau = \frac{x - \xi}{p_x^r}$. Now proceeding to find the unknown variables of phase and amplitude in (2.2.1) as below.

2.2.1. Evaluation of Phase Function

The phase function of the reflected field is given by

$$S(p_z^r) = S_0 + \tau - z_s(x, p_z^r) p_z^r + p_z^r z$$

Using solution of Hamilton's equations (2.1.8), the phase function may be written as

$$\begin{aligned} S(p_z^r) &= \xi \sin \phi_0 + f(\xi) \cos \phi_0 + \frac{x - \xi}{p_x^r} - f(\xi) p_z^r - (p_z^r)^2 \frac{x - \xi}{p_x^r} + p_z^r z \\ &= \xi \sin \phi_0 + f(\xi) \cos \phi_0 + \frac{x - \xi}{p_x^r} (1 - (p_z^r)^2) - f(\xi) p_z^r + p_z^r z \end{aligned} \quad (2.2.2)$$

Using (2.1.7) and (2.1.8), it gives

$$\begin{aligned} S(p_z^r) &= \xi \left[\sin \phi_0 + \sin(2\theta - \phi_0) \right] + f(\xi) \left[\cos \phi_0 + \cos(2\theta - \phi_0) \right] + p_x^r x + p_z^r z \\ &= 2\xi \sin \theta \cos(\theta - \phi_0) + 2f(\xi) \cos \theta \cos(\theta - \phi_0) + p_x^r x + p_z^r z \end{aligned}$$

In the above equation, introducing polar coordinates

$$x = \rho \sin \phi, \quad z = \rho \cos \phi \quad (2.2.3)$$

It yields,

$$S(\theta) = 2 \left[\xi \sin \theta + f(\xi) \cos \theta \right] \cos(\theta - \phi_0) - \rho \cos(2\theta - \phi - \phi_0) \quad (2.2.4)$$

2.2.2. Evaluation of Amplitude Function

The amplitude function means integrand of (2.2.1)

$$\left[\frac{D(\tau)}{D(0)} \frac{\partial p_z^r}{\partial z} \right]^{-\frac{1}{2}} = \left[J(\tau) \frac{\partial p_z^r}{\partial z} \right]^{-\frac{1}{2}} \quad (2.2.5)$$

First of all, it is required to determine $\frac{\partial p_z^r}{\partial z}$ from (2.1.7) and (2.1.8), variable z can be written as

$$z = f(\xi) + \cot(2\theta - \phi_0)(x - \xi) \quad (2.2.6)$$

Differentiation of (2.2.6) w.r.t. θ yields

$$\begin{aligned} \frac{\partial z}{\partial \theta} &= f'(\xi) \frac{\partial \xi}{\partial \theta} - \frac{2(x - \xi)}{\sin^2(2\theta - \phi_0)} - \cot(2\theta - \phi_0) \frac{\partial \xi}{\partial \theta} \\ &= - \left[\tan \theta + \cot(2\theta - \phi_0) \right] \frac{\partial \xi}{\partial \theta} + \frac{2\tau}{\sin(2\theta - \phi_0)} \\ &= - \frac{\cos(\theta - \phi_0)}{\sin(2\theta - \phi_0)} \frac{1}{\cos \theta} \frac{\partial \xi}{\partial \theta} \left[1 - \frac{2 \cos \theta}{\cos(\theta - \phi_0)} \frac{\partial \theta}{\partial \xi} \tau \right] \end{aligned} \quad (2.2.7)$$

Making use of (2.1.7), gives

$$\frac{\partial p_z^r}{\partial \theta} = 2 \sin(2\theta - \phi_0) \quad (2.2.8)$$

As $\tan \theta = -f'(\xi)$ therefore $\frac{\partial \theta}{\partial \xi} = -\cos^2 \theta f''(\xi)$ hence using (2.2.7) and (2.2.8), gives

$$\begin{aligned} \frac{\partial z}{\partial p_z^r} &= \frac{\partial z}{\partial \theta} \frac{\partial \theta}{\partial p_z^r} \\ &= \frac{1}{2 \sin(2\theta - \phi_0)} \frac{\partial z}{\partial \theta} \\ &= -\frac{\cos(\theta - \phi_0)}{2 \sin^2(2\theta - \phi_0) \cos \theta} \frac{\partial \xi}{\partial \theta} \left[1 + \frac{2f''(\xi) \cos^3 \theta}{\cos(\theta - \phi_0)} \tau \right] \\ \frac{\partial p_z^r}{\partial z} &= \frac{2 \sin^2(2\theta - \phi_0) \cos^3 \theta f''(\xi)}{\cos(\theta - \phi_0)} \left[1 + \frac{2f''(\xi) \cos^3 \theta}{\cos(\theta - \phi_0)} \tau \right]^{-1} \end{aligned} \quad (2.2.9)$$

Using (2.1.16) and (2.2.9), yields

$$\begin{aligned} J(\tau) \frac{\partial p_z^r}{\partial z} &= \left[1 + \frac{2f''(\xi) \cos^3 \theta}{\cos(\theta - \phi_0)} \tau \right] \left[\frac{2 \cos^3 \theta \sin^2(2\theta - \phi_0)}{\cos(\theta - \phi_0)} f''(\xi) \right] \left[1 + \frac{2f''(\xi) \cos^3 \theta}{\cos(\theta - \phi_0)} \tau \right]^{-1} \\ &= \frac{2 \cos^3 \theta \sin^2(2\theta - \phi_0)}{\cos(\theta - \phi_0)} f''(\xi) \quad (\text{Appendix A}) \end{aligned} \quad (2.2.10)$$

Also (2.2.8) yields

$$dp_z^r = 2 \sin(2\theta - \phi_0) d\theta \quad (2.2.11)$$

Now substituting (2.2.4), (2.2.10) and (2.2.11) in (2.2.1), gives

$$\begin{aligned} E^r(x, z) &= \sqrt{\frac{k}{\pi}} \exp\left(-j\frac{\pi}{4}\right) \int_{-\Theta/2}^{\Theta/2} A_0^r(\xi) \left[\frac{\cos(\theta - \phi_0)}{\cos^3 \theta f''(\xi)} \right]^{\frac{1}{2}} \\ &\quad \times \exp\left\{-j2k\left[\xi \sin \theta + f(\xi) \cos \theta\right] \cos(\theta - \phi_0)\right\} \\ &\quad \times \exp\left[jk\rho \cos(2\theta - \phi - \phi_0)\right] d\theta \end{aligned} \quad (2.2.12)$$

where Θ is the aperture angle subtended at the caustic such that $\Theta = 2\theta$ at the edge of the reflector. It may be noted that integration variable has been changed from p_z^r to θ . Field expression (2.2.12) yields finite field at all points including caustic region of arbitrary cylinder.

2.3. Validity of Maslov's Method

It is interesting to establish the validity of the field expression (2.2.12) based on Maslov's method that produces finite field value in the neighborhood of caustic region. In order to achieve this, consider a region far away from caustic and evaluate the field by obtaining approximate solution of (2.2.12) through the use of stationary phase method of integration [6]. The results obtained from this approximate solution must agree with those obtained from GO field expression derived in (2.1.19). This serves as an important check on the validity of the field expression (2.2.12) based on Maslov's method. In order to solve the integral of (2.2.12) by using stationary phase method of integration, the stationary point is determined from the phase function

$$S(\theta) = 2 \left[\xi \sin \theta + f(\xi) \cos \theta \right] \cos(\theta - \phi_0) - \rho \cos(2\theta - \phi - \phi_0) \quad (2.3.1)$$

Differentiating (2.3.1) w.r.t. θ , gives

$$S'(\theta) = 2 \left[\xi \cos(2\theta - \phi_0) - f(\xi) \sin(2\theta - \phi_0) \right] + 2\rho \sin(2\theta - \phi - \phi_0) \quad (2.3.2)$$

Stationary point is obtained by setting

$$S'(\theta_s) = 0$$

which yields stationary point

$$\theta_s = \frac{\phi_0 + \phi}{2}$$

The second derivative of the phase function at stationary point is

$$\begin{aligned} S''(\theta_s) &= -4 \left[\xi \sin(2\theta - \phi_0) + f(\xi) \cos(2\theta - \phi_0) \right] \\ &\quad + 2 \left[\cos(2\theta - \phi_0) - f'(\xi) \sin(2\theta - \phi_0) \right] \frac{d\xi}{d\theta} + 4\rho \cos(2\theta - \phi - \phi_0) \\ &= -2 \frac{\cos(\theta - \phi_0)}{\cos^3 f''(\xi)} \left[1 + 2 \frac{\cos^3 \theta}{\cos(\theta - \phi_0)} f''(\xi) \tau \right] \\ &= -2 \frac{\cos(\theta - \phi_0)}{\cos^3 f''(\xi)} J(\tau) \end{aligned} \quad (2.3.3)$$

The phase function at stationary point is

$$\begin{aligned}
 S(\theta_s) &= 2 \left[\xi \sin \theta + f(\xi) \cos \theta \right] \cos(\theta - \phi_0) - \rho \cos(2\theta - \phi - \phi_0) \\
 &= \xi \left[\sin(2\theta - \phi_0) + \sin \phi_0 \right] + f(\xi) \left[\cos(2\theta - \phi_0) + \cos \phi_0 \right] \\
 &\quad - x \sin(2\theta - \phi_0) - z \cos(2\theta - \phi_0) \\
 &= \xi \sin \phi_0 + f(\xi) \cos \phi_0 + \tau
 \end{aligned} \tag{2.3.4}$$

Equation (2.2.12) may be written in the form of a standard integral as

$$E^r(x, z) = \sqrt{\frac{k}{\pi}} \exp\left(-j\frac{\pi}{4}\right) \int_{-\Theta/2}^{\Theta/2} F(\theta) \exp[-jkS(\theta)] d\theta \tag{2.3.5}$$

where

$$F(\theta) = A_0^r(\xi) \left[\frac{\cos(\theta - \phi_0)}{\cos^3 \theta f''(\xi)} \right]^{-\frac{1}{2}}$$

Using stationary phase method of integration, asymptotic solution of (2.3.5) is

$$\begin{aligned}
 E^r(x, z) &\approx \sqrt{\frac{k}{\pi}} \exp\left(-j\frac{\pi}{4}\right) \left[\sqrt{\frac{2\pi j}{k}} F(\theta_s) \exp[-jkS(\theta_s)] \frac{1}{\sqrt{|S''(\theta_s)|}} \right], \quad k \gg 1 \\
 &= A_0^r(\xi) |J(\tau)|^{-\frac{1}{2}} \exp[-jkS(\theta_s)] \\
 &= A_0^r(\xi) |J(\tau)|^{-\frac{1}{2}} \exp[-jk \{ \xi \sin \phi_0 + f(\xi) \cos \phi_0 + \tau \}]
 \end{aligned} \tag{2.3.6}$$

The field expression (2.3.6) obtained as an approximate solution of (2.2.12), is the same as GO field expression (2.1.19). Thus the field expression (2.2.12) reduces to GO field expression (2.1.19) in a region far away from caustic. This confirms the validity of the field expression (2.2.12) obtained using Maslov's method.

2.4. Special Case–Parabolic Cylindrical Reflector

The field expression (2.2.12) derived for an arbitrary cylindrical reflector is now used to determine the field distribution around the focal region of a PEC parabolic cylinder which is used as microwave receiving antenna.

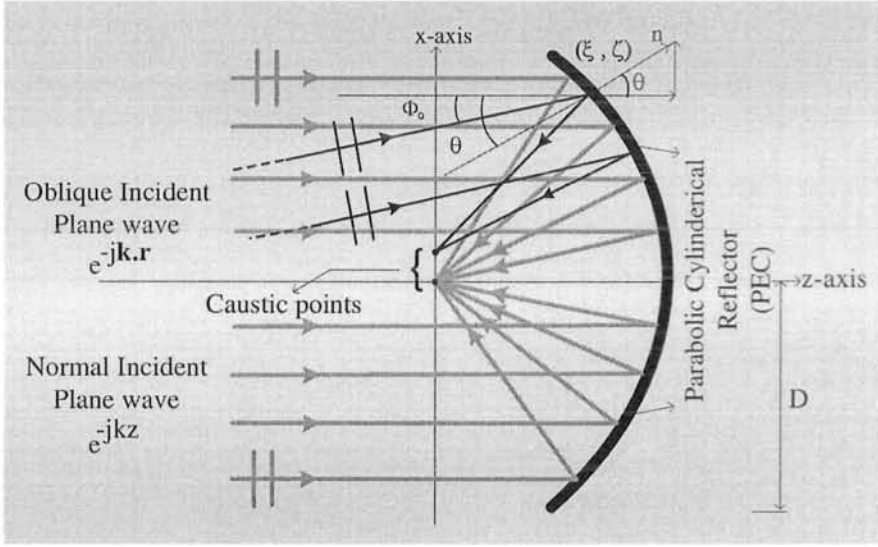


Fig. 2.2. PEC parabolic cylinder being excited by both normal and oblique incident plane electromagnetic wave.

Consider a plane wave reflection from a two dimensional parabolic microwave antenna with its focus at the origin of cartesian coordinates system. The surface contour of parabolic reflector is defined as

$$f(\xi) = \zeta = f - \frac{\xi^2}{4f} \quad (2.4.1)$$

where (ξ, ζ) are the cartesian coordinates of a point on the parabolic reflector. Suppose that a uniform electromagnetic plane wave is obliquely incident from the left on concave side of parabolic reflector as shown in Fig. 2.2. and is given by

$$E^i = e^{-j\mathbf{k}\cdot\mathbf{r}} \quad (2.4.2)$$

Now the differentiation of (2.4.1) w.r.t. ξ yields

$$f'(\xi) = -\frac{\xi}{2f}, \quad f''(\xi) = -\frac{1}{2f} \quad (2.4.3)$$

As from (2.1.7), $f'(\xi) = -\tan \theta$, the relation (2.4.3) and (2.4.1) respectively give

$$\xi = 2f \tan \theta, \quad \text{and} \quad \zeta = f \frac{\cos 2\theta}{\cos^2 \theta} \quad (2.4.4)$$

Now substitute (2.4.3) and (2.4.4) in the field expression (2.2.12) and obtain

$$E^r(x, z) = \sqrt{\frac{2kf}{\pi}} \exp \left[-j2kf - j\frac{\pi}{4} \right] \int_{-\Theta/2}^{\Theta/2} \left[\frac{\cos(\theta - \phi_0)}{\cos^3 \theta} \right]^{\frac{1}{2}} \exp \left[jk\rho \cos(2\theta - \phi_0 - \phi) - j2kf \frac{\cos(\theta - \phi_0) - \cos \theta}{\cos \theta} \right] d\theta \quad (2.4.5)$$

where $x = \rho \sin \phi$, $z = \rho \cos \phi$, and $\Theta = 2\theta$, is the angle subtended at focal point by the aperture of parabolic reflector and is selected by $\Theta = 2 \text{Arctan}(\frac{D}{2f})$. when the observation point is considered far from caustic, it can be shown that (2.4.5) will reduce to GO field expression (2.1.19) by applying stationary phase method of integration. Using numerical computations, the field expression (2.4.5) gives field distribution around the caustic of a parabolic reflector for obliquely incident ϕ_0 plane wave. For normal incident plane wave $\phi_0 = 0$, the field expression (2.4.5) will become,

$$E^r(x, z) = \sqrt{\frac{2kf}{\pi}} \exp \left[-j2kf - j\frac{\pi}{4} \right] \int_{-\Theta/2}^{\Theta/2} \sec \theta \exp \left[jk\rho \cos(2\theta - \phi) \right] d\theta \quad (2.4.6)$$

The field expression (2.4.6) completely agrees with that of Kay and Keller [13]. The field distribution around the caustic region of parabolic reflector is studied for both oblique incident field $\phi_0 = -5^\circ$ and normal incident field $\phi_0 = 0$ as shown in Fig. 2.3–Fig. 2.5.

2.5. Comparison with the Huygens-Kirchhoff's Principle

To testify the validity of the uniform field expression (2.4.5) based on Maslov's method, alternate field expression for a parabolic reflector is derived using Huygens-Kirchhoff's principle based on Green's theorem as

$$E(x, z) = \frac{1}{j4} \int_C \frac{\partial E_y}{\partial n} H_0^{(2)}(k\tau) dl \quad (2.5.1)$$

where $\tau = [(x - \xi)^2 + (z - \zeta)^2]^{\frac{1}{2}}$ and $\frac{\partial E_y}{\partial n}$ can be calculated as

$$\begin{aligned} \frac{\partial E_y}{\partial n} &= \frac{\partial E_y}{\partial x} n_x + \frac{\partial E_y}{\partial z} n_z = -j\omega\mu(\mathbf{n} \times \mathbf{H})_y = -j\omega\mu J_y \\ J_y &= (\mathbf{2n} \times \mathbf{H}^i)_y = -j2\omega\mu \cos(\theta - \phi_0) \exp(-jknS_0) \end{aligned} \quad (2.5.2)$$

where $S_0 = \xi \sin \phi_0 + \zeta \cos \phi_0$ and C is the contour of the reflector. Using the following facts and the asymptotic expression for Hankel function

$$\begin{aligned} dl &= \sqrt{1 + [f'(\xi)]^2} \\ &= \frac{2f}{\cos^3 \theta} d\theta \end{aligned} \quad (2.5.3)$$

$$H_0^{(2)}(k\tau) \simeq \sqrt{\frac{2}{\pi k\tau}} \exp\left[-jk\tau + j\pi/4\right] \quad (2.5.4)$$

Finally the field expression which is valid around the caustic is

$$\begin{aligned} E^r(x, z) &= f \sqrt{\frac{2k}{\pi}} \exp\left[-j2kf - j\frac{\pi}{4}\right] \int_{-\Theta/2}^{\Theta/2} \frac{\cos(\theta - \phi_0)}{\sqrt{\tau} \cos^3 \theta} \\ &\quad \times \exp\left[jk\rho \cos(2\theta - \phi_0 - \phi) - \frac{jk2f \cos(\theta - \phi_0) - \cos \theta}{\cos \theta}\right] d\theta \end{aligned} \quad (2.5.5)$$

where $\Theta = 2 \arctan\left(\frac{D}{2f}\right)$ and Θ signifies the angle which is subtended at the focal point by the aperture of parabolic cylinder. It may be noted that D is the height of the edge of parabolic reflector from horizontal axis. In the vicinity of caustic $\tau = \frac{f \cos(\theta - \phi_0)}{\cos^3 \theta}$. The above field expression assumes the form which completely agrees with (2.4.5). The results of field pattern obtained from field expression (2.5.5) based on Huygens-Kirchhoff's principle are compared with those obtained from field expression (2.4.5) based on Maslov's method for both normal and oblique incident electromagnetic plane wave. The results show complete agreement around caustic region.

2.6. Results and Discussion

The field expression (2.2.12) for an arbitrary reflector has been established using Maslov's method. When observation point is far away from caustic, it has been

shown that (2.2.12) reduces to GO field expression (2.1.19) which is based on solutions of Hamilton's equations. As an application to radio engineering, the field expression (2.2.12) for an arbitrary cylinder is applied to a parabolic cylinder which is of perfect electric conductor. The two field expressions (2.4.5) and (2.5.5) based on Maslov's method and Huygens-Kirchhoff's principle respectively, are evaluated through numerical computations to determine field distribution around the feed point of parabolic cylinder.

Fig. 2.3. provides comparison of the two field patterns around feed point, obtained using both (a) Maslov's method (solid line) and (b) Kirchhoff's approximation (dashed line) respectively. The comparison results of field patterns are found in complete agreement. The above analysis is carried out for a parabolic cylinder having dimensional parameters of $kf = 50$ and $\Theta = \frac{\pi}{2}$. Fig. 2.4. provides the comparison of field patterns around caustic region of parabolic cylinder under normal incident ($\phi_0 = 0$) of plane electromagnetic wave, using both (a) Maslov's method, and (b) Huygens-Kirchhoff's principle. The results of field comparison are found in complete agreement. The above field analysis is carried out for a parabolic cylinder having dimensional parameters of the reflector as $kf = 50$ and $\Theta = \frac{\pi}{3}$. Fig. 2.5. provides the comparison of field distribution around caustic region of parabolic cylinder under oblique ($\phi_0 = 50^\circ$) incident of plane electromagnetic wave using the field expression based on both (a) Maslov's method, and (b) Huygens-Kirchhoff's principle. The caustic region is located off-axis of parabolic cylinder. The results of field comparison are found in complete agreement. The above field analysis is carried out for a parabolic cylinder having dimensional parameters of the reflector as $kf = 50$ and $\Theta = \frac{\pi}{3}$. The discussion is concluded with the observation that the results obtained by comparison of field patterns are in complete agreement, thereby establishing the validity of Maslov's method.

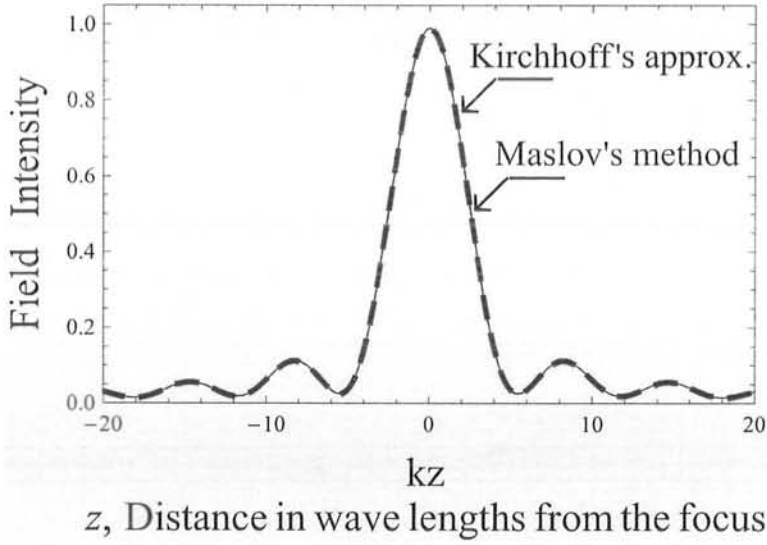


Fig. 2.3. Comparison of reflected field intensity around the caustic region of PEC parabolic cylinder along z -axis for normal incident plane wave ($\phi_0 = 0$) using Maslov's method (solid line) with that using Kirchhoff's approximation (dashed line). The dimension of parabolic cylinder is $\Theta = \frac{\pi}{2}$ and $kf = 50$

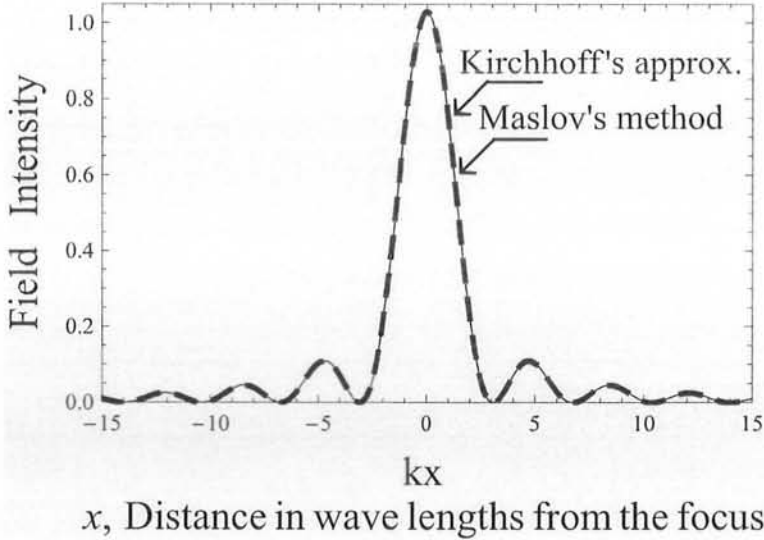


Fig. 2.4. Comparison of field intensity distribution around the caustic region of PEC parabolic cylinder along x -axis for normal incident plane wave ($\phi_0 = 0$) using Maslov's method (solid line) with that using Kirchhoff's approximation (dashed line). The dimension of parabolic cylinder is $\Theta = \frac{\pi}{3}$ and $kf = 50$.

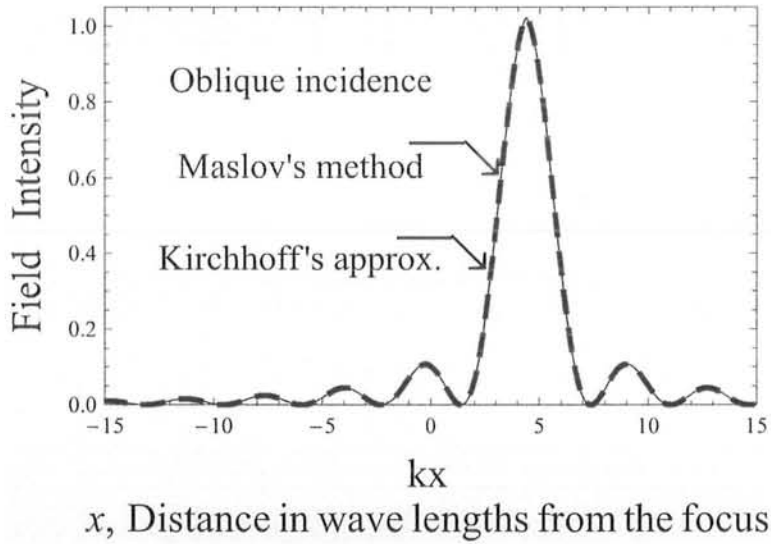


Fig. 2.5. Comparison of field intensity distribution around the caustic region of PEC parabolic cylinder along x -axis for oblique incident plane wave ($\phi_0 = -5^\circ$) using Maslov's method (solid line) with that using Kirchhoff's approximation (dashed line). The dimension of parabolic cylinder is $\Theta = \frac{\pi}{3}$ and $kf = 50$.

Chapter 3

Two Dimensional PEC Dual Reflector Systems

In this Chapter, two dimensional dual reflector systems of perfect electric conductor are considered for the study of field distribution around their caustic regions when they are used as microwave receiving antennas. High frequency field expressions are derived around feed point of two dimensional Cassegrain and Gregorian systems using Maslov's method. Field patterns around feed point of these systems are evaluated using numerical computations. The results of each dual reflector system are compared with the results of their equivalent parabola obtained using field expression based on Huygens-Kirchhoff's integral.

3.1. Cassegrain Dual Reflector System

A Cassegrain dual reflector system as shown in Fig. 3.1., consists of a main-reflector which is a parabolic cylinder and a sub-reflector which is hyperbolic cylinder. Both the cylindrical reflectors are assumed to be perfect electric conductor(PEC). The focal points of the two reflectors overlap each other and the system is being used as high frequency receiving antenna. Cassegrain dual reflector system can be modelled as a single equivalent parabolic reflector as shown in Fig. 3.2. The equivalent parabolic reflector has the same aperture as that of main-reflector of Cassegrain system, $D_{eq} = D$, but its focal length is much longer than that of the main-reflector. The focal length of equivalent parabola is determined using the following relation [Appendix D]

$$f_e = \left(\frac{c+a}{c-a} \right) f$$

where $\frac{c+a}{c-a}$ is called image field magnification. The increased focal length has various advantages regarding its performance i.e., less cross polarization, improved aperture efficiency etc.

The equation takes the form

$$f(\xi_2) = \zeta_2 = a \left[1 + \frac{\xi_2^2}{b^2} \right]^{\frac{1}{2}} \quad (3.1.3)$$

with

$$c^2 = a^2 + b^2 \quad (3.1.4)$$

where (ξ_2, ζ_2) are cartesian co-ordinates of a point on the surface of hyperbolic cylindrical reflector. Further $c + a$ and $c - a$ are the distances from the feed points F_2 and F_1 respectively to the sub-reflector as shown in the Fig. 3.1. Also D and d are the half apertures of the main reflector and sub reflector respectively.

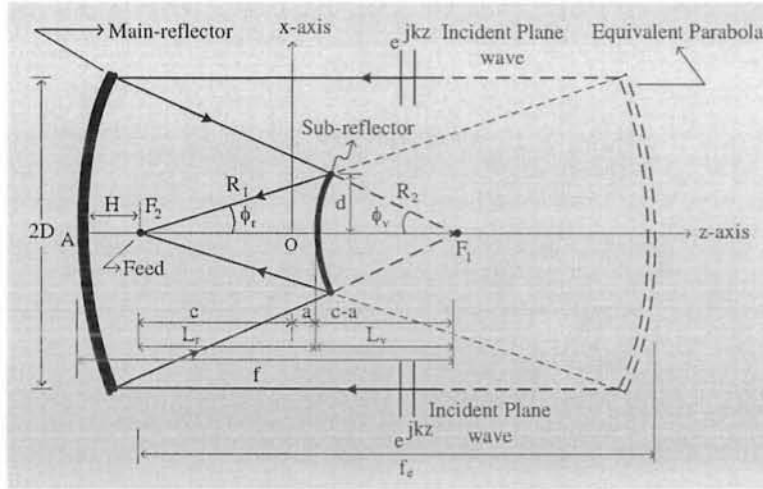


Fig. 3.2. Parameters in cylindrical dual reflector Cassegrain system.

The parameters shown in Fig. 3.2. are defined as

$$\tau = \sqrt{(x - \xi_2)^2 + (z - \zeta_2)^2} \quad (3.1.5)$$

$$\tau_1 = \sqrt{(\xi_2 - \xi_1)^2 + (\zeta_2 - \zeta_1)^2} \quad (3.1.6)$$

$$R_1 = \sqrt{\xi_2^2 + (\zeta_2 + c)^2} \quad (3.1.7)$$

$$R_2 = \sqrt{\xi_2^2 + (\zeta_2 - c)^2} \quad (3.1.8)$$

where τ_1 is distance along the ray between two points located on the two reflectors, τ is a parameter along the ray reflected by sub-reflector, R_1 and R_2 are the distances

from the hyperbolic surface to the focal points F_2 and F_1 respectively. let \mathbf{n}_1 and \mathbf{n}_2 be unit normals at reflection point (ξ_1, ζ_1) and (ξ_2, ζ_2) on the main-reflector and sub-reflector respectively and are defined by

$$\mathbf{n}_1 = -\sin \alpha \mathbf{i}_x + \cos \alpha \mathbf{i}_z \quad (3.1.9a)$$

$$\mathbf{n}_2 = -\sin \psi \mathbf{i}_x + \cos \psi \mathbf{i}_z \quad (3.1.9b)$$

where

$$\sin \alpha = -\frac{f'(\xi_1)}{\sqrt{1 + [f'(\xi_1)]^2}}, \quad \cos \alpha = \frac{1}{\sqrt{1 + [f'(\xi_1)]^2}} \quad (3.1.10)$$

$$\sin \psi = -\frac{f'(\xi_2)}{\sqrt{1 + [f'(\xi_2)]^2}}, \quad \cos \psi = \frac{1}{\sqrt{1 + [f'(\xi_2)]^2}} \quad (3.1.11)$$

where α and ψ are the angles which the unit normals \mathbf{n}_1 and \mathbf{n}_2 make with the z -axis respectively. Referring to (3.1.1), we have $f(\xi_1) = \zeta_1 = \frac{\xi_1^2}{4f} - f + c$ which on differentiating gives

$$f'(\xi_1) = \frac{\xi_1}{2f}$$

therefore

$$\sin \alpha = \frac{-\xi_1}{\sqrt{\xi_1^2 + 4f^2}}, \quad \cos \alpha = \frac{2f}{\sqrt{\xi_1^2 + 4f^2}} \quad (3.1.12)$$

Similarly differentiating (3.1.2) yields $f'(\xi_2) = \frac{a^2}{b^2} \frac{\xi_2}{\zeta_2}$ and substituting in (3.1.11) will produce (Appendix E)

$$\sin \psi = \frac{a\xi_2}{b\sqrt{R_1 R_2}}, \quad \cos \psi = \frac{b\zeta_2}{a\sqrt{R_1 R_2}} \quad (3.1.13)$$

For formulation of other parameters of Cassegrain system [Appendix D].

3.1.2. Derivation of GO Field

Consider a linearly polarized electromagnetic plane wave which is normally incident on the aperture of an axially symmetric parabolic reflector of the Cassegrain system as shown in Fig. (3.1). Let the field be given by

$$\mathbf{E}^i = \mathbf{u}_y \exp(jkz) \quad (3.1.14)$$

As receiving characteristics of the system are considered, so a field expression is derived to determine field distribution around caustic point F_2 of the system. The wave vector associated with the normal incident field is given by $\mathbf{p}^i = -\mathbf{i}_z$, as angle of incident is $\phi_0 = \pi$. The wave vector of the field reflected from parabolic reflector is obtained by substituting \mathbf{p}^i and \mathbf{n} in (2.1.4)

$$\mathbf{p}_1^r = -\sin 2\alpha \mathbf{i}_x + \cos 2\alpha \mathbf{i}_z \quad (3.1.15)$$

This will become incident wave vector \mathbf{p}_2^i for sub-reflector so that wave vector of the field reflected from the hyperbolic cylinder is

$$\mathbf{p}_2^r = -\sin(2\alpha - 2\psi) \mathbf{i}_x - \cos(2\alpha - 2\psi) \mathbf{i}_z \quad (3.1.16)$$

which explicitly gives

$$p_{x_2}^r = -\sin(2\alpha - 2\psi), \quad p_{z_2}^r = -\cos(2\alpha - 2\psi) \quad (3.1.17)$$

The space coordinates (x, z) of a point on the ray reflected from hyperbolic cylinder may be obtained using (3.1.17) and the solutions of Hamilton's equations

$$\begin{aligned} x &= \xi_2 + p_{x_2}^r \tau \\ z &= \zeta_2 + p_{z_2}^r \tau \end{aligned} \quad (3.1.18)$$

The cartesian coordinates of the ray reflected from hyperbolic reflector in terms of coordinates ξ_1, ζ_1 of parabolic reflector are given by

$$\begin{aligned} x &= \xi_2 + p_{x_2}^r \tau = \xi_1 + p_{x_1}^r \tau_1 + p_{x_2}^r \tau \\ z &= \zeta_2 + p_{z_2}^r \tau = \zeta_1 + p_{z_1}^r \tau_1 + p_{z_2}^r \tau \end{aligned} \quad (3.1.19)$$

In the above equations $(p_{x_1}^r, p_{z_1}^r)$ and $(p_{x_2}^r, p_{z_2}^r)$ are the rectangular components of \mathbf{p}_1^r and \mathbf{p}_2^r respectively. Considering the field after reflection from sub-reflector, the

expression for GO field of Cassegrain dual reflector microwave antenna may be given using (1.2.26)

$$E^r(x, z) = E_0^r(\xi_2, \zeta_2)[J(\tau)]^{-\frac{1}{2}} \exp[-jk\{S_0(\xi_1) + \tau_1 + \tau\}] \quad (3.1.20)$$

$$S_0(\xi_1) = -\zeta_1 = 2f \frac{\cos 2\alpha}{1 + \cos 2\alpha} - c$$

where $S_0(\xi_1)$ is the initial phase of the field incident on the parabolic main reflector, τ_1 as given by (3.1.6) is the phase function of the field associated with the ray propagating between the parabolic and hyperbolic reflector, τ as given by (3.1.5), is the phase function variation of the field along the ray between the sub-reflector and feed point of the Cassegrain system and $E_0^r(\xi_2, \zeta_2)$ is the initial amplitude of the field reflected from hyperbolic reflector.

3.1.3. Evaluation of Jacobian of the Field

The Jacobian of the field reflected from the parabolic cylinder is obtained by using (2.1.16) as

$$J_p(\tau) = \frac{D_p(\tau)}{D_p(0)} = 1 + \frac{2 \cos^3 \theta}{\cos(\theta - \phi_0)} f''(\xi) \tau$$

Substituting $\phi_0 = \pi$, $f''(\xi) = \frac{1}{2f}$, $\theta = -\alpha$ in the above relation yields

$$J_p(\tau) = \frac{D_p(\tau)}{D_p(0)} = 1 - \frac{\cos^2 \alpha}{f} \tau \quad (3.1.21)$$

Now consider the field after reflection from the hyperbolic cylinder, the Jacobian of transformation from ray co-ordinates (ξ_1, τ) to cartesian co-ordinates (x, y) is given by [Appendix B]

$$\begin{aligned} D(\tau) &= \frac{\partial(x, z)}{\partial(\xi_1, \tau)} = \begin{vmatrix} \frac{\partial \xi_2}{\partial \xi_1} + \frac{\partial p_{x2}}{\partial \xi_1} \tau & \frac{\partial \zeta_2}{\partial \xi_1} + \frac{\partial p_{z2}}{\partial \xi_1} \tau \\ p_{x2} & p_{z2} \end{vmatrix} \\ &= 2 \frac{\partial(\alpha - \psi)}{\partial \xi_1} \tau - \frac{\cos(2\alpha - \psi)}{\cos \psi} \frac{\partial \xi_2}{\partial \xi_1} \end{aligned} \quad (3.1.22)$$

where relation being used is $\frac{\partial \zeta_2}{\partial \xi_1} = \frac{\partial \zeta_2}{\partial \xi_2} \frac{\partial \xi_2}{\partial \xi_1} = \tan \psi \frac{\partial \xi_2}{\partial \xi_1}$. And

$$\frac{\partial \xi_2}{\partial \xi_1} = \frac{\cos \psi}{\cos(2\alpha - \psi)} \left[1 - \frac{\zeta_2 - \zeta_1}{f} \frac{\cos^2 \alpha}{\cos 2\alpha} \right] = \frac{\cos \psi}{\cos(2\alpha - \psi)} \frac{R_2 \cos^2 \alpha}{f}$$

Furthermore,

$$\frac{\partial \alpha}{\partial \xi_1} = \frac{1}{2f} \cos^2 \alpha, \quad \frac{\partial \psi}{\partial \xi_1} = \frac{\partial \psi}{\partial \xi_2} \frac{\partial \xi_2}{\partial \xi_1} = \cos^2 \psi \frac{a^4}{b^2 \zeta_2^3} \frac{1}{\partial \xi_1} \frac{\partial \xi_2}{\partial \xi_1}$$

Therefore

$$D(\tau) = \frac{\cos^2 \alpha}{f} \left\{ \left[1 - \frac{2 \cos^3 \psi}{\cos(2\alpha - \psi)} \frac{a^4}{b^2 \zeta_2^3} R_2 \right] \tau - R_2 \right\} \quad (3.1.23)$$

As

$$\begin{aligned} \cos(2\alpha - \psi) &= \frac{c - \zeta_2}{R_2} \cos \psi + \frac{\xi_2}{R_2} \sin \psi \\ &= \frac{1}{R_2 \sqrt{R_1 R_2}} \frac{b}{a} (c\zeta_2 - a^2) = \frac{b}{\sqrt{R_1 R_2}} \end{aligned}$$

Also

$$1 - \frac{2 \cos^3 \psi}{\cos(2\alpha - \psi)} \frac{a^4}{b^2 \zeta_2^3} R_2 = 1 - \frac{2abR_2}{(R_1 R_2)^{\frac{3}{2}}} \frac{aR_2 \sqrt{R_1 R_2}}{b(c\zeta_2 - a^2)} = 1 - \frac{2a}{R_1} = \frac{R_2}{R_1}$$

So that

$$D(\tau) = \frac{\cos^2 \alpha}{f} R_2 \left[1 - \frac{\tau}{R_1} \right] \quad (3.1.24)$$

Therefore the normalized Jacobian of the field reflected from hyperbolic reflector of Cassegrain system becomes

$$J(\tau) = \frac{D(\tau)}{D(0)} = 1 - \frac{\tau}{R_1} \quad (3.1.25)$$

Substituting (3.1.25) in (3.1.20) will produce the GO field expression for Cassegrain system

$$E^r = E_0^r(\xi_2, \zeta_2) \left[1 - \frac{\tau}{R_1} \right]^{-\frac{1}{2}} \exp \left[-jk(S_0 + \tau_1 + \tau) \right] \quad (3.1.26)$$

with

$$S_0 = -\zeta_1 = 2f \frac{\cos 2\alpha}{1 + \cos 2\alpha} - c$$

It is readily seen that the value of the field given by GO field expression becomes infinite at feed point F_2 when $\tau = R_1$ so that $J(\tau) = 0$ as expected. Thus in order to overcome the problem of singularity at caustic, Maslov's method is used to derive field expression that remains valid in the neighborhood of caustic and gives finite field value.

3.2. Derivation of Field near Caustic

The refined field expression may be derived using the field expression (1.2.16) based on Maslov's method and is given by

$$E_{(x,y)}^r(\mathbf{r}) = \sqrt{\frac{k}{j2\pi}} \int_{-\infty}^{\infty} E_0^r(\xi_2, \zeta_2) \left[\frac{D(\tau)}{D(0)} \frac{\partial p_{z2}}{\partial z} \right]^{-\frac{1}{2}} \times \exp \left\{ -jk \left[S_0 + \tau + \tau_1 - z(x, p_z)p_{z2} + p_{z2}z \right] \right\} dp_{z2} \quad (3.2.1)$$

In order to solve above integral, it is required to determine amplitude and phase of the field in the caustic region.

(i) Evaluation of Field Amplitude

The integrand of (3.2.1) gives the amplitude of the reflected field as

$$\begin{aligned} E^r(x, z) &= E_0^r(\xi_2, \zeta_2) \left[\frac{D(\tau)}{D(0)} \frac{\partial p_{z2}^r}{\partial z} \right]^{-\frac{1}{2}} \\ &= E_0^r(\xi_2, \zeta_2) \left[J(\tau) \frac{\partial p_{z2}^r}{\partial z} \right]^{-\frac{1}{2}} \end{aligned} \quad (3.2.2)$$

The value of $\left[J(\tau) \frac{\partial p_{z2}}{\partial z} \right]^{-\frac{1}{2}}$ has been evaluated below, for detailed work [Appendix C].

As,

$$\begin{aligned} z &= \zeta_2 + \frac{p_{z2}}{p_{x2}}(x - \xi_2) = \zeta_2 + \cot(2\alpha - 2\psi)(x - \xi_2) \\ p_{z2}^r &= -\cos(2\alpha - 2\psi) \end{aligned}$$

so that

$$\begin{aligned} \frac{\partial z}{\partial \xi_2} &= \frac{1}{\sin(2\alpha - 2\psi)} \frac{\partial \xi_1}{\partial \xi_2} \left[2\tau \frac{\partial(\alpha - \psi)}{\partial \xi_1} - \frac{\cos(2\alpha - \psi)}{\cos \psi} \frac{\partial \xi_2}{\partial \xi_1} \right] \\ \frac{\partial p_{z2}}{\partial \xi_2} &= 2 \sin(2\alpha - 2\psi) \frac{\partial(\alpha - \psi)}{\partial \xi_2} \\ &= 2 \sin(2\alpha - 2\psi) \frac{\partial \xi_1}{\partial \xi_2} \frac{\partial(\alpha - \psi)}{\partial \xi_1} \end{aligned}$$

$$\begin{aligned} \frac{\partial p_{z2}}{\partial z} &= \frac{\partial \xi_2}{\partial z} \frac{\partial p_{z2}}{\partial \xi_2} = 2 \sin(2\alpha - 2\psi) \frac{\partial \xi_1}{\partial \xi_2} \frac{\partial(\alpha - \psi)}{\partial \xi_1} \sin(2\alpha - 2\psi) \frac{\partial \xi_2}{\partial \xi_1} \\ &\times \left[2\tau \frac{\partial(\alpha - \psi)}{\partial \xi_1} - \frac{\cos(2\alpha - \psi)}{\cos \psi} \frac{\partial \xi_2}{\partial \xi_1} \right]^{-1} \quad (3.2.3) \\ \frac{D(\tau)}{D(0)} \frac{\partial p_{z2}}{\partial z} &= \left[2\tau \frac{\partial(\alpha - \psi)}{\partial \xi_1} - \frac{\cos(2\alpha - \psi)}{\cos \psi} \frac{\partial \xi_2}{\partial \xi_1} \right] \left[\frac{\cos \psi}{\cos(2\alpha - \psi)} \frac{\partial \xi_2}{\partial \xi_2} \right] \frac{\partial p_{z2}}{\partial z} \end{aligned}$$

Finally it gives

$$\frac{D(\tau)}{D(0)} \frac{\partial p_{z2}}{\partial z} = \frac{\sin^2(2\alpha - 2\psi)}{R_1} \quad (3.2.4)$$

$$\left[J(\tau) \frac{\partial p_z}{\partial z} \right]^{-\frac{1}{2}} = \frac{\sqrt{R_1}}{\sin(2\alpha - 2\psi)} \quad (3.2.5)$$

Substituting (3.2.5) in (3.2.2) yields

$$E^r(x, z) = E_0^r(\xi_2, \zeta_2) \frac{\sqrt{R_1}}{\sin(2\alpha - 2\psi)} \quad (3.2.6)$$

which is field amplitude between sub-reflector and the feed point F_2 of Cassegrain microwave antenna.

(ii) Evaluation of Phase Function

The phase function of the field in Caustic region is contained in (3.2.1) and is given by

$$\begin{aligned} S &= S_0 + \tau_1 + \tau - z(x, p_{z2}) p_{z2}^r + z p_{z2}^r \\ S &= S_0 + \tau_1 + S_{ext} \quad (3.2.7) \end{aligned}$$

where S_0 and τ_1 have been defined in equations (3.1.20) and (3.1.6) respectively. The extra phase term S_{ext} is given by

$$\begin{aligned} S_{ext} &= \tau - z(x, p_{z2}) p_{z2}^r + z p_{z2}^r \\ &= \tau - [\zeta_2 + p_{z2} \tau] p_{z2}^r + z p_{z2}^r \\ &= (1 - [p_{z2}^r]^2) \tau + (z - \zeta_2) p_{z2}^r \\ &= [p_{x2}^r]^2 \tau + (z - \zeta_2) p_{z2}^r \\ &= p_{x2}^r (x - \xi_2) + p_{z2}^r (z - \zeta_2) \quad (3.2.8) \end{aligned}$$

Now expressing cartesian coordinates x and z in terms of polar coordinates to obtain the field near caustic, $x = \rho \sin \phi$ and $z = \rho \cos \phi$. Now substituting these values and (3.1.17) in (3.2.8) gives

$$S_{ext} = -\rho \cos(2\alpha - 2\psi - \phi) + \left[\sin(2\alpha - 2\psi)\xi_2 + \cos(2\alpha - 2\psi)\zeta_2 \right] \quad (3.2.9)$$

where

$$\begin{aligned} \xi_2 &= \frac{b^2 \sin \psi}{\sqrt{a^2 \cos^2 \psi + b^2 \sin^2 \psi}} \\ \zeta_2 &= \frac{a^2 \cos \psi}{\sqrt{a^2 \cos^2 \psi + b^2 \sin^2 \psi}} \\ \rho &= \sqrt{x^2 + z^2} \end{aligned}$$

Also from (3.1.17)

$$dp_{z_2}^r = \sin(2\alpha - 2\psi)d(2\alpha)$$

Thus substituting (3.2.5) (3.2.7),(3.2.9) and the value of $dp_{z_2}^r$ in (3.2.1) produces

$$E^r(x, z) = \sqrt{\frac{k}{j2\pi}} \left[\int_{A_1}^{A_2} + \int_{-A_2}^{-A_1} \right] \sqrt{R_1} \exp \left[-jk(S_0 + \tau_1 + S_{ext}) \right] d(2\alpha) \quad (3.2.10)$$

In the above field expression, R_1 , S_0 , τ_1 , and S_{ext} have been expressed in terms of α . Further in (3.2.10), A_1 and A_2 are the subtention angles equal to ϕ_ν and ϕ_r at the edges of the parabolic and hyperbolic cylinders respectively as shown in Fig. 3.2. It may be noted here that limits of the integrals in equation (3.2.10) are selected using the following relations [Appendix D]

$$\begin{aligned} A_1 &= \phi_\nu = 2 \arctan \left(\frac{D}{2f} \right) \\ A_2 &= \phi_r = 2 \arctan \left(\frac{D}{2f_e} \right) \end{aligned}$$

where D and d are the heights of the edge of the parabolic and hyperbolic cylinders respectively from horizontal axis.

3.2.1. Results and Discussion

The field expression (3.2.10) obtained using Maslov's method is valid around caustic region. So that it could be used to determine field patterns around feed point of Cassegrain dual reflector system. Mathematica software has been used to find the solutions of (3.2.10) by performing numerical computations. The solutions obtained thereby are plotted along x -axis and z -axis to give pictorial view of field distribution around caustic region. The field patterns around the caustic region of Cassegrain dual reflector system and its equivalent parabolic cylinder are obtained using Maslov's method (solid line) and Huygens-Kirchhoff's integral (dashed line) respectively. The field patterns are determined for three set of parameters of Cassegrain system in order to study the field behavior around caustic region.

Fig. 3.3. provides comparison of two field patterns both along (a) x -axis and (b) z -axis around the focal region of Cassegrain system (solid line) and its equivalent parabola (dotted line). The comparison results of field patterns are found in close agreement. It is observed that the field spread region around the feed point is "small" as compared to other two cases. The above analysis is carried out for Cassegrain dual reflector system having dimensional parameters as $kf = 55$, $ka = 6.2$, $kb = 6.8$, $kd = 6$, $kD = 90$ and $kf_e = 282.2$

In Fig. 3.4., the results of Cassegrain dual reflector system obtained by Maslov's method (solid line), along (a) x -axis and (b) z -axis, are compared with the results of its equivalent parabola (dotted line) obtained using Huygens-Kirchhoff's integral respectively. The agreement of comparison results is fairly good. It is observed that the field spread region around the feed point is "medium" as compared to other two cases. The above analysis is carried out for Cassegrain dual reflector system having dimensional parameters as $kf = 65$, $ka = 6.2$, $kb = 6.8$, $kd = 6$, $kD = 70$ and $kf_e = 333.5$

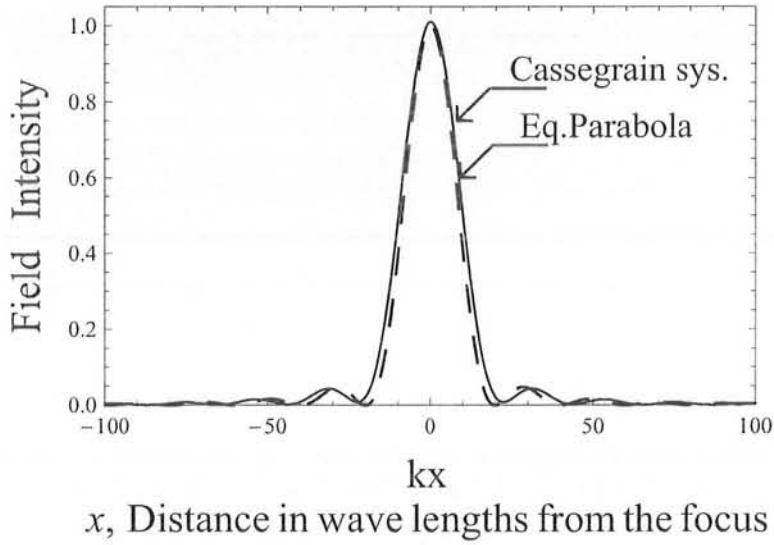
Fig. 3.5. again provides comparison of two field patterns both along (a) x -axis and (b) z -axis around the focal region of Cassegrain system (solid line) and its equivalent parabola (dotted line). The comparison results of field patterns are found in close agreement. It is observed that the field spread region around the feed point is “large” as compared to other two cases. The above analysis is carried out for Cassegrain dual reflector system having dimensional parameters as $kf = 100$, $ka = 18.7$, $kb = 15$, $kd = 12$, $kD = 125$ and $kf_e = 809$

Fig. 3.3–3.5 show comparison of field plots around caustic region of Cassegrain system and its equivalent parabola, the field is obtained using both Maslov’s method and Huygens-Kirchhoff’s integral respectively. The slight difference in field space regions by two methods appears due to consideration of equivalent parabola of Cassegrain system.

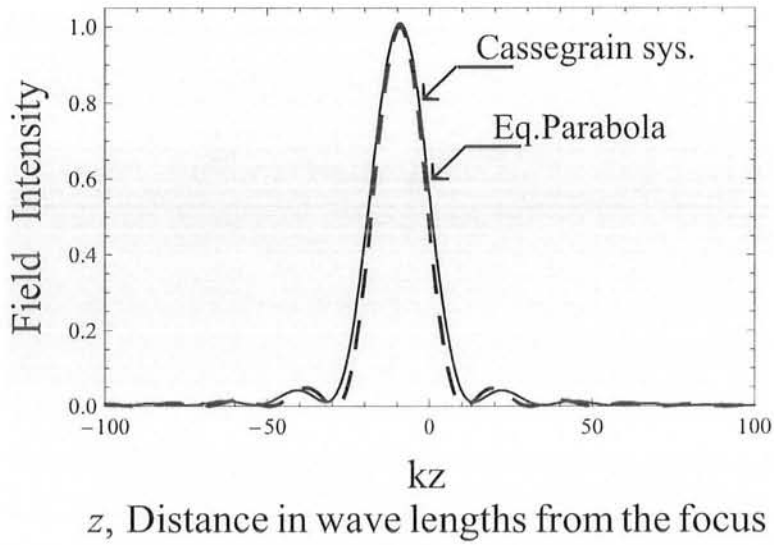
The field behavior in terms of field space variation around the feed point is studied. Fig. 3.6 contains the three field plots designated as image field-1, image field-2 and image field-3 and they correspond respectively to the following three set of parameters of Cassegrain system,

- (i) $kf = 55$, $ka = 6.2$, $kb = 6.8$, $kd = 6$, $kD = 90$ and $kf_e = 282.2$,
- (ii) $kf = 65$, $ka = 6.2$, $kb = 6.8$, $kd = 6$, $kD = 70$ and $kf_e = 333.5$,
- (iii) $kf = 100$, $ka = 18.7$, $kb = 15$, $kd = 12$, $kD = 125$ and $kf_e = 809$.

The variation of field spread region around feed point against the change in parameters of Cassegrain system, is observed. The knowledge of the size of field region around the feed point is useful in selecting the physical size of transmitter or receiver for electromagnetic waves.

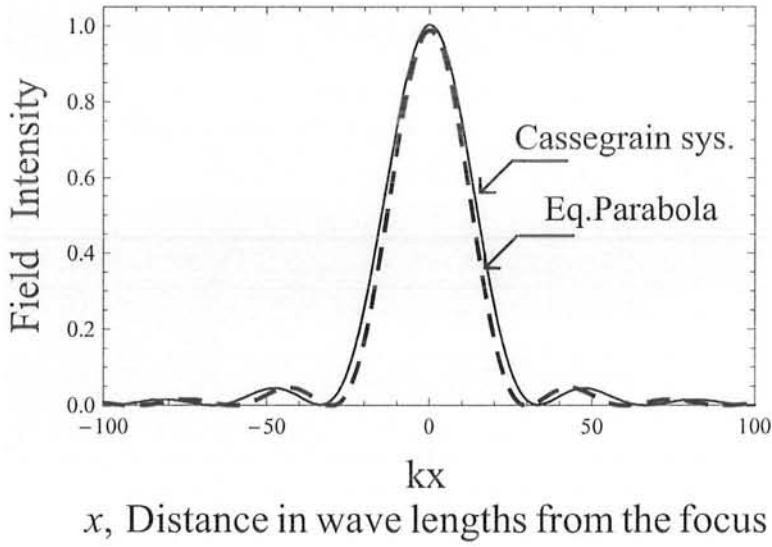


(a)

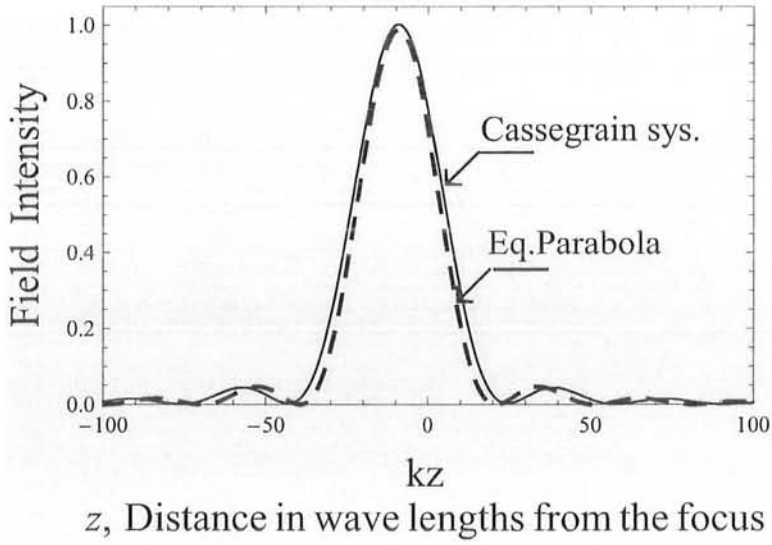


(b)

Fig. 3.3. Comparison of field intensity distribution around the caustic region of PEC Cassegrain dual reflector system along (a) x -axis and along (b) z -axis for normal incident plane wave using Maslov's method with that of system equivalent parabola using induced current method with $kf = 55$, $ka = 6.2$, $kb = 6.8$, $kd = 6$, $kD = 90$. and $kf_e = 282.2$

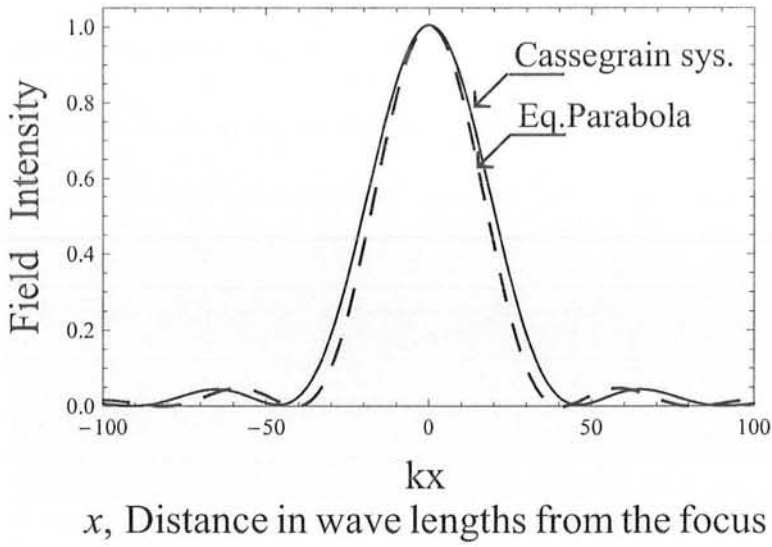


(a)

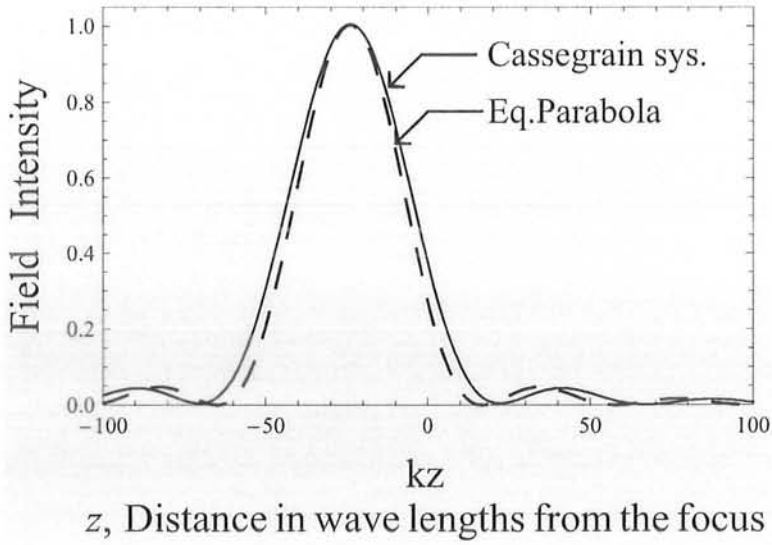


(b)

Fig. 3.4. Comparison of field intensity distribution around the caustic region of PEC Cassegrain dual reflector system along (a) x -axis and along (b) z -axis for normal incident plane wave using Maslov's method with that of system equivalent parabola using induced current method with $kf = 65$, $ka = 6.2$, $kb = 6.8$, $kd = 6$, $kD = 70$. and $kf_e = 333.5$



(a)



(b)

Fig. 3.5. Comparison of field intensity distribution around the caustic region of PEC Cassegrain dual reflector system along (a) x -axis and along (b) z -axis for normal incident plane wave using Maslov's method with that of system equivalent parabola using induced current method with $kf = 100$, $ka = 18.7$, $kb = 15$, $kd = 12$, $kD = 125$. and $kf_e = 809$

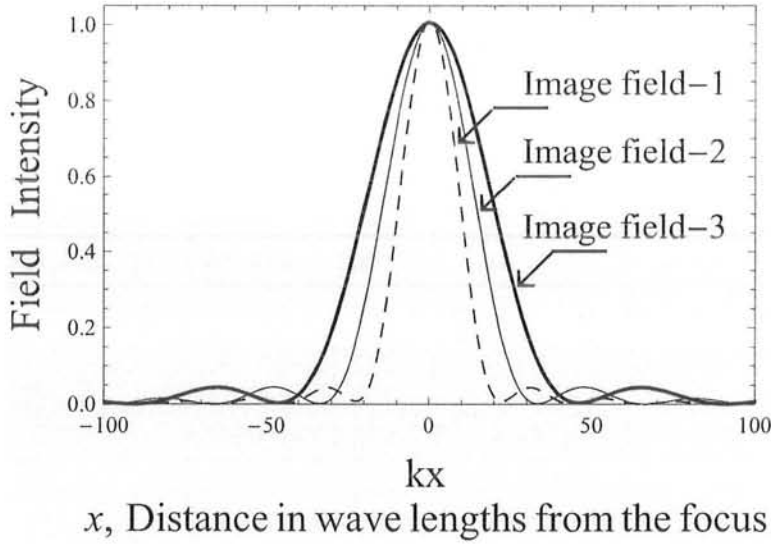


Fig. 3.6. Comparison of image field spread region around caustic of Cassegrain dual reflector system by considering three different set of parameters of focussing system.

3.3. Gregorian Dual Reflector System

The configuration of Gregorian dual reflector system is shown in Fig. 3.7. It consists of two cylindrical reflectors, a parabolic main-reflector and another elliptical sub-reflector both are considered to be perfect electric conductor. The focal point F_2 of the sub-reflector coincides with the focal point of parabolic reflector. The field investigation of the dual reflector antenna is carried out from the receiving point of view. The derivation of high frequency field expression for Gregorian system is based on Maslov's method.

Gregorian dual reflector antenna can be replaced with a single equivalent parabolic reflector as shown in Fig. 3.8. The equivalent parabolic reflector has the same aperture as that of main-reflector of Gregorian system $D_{eq} = D$, but its focal length is much longer than that of the main-reflector. The focal length of equivalent parabola is determined using the following relation [Appendix D]

$$f_e = - \left(\frac{c+a}{c-a} \right) f$$

Here $(c + a)/(c - a)$ is called image field magnification. The increased focal length has various advantages in terms of its performance i.e., less cross polarization, improved aperture efficiency etc.

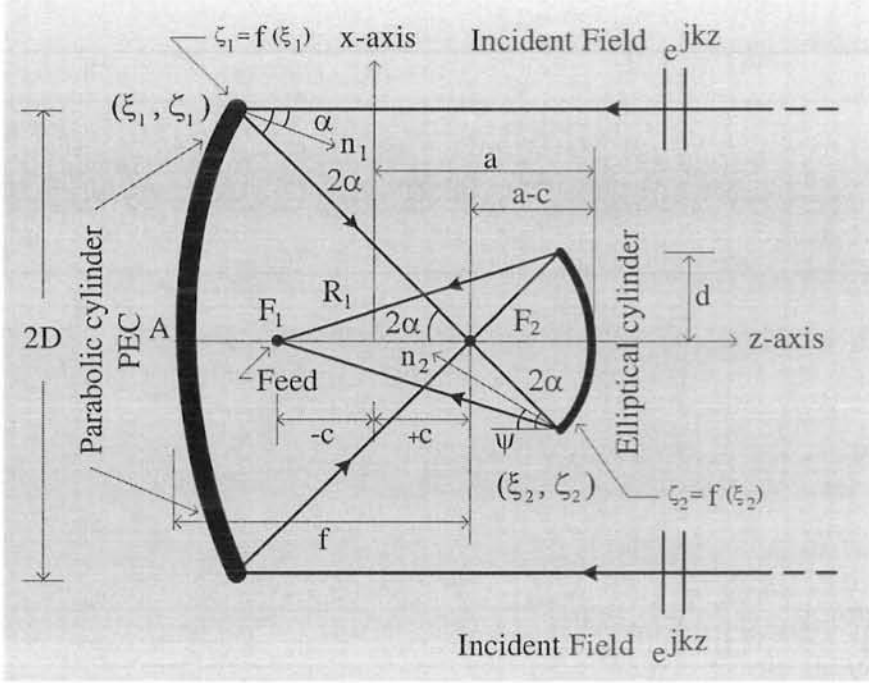


Fig. 3.7. A schematic diagram showing PEC cylindrical dual reflector Gregorian system being excited by a normal incident plane wave field .

3.3.1. GO Field Expression

The equation describing the surface contour of main-reflector is given by (3.1.1) and for elliptical sub-reflector may be given as

$$f(\xi_2) = \zeta_2 = a \left[\frac{\xi_2^2}{b^2} - 1 \right]^{\frac{1}{2}} \quad (3.3.1)$$

$$c^2 = a^2 - b^2 \quad (3.3.2)$$

where (ξ_2, ζ_2) are the cartesian coordinates of a point on the surface of sub-reflector. In Fig. 3.7., f is the focal distance of the main-reflector, D and d are the half apertures

of the main and sub-reflector respectively. Let \mathbf{n}_1 and \mathbf{n}_2 be the unit normals at points (ξ_1, ζ_1) and (ξ_2, ζ_2) on the surface of main-reflector and sub-reflector respectively. The unit vector \mathbf{n}_1 is completely defined by (3.1.9) and (3.1.12), whereas \mathbf{n}_2 may be given by [Appendix E]

$$\mathbf{n}_2 = -\sin \psi \mathbf{i}_x + \cos \psi \mathbf{i}_z \quad (3.3.3)$$

where

$$\sin \psi = -\frac{1}{\sqrt{R_1 R_2}} \frac{a}{b} \xi_2, \quad \cos \psi = \frac{1}{\sqrt{R_1 R_2}} \frac{b}{a} \zeta_2 \quad (3.3.4)$$

and R_1 and R_2 are defined by (3.1.7) and (3.1.8) respectively.

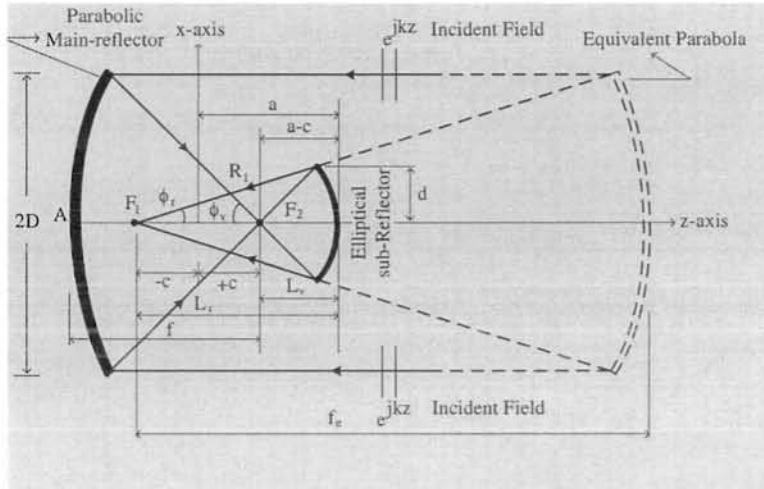


Fig. 3.8. Parameters in PEC dual reflector Gregorian system.

Suppose the main-reflector is excited by a linearly polarized plane wave which is defined by equation (3.1.14) and corresponding wave vector is given by (2.1.3) with $\phi_0 = \pi$. The wave vector of the field reflected by main-reflector is given by equation (3.1.16) and that reflected by the sub-reflector may be given by

$$\mathbf{p}_2^r = -\sin(2\alpha - 2\psi) \mathbf{i}_x - \cos(2\alpha - 2\psi) \mathbf{i}_z \quad (3.3.5)$$

with the condition $\psi > \alpha$. It may be noted that the condition $\psi > \alpha$ comes from the physical picture of the system for which the above relation has been established. The

Jacobian associated with the wave reflected by parabolic cylindrical reflector is given in (3.1.21). Now considering the field after reflection from sub-reflector, GO field of the Gregorian system may be given using (1.1.24) as

$$E^r(x, z) = E_0^r(\xi_2, \zeta_2) \left[\frac{D(\tau)}{D(0)} \right]^{-\frac{1}{2}} \exp \left[-jk(S_0 + \tau_1 + \tau) \right] \quad (3.3.6)$$

The phase function S_0 , τ_1 and τ are given by (3.1.20), (3.1.6) and (3.1.5) respectively. The Jacobian of transformation from the ray co-ordinates (ξ_1, τ) to the space co-ordinates (x, z) of the field is given

$$\begin{aligned} J(\tau) &= \frac{D(\tau)}{D(0)} = \frac{1}{D(0)} \frac{\partial}{\partial(\xi_1, \tau)} \\ &= \frac{1}{D(0)} \begin{vmatrix} \frac{\partial \xi_2}{\partial \xi_1} + \frac{\partial p_{x2}}{\partial \xi_1} \tau & \frac{\partial \zeta_2}{\partial \xi_1} + \frac{\partial p_{z2}}{\partial \xi_1} \tau \\ p_{x2} & p_{z2} \end{vmatrix} \\ &= \frac{1}{D(0)} \left[2 \frac{\partial(\alpha - \psi)}{\partial \xi_1} \tau - \frac{\cos(2\alpha - \psi)}{\cos \psi} \frac{\partial \zeta_2}{\partial \xi_1} \right] \\ &= 1 - \frac{\tau}{R_1} \end{aligned} \quad (3.3.7)$$

Around caustic region $\tau = R_1$ and hence $J(\tau) = 0$, GO field expression (3.3.6), gives infinite field. Therefore the G.O field expression fails to quantify the field around caustic region. In order to determine finite field value $E^r(x, z)$ at caustic, field expression based on Maslov's method is derived.

3.3.2. Field Determination Around Caustics

According to the Maslov's method, the field expression which is valid around caustic may be derived using (1.2.12) as

$$\begin{aligned} E^r(x, z) &= \sqrt{\frac{k}{j2\pi}} \int_{-\infty}^{\infty} A_0(\xi) \left[\frac{D(\tau)}{D(0)} \frac{\partial p_z}{\partial z} \right]^{-\frac{1}{2}} \\ &\quad \times \exp \left\{ -jk \left[S_0 + \tau_1 + \tau - z(x, p_{z2}) p_{z2} + p_{z2} \right] \right\} dp_z \end{aligned} \quad (3.3.8)$$

where S_0 , τ_1 and τ have been defined in equation (3.1.20), (3.1.6), (3.1.5) respectively. The amplitude term $\left[\frac{D(\tau)}{D(0)} \frac{\partial p_z}{\partial z} \right]^{-\frac{1}{2}}$ in field expression (3.3.8) has been evaluated in

[Appendix C] as

$$\left[\frac{D(\tau)}{D(0)} \frac{\partial p_z}{\partial z} \right]^{-\frac{1}{2}} = \frac{\sqrt{R_1}}{\sin(2\psi - 2\alpha)} \quad (3.3.9)$$

The phase function is given by

$$\begin{aligned} S &= S_0 + \tau_1 + \tau - z(x, p_{z_2})p_{z_2} + p_{z_2}^r z \\ &= S_0 + \tau_1 + S_{ex} \end{aligned} \quad (3.3.10)$$

where S_0 and τ_1 are determined from equations (3.1.20) and (3.1.6) respectively.

The extra term of the phase function is given by

$$\begin{aligned} S_{ex} &= \tau - z(x, p_{z_2}^r)p_{z_2}^r + p_{z_2}^r z \\ &= \tau - (\zeta_2 + p_{z_2}^r \tau)p_{z_2}^r + p_{z_2}^r z \\ &= \tau(1 - p_{z_2}^{2r}) + (z - \zeta_2)p_{z_2}^r \\ &= p_{x_2}^r(x - \xi_2) + p_{z_2}^r(z - \zeta_2) \end{aligned} \quad (3.3.11)$$

On substituting $x = \rho \sin \phi$ and $z = \rho \cos \phi$, using (3.3.5) and $p_z = -\cos(2\psi - 2\alpha)$ in the above extra phase relation, one obtains

$$S_{ex} = -\rho \cos(2\psi - 2\alpha + \phi) + \xi_2 \sin(2\psi - 2\alpha) - \zeta_2 \cos(2\psi - 2\alpha) \quad (3.3.12)$$

where

$$\xi_2 = b \sqrt{1 - \frac{\cos^2 \psi}{\cos^2(\psi - 2\alpha)}}, \quad \zeta_2 = \frac{a \cos \psi}{\cos(\psi - 2\alpha)}, \quad \rho = \sqrt{x^2 + z^2}$$

Substituting (3.3.9), (3.3.10) and $dp_z = \sin(2\psi - 2\alpha)d(2\alpha)$ in (3.3.8) yields

$$E^r(x, z) = \sqrt{\frac{k}{j2\pi}} \left[\int_{A_1}^{A_2} + \int_{-A_1}^{-A_2} \right] \sqrt{R_1} \exp[-jk(S_0 + \tau_1 + S_{ex})] d(2\alpha) \quad (3.3.13)$$

where R_1 , S_0 , τ_1 and S_{ex} in above equation have been expressed in terms of α . Moreover A_1 and A_2 are the subtention angles equal to ϕ_ν and ϕ_r at the edges of the parabolic and elliptical cylinders respectively as shown in Fig. 3.8. It may be noted

here that limits of the integrals in equation (3.3.13) are selected using the following relations [Appendix D]

$$A_1 = \phi_\nu = 2 \arctan \left(\frac{D}{2f} \right)$$

$$A_2 = \phi_r = 2 \arctan \left(\frac{D}{2f_e} \right)$$

where D and d are the heights of the edge of the parabolic and elliptical cylinders respectively from the horizontal axis.

3.4. Results and Discussion

The field patterns around the caustic of dual reflector Gregorian system are obtained by solving (3.3.13) through numerical computations. Note that the focal region is located between the two cylindrical reflectors, that is point F_1 as shown in Fig. 3.7. The field patterns are determined for three set of parameters of Gregorian system in order to study the field behavior around caustic region. The location of the caustic may be observed and verified easily. The results of field distribution around caustic of Gregorian dual reflector system obtained using Maslov's method are compared with the results of its equivalent parabola obtained using Huygens-Kirchhoff's principle. Fig. 3.9. contains comparison plots of field distribution around the caustic region of a Gregorian system (solid line) and an equivalent parabolic reflector (dotted line) both along x -axis and z -axis. The comparison results are found in close agreement thereby reaffirming the validity of Maslov's method when it is applied to Gregorian dual reflector system. It is also observed that the field spread region around the feed point is "small" as compared to the other two cases considered for the study. The above analysis is carried out for Gregorian dual reflector system having dimensional parameters as $kf = 55$, $ka = 14$, $kb = 12.1$, $kd = 10$, $kD = 80$ and $kf_e = 168.4$

In Fig. 3.10., the results of Gregorian dual reflector system obtained by Maslov's method (solid line), along (a) x -axis and (b) z -axis, are compared with the results of its

equivalent parabola (dotted line) obtained using induced current method respectively. The agreement of results of comparison is fairly good and it validates Maslov's method. It is also observed that the field spread region around the feed point is "medium" as compared to other two cases. The above analysis is based on the parameters chosen for Gregorian dual reflector system as $kf = 62.5$, $ka = 10$, $kb = 8.7$, $kd = 8.2$, $kD = 70$ and $kf_e = 191.5$

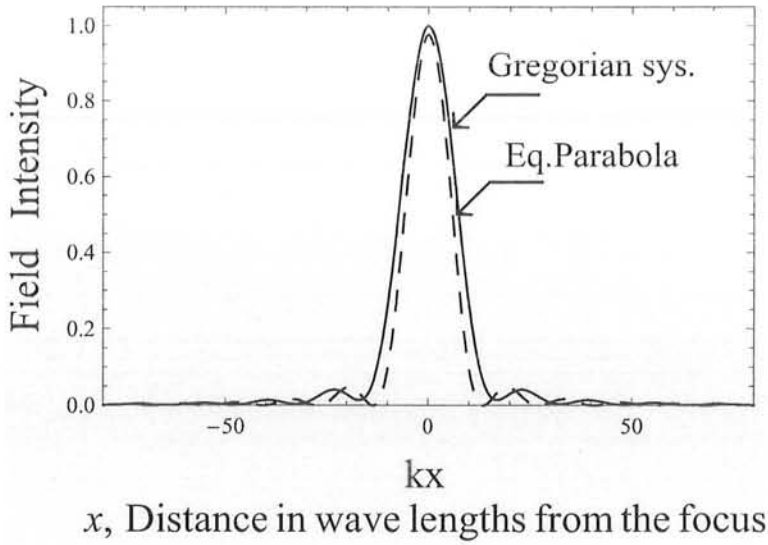
Fig. 3.11. again provides comparison of two field patterns both along (a) x -axis and (b) z -axis around the focal region of Gregorian system (solid line) and its equivalent parabola (dotted line). The comparison results of field patterns are found in close agreement, validating Maslov's method for Gregorian dual reflector system. It is also observed that the field spread region around the feed point is "large" as compared to other two cases. The above analysis is carried out by choosing parameters of Gregorian dual reflector system as $kf = 100$, $ka = 35$, $kb = 30$, $kd = 15$, $kD = 80$ and $kf_e = 3535$

The field behavior in terms of spread of field region around the feed point against change in system parameters is studied. Fig. 3.12. contains the four field plots designated as image field-1, image field-2, image field-3 and image field-4 and they correspond respectively to the following set of parameters of Gregorian system

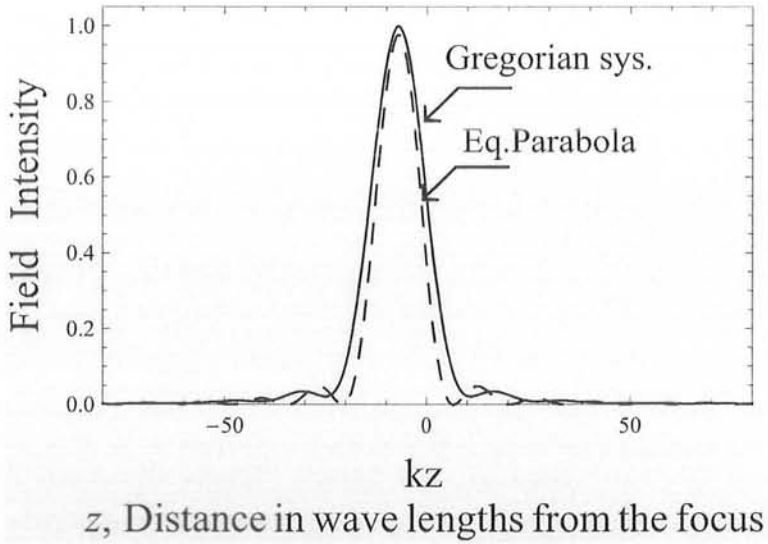
- (i) $kf = 55$, $ka = 14$, $kb = 12.1$, $kd = 10$, $kD = 80$ and $kf_e = 168.4$,
- (ii) $kf = 62.5$, $ka = 10$, $kb = 8.7$, $kd = 8.2$, $kD = 70$ and $kf_e = 191.5$,
- (iii) $kf = 100$, $ka = 35$, $kb = 30$, $kd = 15$, $kD = 80$ and $kf_e = 3535$,
- (iv) $kf = 100$, $ka = 45$, $kb = 30$, $kd = 40$, $kD = 150$ and $kf_e = 353.5$

The variation of field region around feed point in response to change in parameters of Gregorian system, is observed so as to know the size of region occupied by the field.

The knowledge of the size of field region around the feed point is useful to fix physical size of transmitter or receiver for electromagnetic waves.

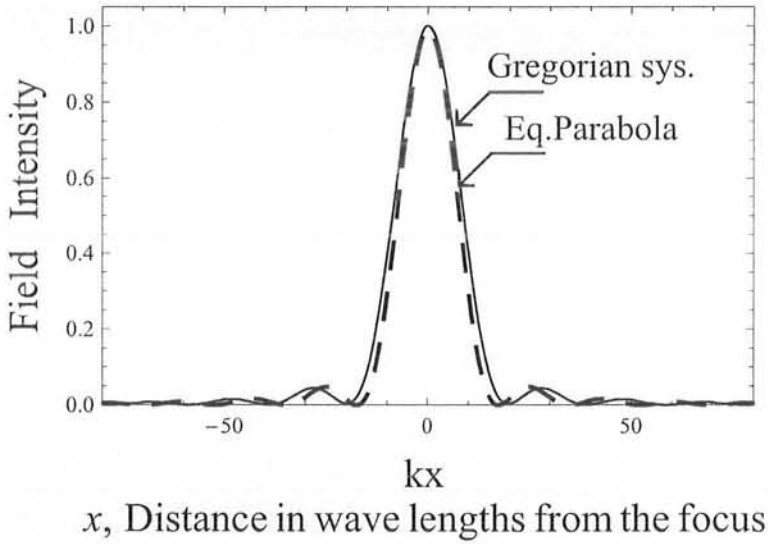


(a)

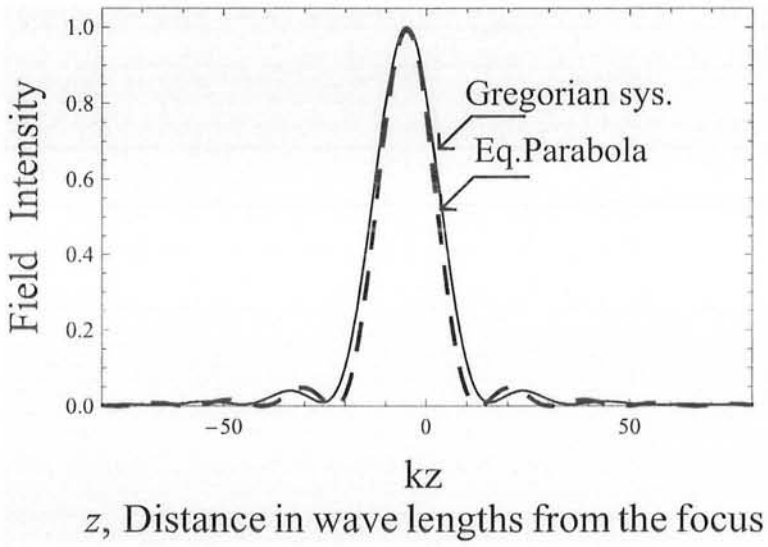


(b)

Fig. 3.9. Comparison of field distribution around the caustic region of PEC Gregorian dual reflector system using Maslov's method along (a) x -axis and along (b) z -axis with that of equivalent parabola using induced current method with parameters $kf = 55$, $ka = 14$, $kb = 12$, $kd = 10$, $kD = 80$ and $kf_e = 168.4$

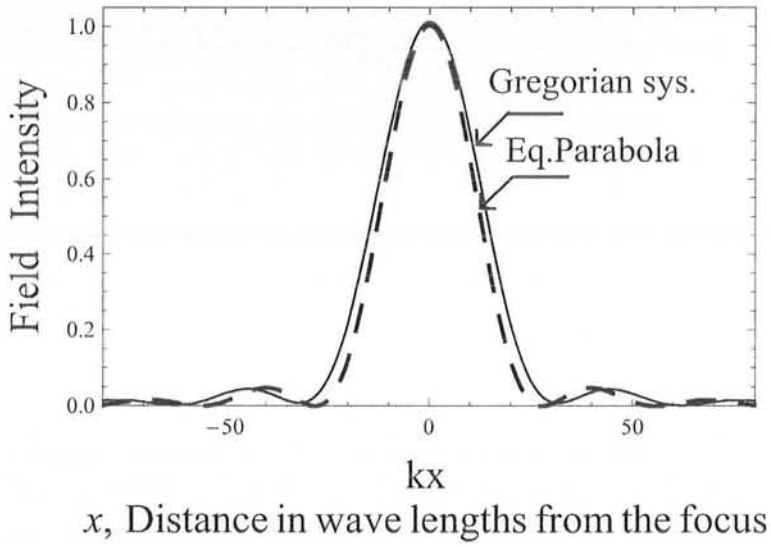


(a)

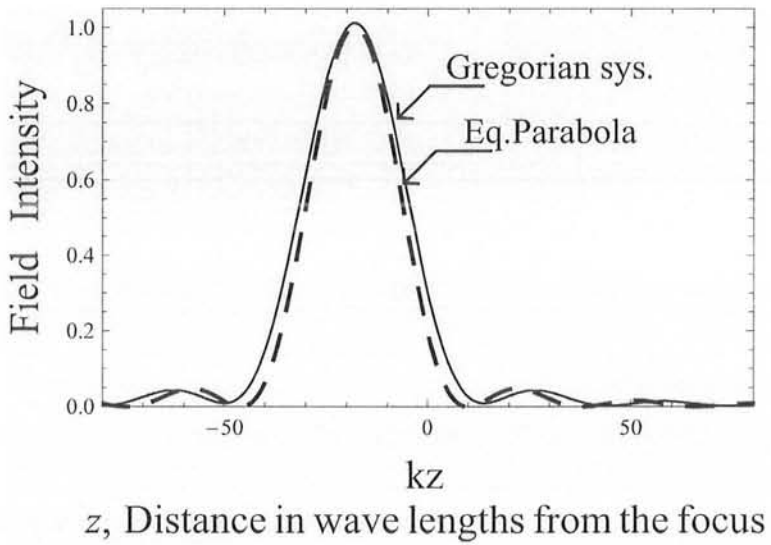


(b)

Fig. 3.10. Comparison of field distribution around the caustic region of PEC Gregorian dual reflector system using Maslov's method along (a) x -axis and (b) z -axis for normal incident plane wave, with that of equivalent parabola using induced current method with parameters $kf = 62.5$, $ka = 10$, $kb = 8.7$, $kd = 8.2$, $kD = 70$ and $kf_e = 191.5$



(a)



(b)

Fig. 3.11. Comparison of field distribution around the caustic region of PEC Gregorian dual reflector system using Maslov's method along (a) x -axis and (b) z -axis for normal incident plane wave, with that of its equivalent parabola using induced current method with $kf = 100$, $ka = 35$, $kb = 30$, $kd = 15$, $kD = 8$ and $kf_e = 353.5$

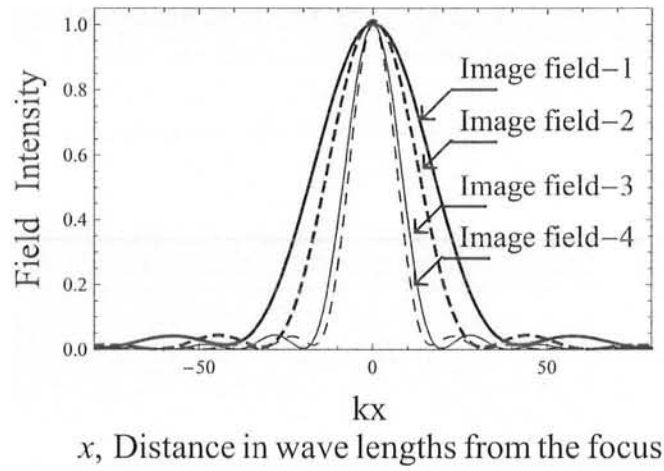


Fig. 3.12. Comparison of image field spread around caustic of Gregorian dual reflector system for normal incident plane wave, by selecting four set of parameters of focussing system.

Chapter 4

The PEMC Dual Reflector Systems

The Chapter is divided into two parts. The first part deals with the study of field pattern around focal region of PEMC Gregorian and Cassegrain microwave antennas, while the second part is concerned with PEMC backed chiral nihility Gregorian and Cassegrain systems.

4.1. Plane Wave Reflection from PEMC Plane Surface

Consider a linearly polarized plane wave obliquely incident on interface of PEMC plane surface as shown in Fig. 4.1. Let the field of incident wave be given by

$$\mathbf{E}_i = \mathbf{E}_{i0} \exp[-jk(x \sin \phi_0 + z \cos \phi_0)]$$

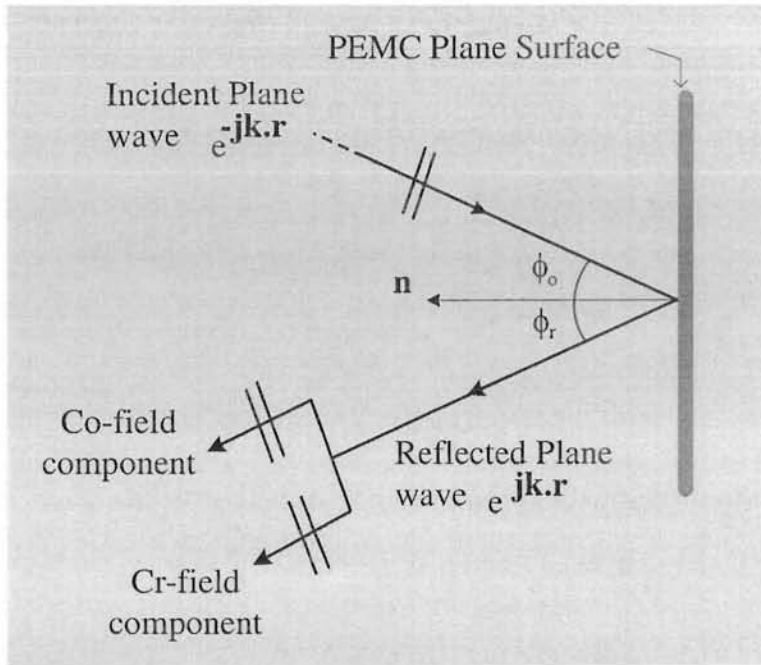


Fig. 4.1. A plane wave obliquely incident upon the interface of PEMC plane surface, creates both co and cr-filed components.

The wave vector associated with incident field is

$$\mathbf{p}_i = \sin \phi_0 \mathbf{u}_x + \cos \phi_0 \mathbf{u}_z$$

where ϕ_0 is the oblique incident angle on PEMC plane surface. The reflected field contains both electric and magnetic fields given by

$$\begin{aligned} \mathbf{E}_r &= \mathbf{E}_{r0} \exp[-jk(x \sin \phi_r + z \cos \phi_r)] \\ \mathbf{H}_r &= \frac{\cos \phi_0 \mathbf{u}_z \times \mathbf{E}_{r0}}{\eta} \exp[-jk(x \sin \phi_r + z \cos \phi_r)] \end{aligned}$$

where it is assumed that $\eta = \eta_0 = \sqrt{\frac{\mu_0}{\epsilon_0}}$. On substituting \mathbf{E} and \mathbf{H} in vector boundary condition [Appendix F], yields

$$M\eta(\mathbf{E}_{i0} + \mathbf{E}_{r0}) = -(\cos \phi_0 \mathbf{u}_z \times \mathbf{E}_{i0} - \cos \phi_0 \mathbf{u}_z \times \mathbf{E}_{r0}) \quad (4.1.1)$$

Taking the dot product with dyadic \tilde{I} of both sides and rearranging the terms, gives

$$(\cos \phi_0 \mathbf{u}_z \times \tilde{I} - M\eta\tilde{I}) \cdot \mathbf{E}_{r0} = (\cos \phi_0 \mathbf{u}_z \times \tilde{I} + M\eta\tilde{I}) \cdot \mathbf{E}_{i0} \quad (4.1.2)$$

where dyadic \tilde{I} is defined as

$$\tilde{I} = \mathbf{u}_x \mathbf{u}_x + \mathbf{u}_y \mathbf{u}_y$$

Solving (4.1.2), gives

$$\mathbf{E}_0^r(\xi, \zeta) = -\frac{(M^2\eta^2 - \cos^2 \phi_0)\mathbf{E}_{i0} + 2M\eta \cos \phi_0(\mathbf{u}_z \times \mathbf{E}_{i0})}{\cos^2 \phi_0 + M^2\eta^2} \quad (4.1.3)$$

which is the initial value of the field at the reflection point (ξ, ζ) on the PEMC reflector.

The initial value of the field on PEMC plane reflector, may also be obtained as

$$\mathbf{E}_0^r(\xi, \zeta) = \tilde{R} \cdot \mathbf{E}_{i0} \quad (4.1.4)$$

The reflection dyadic \tilde{R} is defined by

$$\tilde{R} = R_{co}\tilde{I} + R_{cr}\tilde{J} \quad (4.1.5)$$

where $\tilde{I} = \mathbf{u}_x \mathbf{u}_x + \mathbf{u}_y \mathbf{u}_y$ and $\tilde{J} = \mathbf{u}_z \times \tilde{I}$ where *co* means co-polarized and *cr* means cross-polarized components of the reflected field. Comparing (4.1.3) with (4.1.4) yields

$$\tilde{R} = -\frac{1}{\cos^2 \phi_0 + M^2 \eta^2} [(M^2 \eta^2 - \cos^2 \phi_0) \tilde{I} + 2M\eta \cos \phi_0 \tilde{J}] \quad (4.1.6)$$

$$R_{co} = -\frac{M^2 \eta^2 - \cos^2 \phi_0}{\cos^2 \phi_0 + M^2 \eta^2} \quad (4.1.7)$$

$$R_{cr} = -\frac{2M\eta \cos \phi_0}{\cos^2 \phi_0 + M^2 \eta^2} \quad (4.1.8)$$

The rotation angle ϕ_1 between co and cr-polarized field components caused as a result of field reflection from PEMC interface, is obtained below

$$\tan \phi_1 = \frac{R_{cr}}{R_{co}} = \frac{2M\eta \cos \phi_0}{M^2 \eta^2 - \cos^2 \phi_0} \quad (4.1.9)$$

The rotation angle ϕ_1 depends on the characteristics of both the surrounding medium and PEMC interface.

4.2. PEMC Gregorian Dual Reflector Antenna

Gregorian dual reflector system shown in Fig. 4.2., consists of two reflectors, one is PEMC parabolic main-reflector and another is PEC elliptical sub-reflector. The equations describing the surface contour of both main-reflector and sub-reflector are given by (3.1.1) and (3.3.1) respectively. The unit normals \mathbf{n}_1 and \mathbf{n}_2 on the surface of main-reflector and sub-reflector and are given by (3.1.7) and (3.3.3) respectively. Let the main-reflector of Gregorian dual reflector system be excited by a plane electromagnetic wave which is given by

$$\mathbf{E}^i = \mathbf{u}_y \exp(jkz) \quad (4.2.1)$$

The wave vector associated with incident field (4.2.1) is given by

$$\mathbf{p}^i = -\mathbf{i}_z$$

The wave vector of the field reflected by the PEMC main-reflector and that reflected by PEC sub-reflector are given by (3.1.16) and (3.3.5) respectively. The geometrical optics field expression for the Gregorian system consisting of PEMC parabolic and PEC elliptical cylinder may be obtained from (3.3.6) by including phase angle ϕ_1 in the phase term. The phase angle ϕ_1 is the rotation angle caused due to reflection from PEMC interface of main-reflector. The GO field expression becomes,

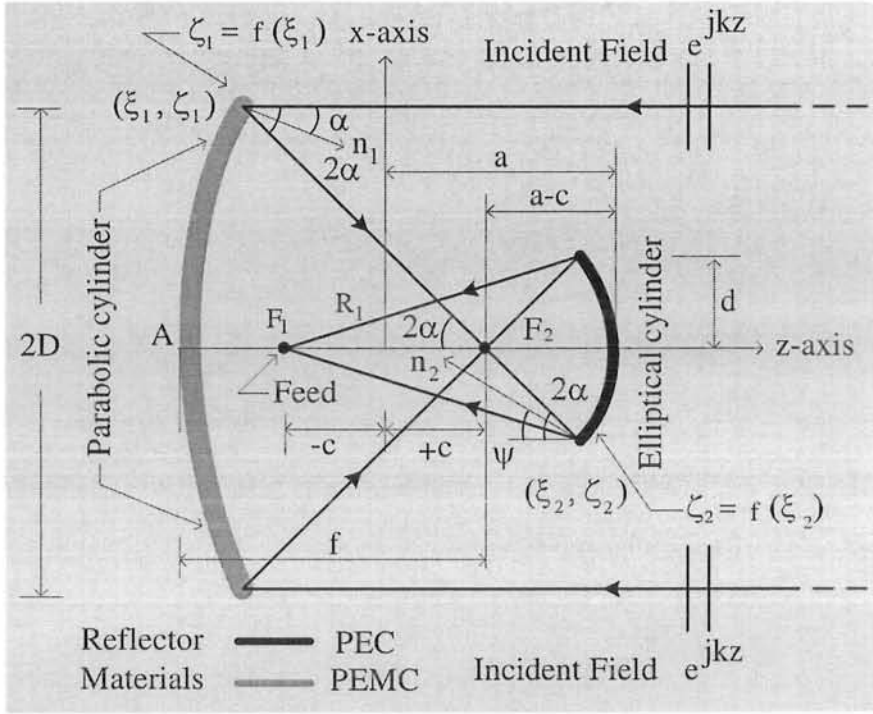


Fig. 4.2. A schematic diagram showing a PEMC Gregorian dual cylindrical reflector system being excited by a plane electromagnetic wave, the reflected field contains both co and cr -field components around Caustic region.

$$\mathbf{E}^r(x, z) = \mathbf{E}_0^r(\xi_2, \zeta_2) \left[\frac{D(\tau)}{D(0)} \right]^{\frac{-1}{2}} \exp[-jk(S_0 + \tau_1 + \tau) + \phi_1] \quad (4.2.2)$$

where phase function includes S_0 , τ_1 and τ given by (3.1.20), (3.1.6) and (3.1.5) respectively. The Jacobian of transformation associated with the wave after reflection from

sub-reflector is given by using the relation (3.3.7) so that equation (4.2.2) becomes

$$\mathbf{E}^r(x, z) = \mathbf{E}_0^r(\xi_2, \zeta_2) \left[1 - \frac{\tau}{R1}\right]^{\frac{-1}{2}} \exp[-jk(S_0 + \tau_1 + \tau) + \phi_1] \quad (4.2.3)$$

where

$$\tan \phi_1 = \frac{R_{cr}}{R_{co}}$$

4.2.1. Determination of Surface Field

In field expression (4.2.3), $\mathbf{E}_0^r(\xi_2, \zeta_2)$ is the amplitude of the field at the reflection point (ξ_2, ζ_2) on the sub-reflector. For normal incident field, the incident angle becomes $\phi_0 = \pi$, further let α be the angle made with z -axis by unit normal on the main-reflector as shown in Fig. 4.2. Now using the relations (4.1.3) and (4.1.6) through (4.1.9) one can obtain $\mathbf{E}_0^r(\xi_1, \zeta_1)$, \tilde{R} and its co and cr-polarized reflection coefficients R_{co} , R_{cr} and rotation angle ϕ_1 for PEMC main-reflector of Gregorian system as

$$\mathbf{E}_0^r(\xi_1, \zeta_1) = -\frac{(M^2\eta^2 - \cos^2 \alpha)\mathbf{E}_{io} - 2M\eta \cos \alpha(\mathbf{u}_z \times \mathbf{E}_{io})}{\cos^2 \alpha + M^2\eta^2} \quad (4.2.4)$$

$$\begin{aligned} \tilde{R} &= -\frac{(M^2\eta^2 - \cos^2 \alpha)\tilde{I} + 2M\eta \cos \alpha \tilde{J}}{\cos^2 \alpha - M^2\eta^2} \\ &= R_{co}\tilde{I} + R_{cr}\tilde{J} \end{aligned} \quad (4.2.5)$$

$$\begin{aligned} R_{co} &= -\frac{M^2\eta^2 - \cos^2 \alpha}{\cos^2 \alpha + M^2\eta^2} \\ R_{cr} &= \frac{2M\eta \cos \alpha}{\cos^2 \alpha + M^2\eta^2} \\ \tan \phi_1 &= \frac{R_{cr}}{R_{co}} = \frac{-2M\eta \cos \alpha}{M^2\eta^2 - \cos^2 \alpha} \end{aligned} \quad (4.2.6)$$

where $\mathbf{E}_0^r(\xi_1, \zeta_1)$, is the surface field of main-reflector and the field after reflection is fully intercepted by the sub-reflector. Therefore it is logical to assume that $\mathbf{E}_0^r(\xi_1, \zeta_1) = \mathbf{E}_0^r(\xi_2, \zeta_2)$, the surface field of the sub-reflector. Substituting(4.2.1) and (4.2.4) in (4.1.4), gives

$$\mathbf{E}_0^r(\xi_2, \zeta_2) = R_{co}\mathbf{u}_y - R_{cr}\mathbf{u}_x \quad (4.2.7)$$

where R_{co} and R_{cr} are given by (4.2.5). On substituting (4.2.7) in (4.2.3), it is readily seen that the amplitude of the field around caustic at $\tau = R_1$ where $J=0$, becomes infinite. In order to determine finite field value around the caustic, field expression based on Maslov's method is derived in the next section.

4.2.2. Derivation of Caustic Field Expression

The field expression which should remain valid around the focal region of PEMC Gregorian system, may be derived using Maslov's method. The field expression for the system may be written using (3.3.8) as

$$\mathbf{E}^r(x, z) = \sqrt{\frac{k}{j2\pi}} \int_{-\infty}^{\infty} \mathbf{E}_0^r(\xi_2, \zeta_2) \left[\frac{D(\tau)}{D(0)} \frac{\partial p_z}{\partial z} \right]^{-\frac{1}{2}} \times \exp \left[-jk(S_0 + \tau + \tau_1 - z_s(x, p_z)p_{z_2} - zp_{z_2}) + \phi_1 \right] dp_{z_2} \quad (4.2.8)$$

The amplitude term $\left[\frac{D(\tau)}{D(0)} \frac{\partial p_z}{\partial z} \right]^{-\frac{1}{2}}$ in (4.2.8) is evaluated in (Appendix C) and is given by

$$\left[\frac{D(\tau)}{D(0)} \frac{\partial p_z}{\partial z} \right]^{-\frac{1}{2}} = \frac{\sqrt{R_1}}{\sin(2\psi - 2\alpha)} \quad (4.2.9)$$

The phase function $S(p_z)$ is given by

$$S(p_z) = S_0 + \tau_1 + S_{ex} + \phi_1 \quad (4.2.10)$$

where S_0 , τ_1 , and S_{ex} are given by (3.1.20), (3.1.6) and (3.3.12) respectively and phase angle ϕ_1 by (4.2.6). Substituting (4.2.7), (4.2.9) and (4.2.10) into (4.2.8) and converting dp_{z_2} into α , gives

$$E^r(x, z) = \sqrt{\frac{k}{j2\pi}} \left[\int_{A_1}^{A_2} + \int_{-A_2}^{-A_1} \right] (R_{co}\mathbf{u}_y - R_{cr}\mathbf{u}_x) \sqrt{R_1} \times \exp[-jk(S_0 + \tau_1 + S_{ex}) + \phi_1] d(2\alpha) \quad (4.2.11)$$

This gives field distribution around feed point F_1 of PEMC Gregorian microwave antenna. The field reflected from PEMC parabolic cylindrical reflector has both co-polarized (R_{co}) and cr-polarized (R_{cr}) field components. When $M\eta \rightarrow \pm\infty$, (for

PEC reflector) in the expression (4.2.11) containing both co and cr-polarized field components, produces $R_{cr} = 0$ and $R_{co} = -1$, consequently $\phi_1=0$ so that (4.2.11) becomes

$$E^r(x, z) = \sqrt{\frac{k}{j2\pi}} \left[\int_{A1}^{A2} + \int_{-A2}^{-A1} \right] \sqrt{R_1} \exp[-jk(S_0 + \tau_1 + S_{ex})] d(2\alpha) \quad (4.2.12)$$

The field expression (4.2.12) is same as (3.3.13), the field expression of PEC Gregorian microwave antenna. It may be noted that in all the field plots here in this discussion, it is assumed that $M\eta_1, M\eta_2, M\eta_3, M\eta_4,$ and $M\eta_5$ are used to represent different values of $M\eta$

4.2.3. Results and Discussion

The field expression (4.2.11) based on Maslov's method remains valid at all points and gives finite field around caustic region of PEMC Gregorian dual reflector system. The solution of (4.2.11) is obtained through numerical integration. For all plots, the focussing system having parameters $kf = 62.5, ka = 10, kb = 8.7, kd = 8.2$ and $kD = 70$, is considered for the study of field behavior around caustic region. Fig. 4.3. and Fig. 4.4. contain the comparison plots along x -axis and z -axis of co-polarized field distribution around feed point F_1 of microwave antenna for different values of $M\eta_0$. Plot for $M\eta = 6000$ is in good agreement with two dimensional PEC Gregorian reflector antenna, that is, field pattern of (4.2.12) as shown in Fig. 4.11. Now Fig. 4.5. and Fig. 4.6. contain the comparison of plots of cr-polarized field distribution around caustic region for different values of $M\eta$. For $M\eta = 6000$ cr-field component vanishes. Fig. 4.7. to Fig. 4.10. contain the comparison of plots of co-polarized and cr-polarized field distribution around caustic region for some other values of $M\eta$. The location of the caustic may be observed and verified easily. It is observed from comparison that cr-polarized field intensity component decreases as $M\eta$ increases and it finally vanishes as $M\eta$ approaches infinity, whereas co-polarized field intensity component increases as $M\eta$ increases till it approaches the results of field pattern determined from (4.2.12) for two dimensional PEC Gregorian dual reflector antenna.

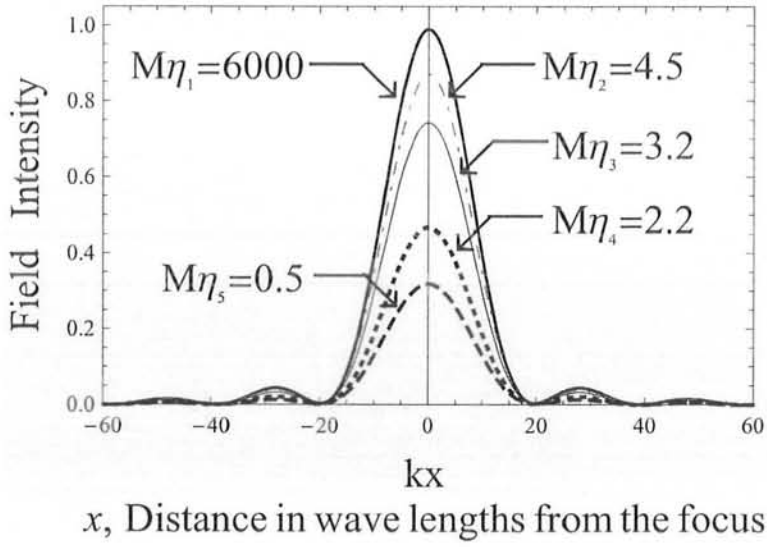


Fig. 4.3. Comparison of co-polarized field intensity distribution pattern along x -axis around the caustic region of PEMC Gregorian system for $M\eta_1 = 6000$, $M\eta_2 = 4.5$, $M\eta_3 = 3.2$, $M\eta_4 = 2.2$ and $M\eta_5 = 0.5$.

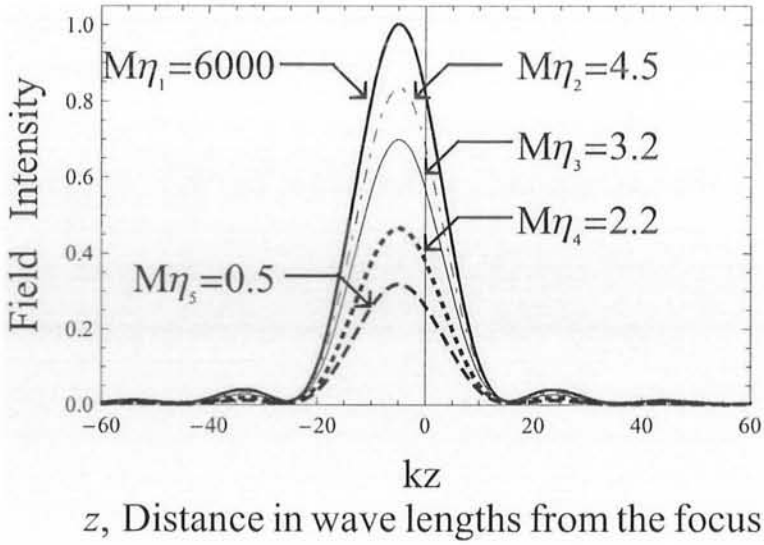


Fig. 4.4. Comparison of co-polarized field intensity distribution in the caustic region along z -axis of PEMC Gregorian system with parameters $M\eta_1 = 6000$ (zero field intensity), $M\eta_2 = 4.5$, $M\eta_3 = 3.2$, $M\eta_4 = 2.2$ and $M\eta_5 = 0.5$.

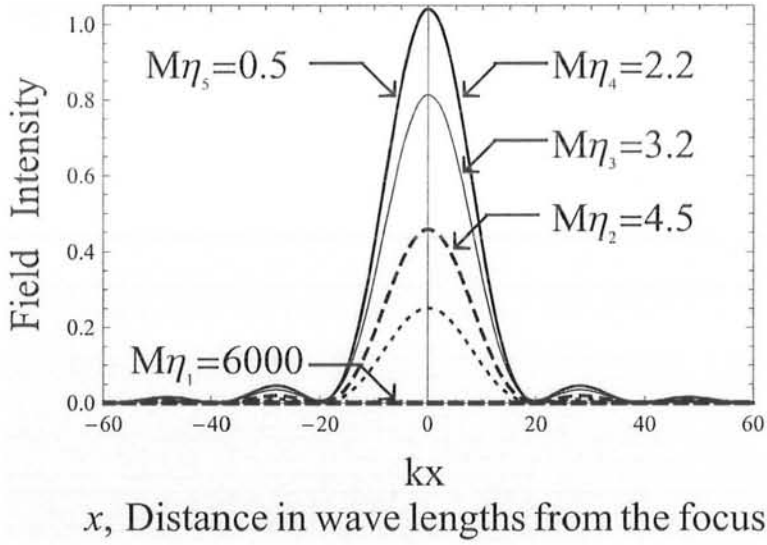


Fig. 4.5. Comparison of *cr*-polarized field intensity distribution pattern along *x*-axis around the caustic region of PEMC Gregorian system for $M\eta_1 = 6000$, $M\eta_2 = 4.5$, $M\eta_3 = 3.2$, $M\eta_4 = 2.2$ and $M\eta_5 = 0.5$.

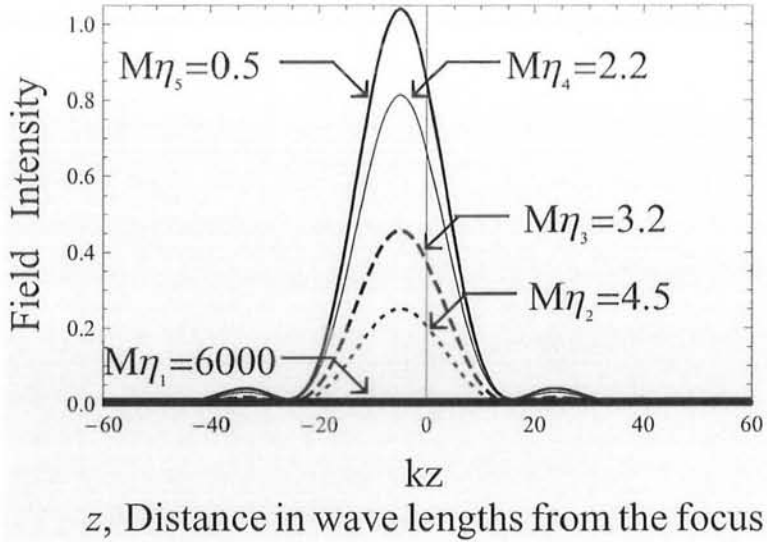


Fig. 4.6. Comparison of *cr*-polarized field intensity distribution in the caustic region along *z*-axis of PEMC Gregorian system having PEMC parameter values as $M\eta_1 = 6000$ (zero field intensity), $M\eta_2 = 4.5$, $M\eta_3 = 3.2$, $M\eta_4 = 2.2$ and $M\eta_5 = 0.5$.

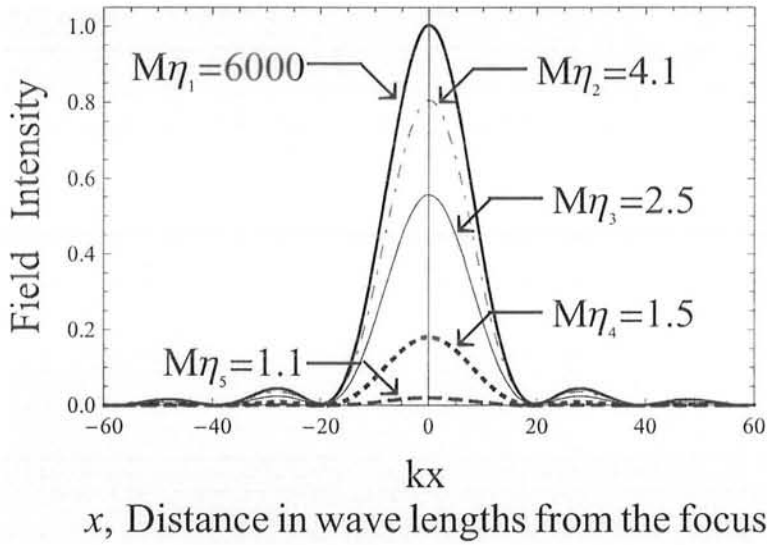


Fig. 4.7. Comparison of co-polarized field intensity distribution along x -axis in the caustic region of PEMC Gregorian system having PEMC parameter values as $M\eta_1 = 6000$ (maximum field intensity), $M\eta_2 = 4.1$, $M\eta_3 = 2.5$, $M\eta_4 = 1.5$ and $M\eta_5 = 1.1$.

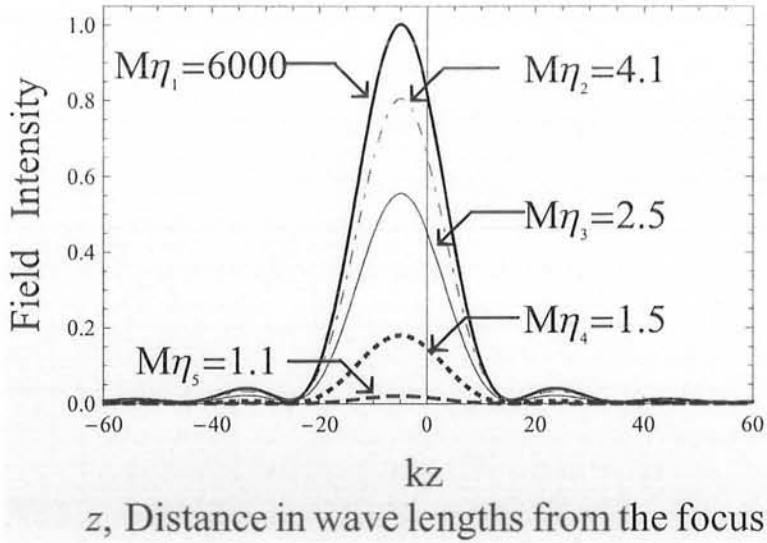


Fig. 4.8. Comparison of co-polarized field intensity distribution along z -axis in the caustic region of PEMC Gregorian system having PEMC parameter values as $M\eta_1 = 6000$ (maximum field intensity), $M\eta_2 = 4.1$, $M\eta_3 = 2.5$, $M\eta_4 = 1.5$ and $M\eta_5 = 1.1$.

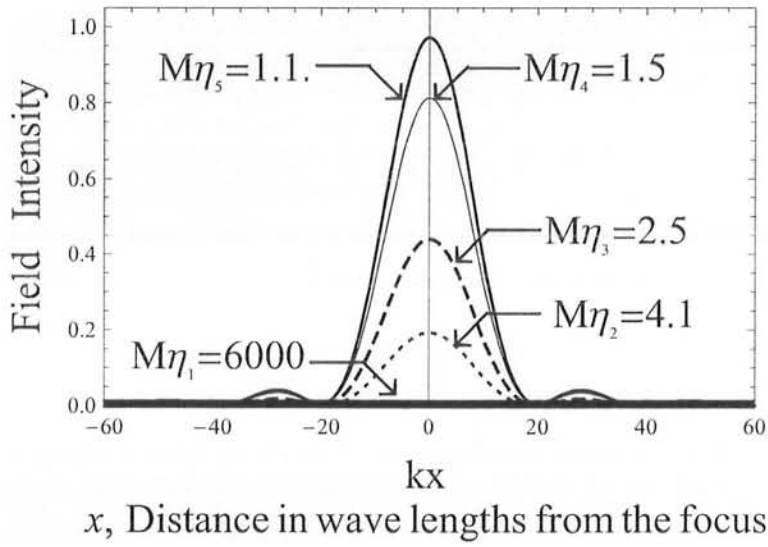


Fig. 4.9. Comparison of *cr*-polarized field intensity distribution along *x*-axis in the caustic region of a PEMC Gregorian system having PEMC parameter of $M\eta_1 = 6000$ (zero field intensity), $M\eta_2 = 4.1$, $M\eta_3 = 2.5$, $M\eta_4 = 1.5$ and $M\eta_5 = 1.1$.

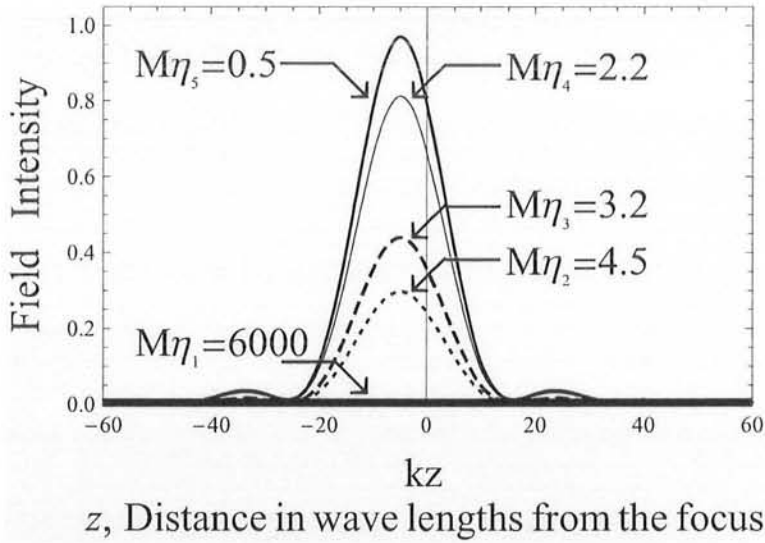


Fig. 4.10. Comparison of *cr*-polarized field intensity distribution along *z*-axis in the caustic region of a PEMC Gregorian system having parameter values of $M\eta_1 = 6000$ (zero field intensity), $M\eta_2 = 4.1$, $M\eta_3 = 2.5$, $M\eta_4 = 1.5$ and $M\eta_5 = 1.1$.

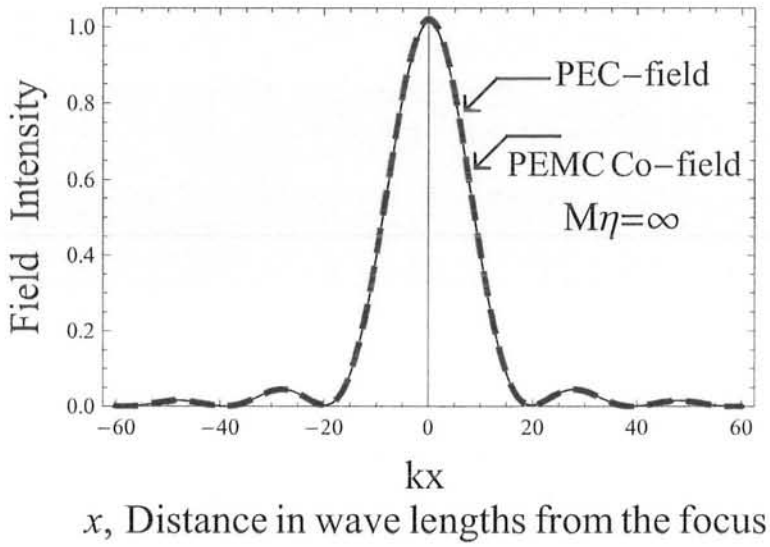


Fig. 4.11. Comparison of field intensity distribution along x -axis around caustic region of PEC and PEMC Gregorian system with PEMC parameter $M\eta \rightarrow \pm\infty$

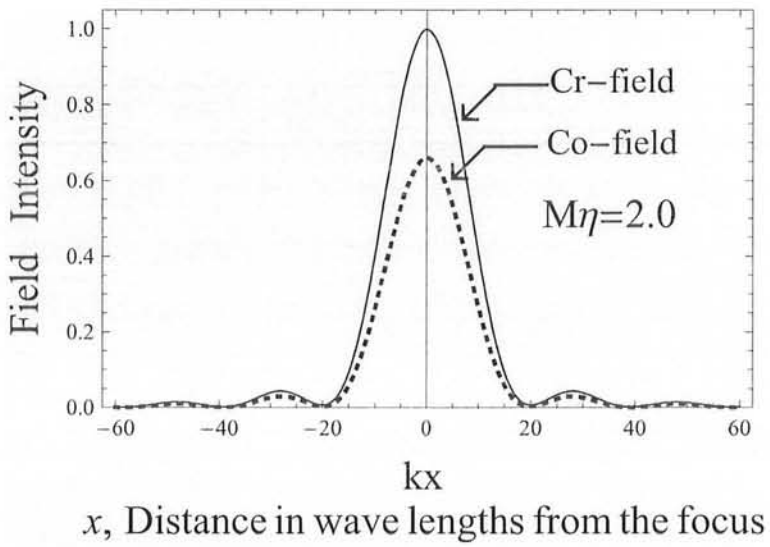


Fig. 4.12. Comparison of co and cr-polarized field intensity distribution along x -axis around caustic region of a PEMC Gregorian system with $M\eta = 2$.

4.3. PEMC Cassegrain Dual Reflector Antenna

Geometry of a two dimensional Cassegrain microwave antenna is as shown in schematic diagram of Fig. 4.13. In present work, it is assumed that both the reflectors are perfect electromagnetic conductor (PEMC). The equations describing the surfaces of both main-reflector and sub-reflector are given by (3.1.1) and (3.1.2) respectively. The surface of main-reflector is excited by the field of linearly polarized plane wave propagating along z-axis, and is given by

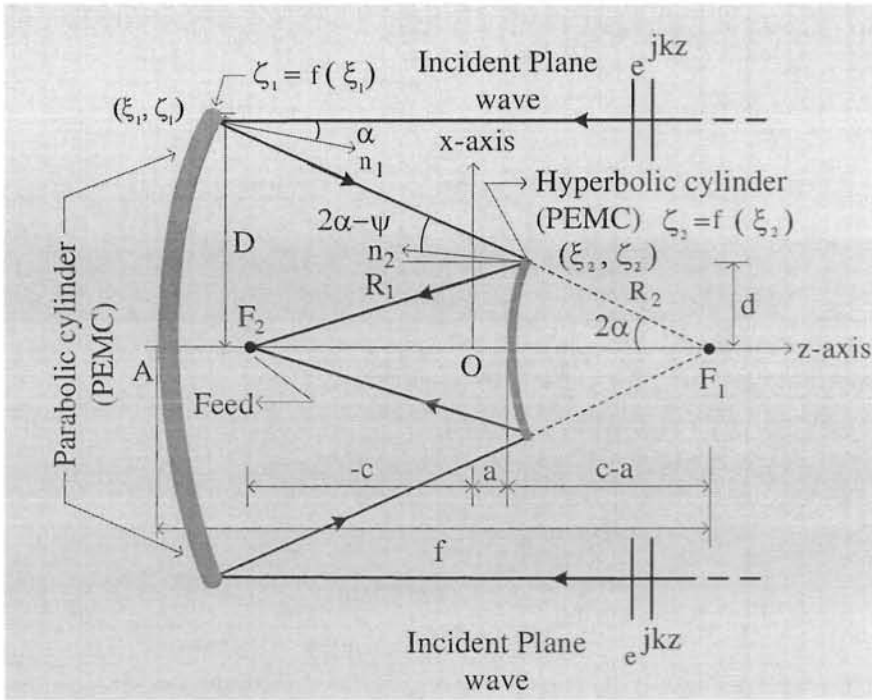


Fig. 4.13. PEMC Cassegrain dual cylindrical reflector system being excited by plane electromagnetic wave, creates both co and cr-field components around feed point.

$$\mathbf{E}^i = \mathbf{u}_y \exp(jkz) \quad (4.3.1)$$

Field after reflection from the parabolic reflector hits the hyperbolic reflector and therefore converges around feed point of the Cassegrain microwave antenna. The objective is to determine the field expression which should remain valid around caustic

region of the system. To achieve this, the discussion may be divided into two main parts:

In the first part, GO field expression is determined, which of course contains singularity at the feed point. Maslov's method is used to derive a field expression that should also be valid around focal region. The method transforms the expression of GO field from spatial domain into spectral domain. To do this it requires to find components of ray vector after reflection from both surfaces, we need expressions for the unit normals on the surfaces of each reflector. Unit normals \mathbf{n}_1 and \mathbf{n}_2 of parabolic reflector and hyperbolic reflector have been given by (3.1.9). GO field expression of PEC Cassegrain dual reflector microwave antenna is given by (3.1.20), and on including field rotation angle ϕ_2 due to plane wave reflection from PEMC interface, in the phase term, yields GO field expression for PEMC Cassegrain system.

$$\mathbf{E}^r = \mathbf{E}_{20}^r J(\tau) \frac{-1}{2} \exp[-jk(S_0 + \tau_1 + \tau) + \phi_2] \quad (4.3.2)$$

where phase function includes S_0 , τ_1 and τ which are given by (3.1.20), (3.1.6) and (3.1.5) respectively. The Jacobian of field reflected from sub-reflector of Cassegrain system has been evaluated in (3.1.25) and is given by

$$J(\tau) = \frac{D(\tau)}{D(0)} = 1 - \frac{\tau}{R_1} \quad (4.3.3)$$

4.3.1. Evaluation of Surface Field

\mathbf{E}_{20}^r is the amplitude of the field on the surface of PEMC hyperbolic cylinder and may be evaluated by considering the field reflected from PEMC main-reflector \mathbf{E}_{10}^r as incident field on sub-reflector. The field \mathbf{E}_{10}^r and reflection coefficients have already been evaluated in (4.2.4) and (4.2.5) respectively and are given as

$$\mathbf{E}_{10}^r = -\frac{1}{\cos^2 \alpha + M_1^2 \eta^2} [(M_1^2 \eta^2 - \cos^2 \alpha) \mathbf{E}_i - 2M_1 \eta \cos \alpha (\mathbf{u}_z \times \mathbf{E}_i)] \quad (4.3.4)$$

$$\begin{aligned}
 \tilde{R}_1 &= -\frac{1}{\cos^2 \alpha + M_1^2 \eta^2} [(M_1^2 \eta^2 - \cos^2 \alpha) \tilde{I} - 2M_1 \eta \cos \alpha \tilde{J}] \tilde{R} \\
 &= R_{co} \tilde{I} + R_{cr} \tilde{J} \\
 R_{1co} &= -\frac{M_1^2 \eta^2 - \cos^2 \alpha}{\cos^2 \alpha + M_1^2 \eta^2} \\
 R_{1cr} &= \frac{2M_1 \eta \cos \alpha}{\cos^2 \alpha + M_1^2 \eta^2}
 \end{aligned} \tag{4.3.5}$$

R_{1co} and R_{1cr} are co and cr reflection coefficients of the main reflector. The wave reflected by main-reflector acts as incident wave to sub-reflector. Therefore the field reflected by sub-reflector is given below

$$\begin{aligned}
 \mathbf{E}_{20}^r &= -\frac{1}{\cos^2(2\alpha + \psi) + M_2^2 \eta^2} [(M_2^2 \eta^2 - \cos^2(2\alpha + \psi)) \mathbf{E}_{10}^r \\
 &\quad - 2M_2 \eta \cos(2\alpha + \psi) (\mathbf{u}_z \times \mathbf{E}_{10}^r)] \\
 &= -\frac{1}{\cos^2(2\alpha + \psi) + M_2^2 \eta^2} [(M_2^2 \eta^2 - \cos^2(2\alpha + \psi)) (R_{1co} \mathbf{u}_y - R_{1cr} \mathbf{u}_x) \\
 &\quad - 2M_2 \eta \cos(2\alpha + \psi) (\mathbf{u}_z \times (R_{1co} \mathbf{u}_y - R_{1cr} \mathbf{u}_x))]
 \end{aligned} \tag{4.3.6}$$

Set

$$\begin{aligned}
 R_{21} &= -\frac{M_2^2 \eta^2 - \cos^2(2\alpha + \psi)}{\cos^2(2\alpha + \psi) + M_2^2 \eta^2} \\
 R_{22} &= \frac{2M_2 \eta \cos(2\alpha + \psi)}{\cos^2(2\alpha + \psi) + M_2^2 \eta^2}
 \end{aligned}$$

The relation (4.3.6) will become,

$$\begin{aligned}
 \mathbf{E}_{20}^r &= R_{21} (R_{1co} \mathbf{u}_y - R_{1cr} \mathbf{u}_x) + R_{22} (\mathbf{u}_z \times (R_{1co} \mathbf{u}_y - R_{1cr} \mathbf{u}_x)) \\
 &= R_{21} R_{1co} \mathbf{u}_y - R_{21} R_{1cr} \mathbf{u}_x - R_{22} (R_{1co} \mathbf{u}_x + R_{1cr} \mathbf{u}_y) \\
 &= (R_{21} R_{1co} - R_{22} R_{1cr}) \mathbf{u}_y - (R_{21} R_{1cr} + R_{22} R_{1co}) \mathbf{u}_x \\
 &= R_{2co} \mathbf{u}_y - R_{2cr} \mathbf{u}_x
 \end{aligned} \tag{4.3.7}$$

where

$$R_{2co} = R_{21} R_{1co} - R_{22} R_{1cr}$$

$$R_{2cr} = R_{21}R_{1cr} + R_{22}R_{1co}$$

R_{2co} and R_{2cr} are co and cr reflection coefficients of PEMC Cassegrain microwave antenna. The rotation angle ϕ_2 produced between the field components after reflection from PEMC interface is obtained as

$$\tan \phi_2 = \frac{R_{2cr}}{R_{2co}}$$

On substituting (4.3.7) and (4.3.3) in GO field expression (4.3.2), It is readily seen that the Geometrical optics field expression gives infinite field value around feed point F_1 of microwave antenna as is expected. The field expression valid around caustic has been formulated by using Maslov's method in (3.2.1) and may be used for PEMC Cassegrain system by including rotation angle ϕ_2 caused by PEMC interface as,

$$\mathbf{E}^r = \sqrt{\frac{k}{j2\pi}} \int_{-\infty}^{\infty} \mathbf{E}_{20}^r \left[\frac{D(\tau)}{D(0)} \frac{\partial p_{z2}}{\partial z} \right]^{\frac{-1}{2}} \exp[-jk(S_0 + \tau_1 + S_{ext}) + \phi_2] dp_{z2} \quad (4.3.8)$$

where integrand in square bracket of above equation has been given in (3.2.5), whereas S_0 , τ_1 and S_{ext} are obtained from (3.1.20), (3.1.6) and (3.1.9) respectively. The rotation angle ϕ_2 is obtained from $\tan \phi_2 = \frac{R_{2cr}}{R_{2co}}$. On substituting these values, the equation (4.3.8) may be written as

$$\mathbf{E}^r(x, z) = \sqrt{\frac{k}{j2\pi}} \left[\int_{A_1}^{A_2} + \int_{-A_2}^{-A_1} \right] (R_{co}\mathbf{u}_y - R_{cr}\mathbf{u}_x) \sqrt{R_1} \exp[-jk(S_0 + \tau_1 + S_{ex}) + \phi_2] d(2\alpha) \quad (4.3.9)$$

When $M_1 = M_2 = \pm\infty$ (PEC), $R_{cr} = 0$, $R_{co} = -1$, therefore (4.3.9) reduces to the field expression of PEC Cassegrain system (3.2.10)

$$E^r(x, z) = \sqrt{\frac{k}{j2\pi}} \left[\int_{A_1}^{A_2} + \int_{-A_2}^{-A_1} \right] \sqrt{R_1} \exp[-jk(S_0 + \tau_1 + S_{ex})] d(2\alpha) \quad (4.3.10)$$

4.3.2. Results and Discussion

Field patterns around the caustic of a two dimensional PEMC Cassegrain dual reflector antenna are evaluated using field expression (4.3.9) by solving it through numerical integration. The dual reflector focussing system, having parameters $kf = 60$, $ka = 6.2$, $kb = 6.8$, $kd = 6$ and $kD = 70$, is chosen for the study of field behavior around caustic region. Fig. 4.14.to Fig. 4.20., contain the plots of co-polarized and cr-polarized field components around feed point both along x -axis and z -axis. For all plots, we assume $M\eta = M_1\eta = M_2\eta$ with quantities M_1 and M_2 as the admittances of parabolic and hyperbolic reflector respectively. Fig. 4.14.to Fig. 4.15., contain the comparison plots of co-polarized component of field distribution for different values of $M\eta$ along x -axis and z -axis respectively. Fig. 4.16. to Fig. 4.17., contain the comparison of field plots for cr-polarized field distribution for different values of $M\eta$ along x -axis and z -axis respectively.

Plot for $M\eta \rightarrow \pm\infty$ i.e., ($M\eta = 6000$) is in good agreement with the plot of field distribution resulting from field expression (4.3.10) of two dimensional PEC Cassegrain dual reflector antenna and for $M\eta=0$ it gives the results of PMC Cassegrain system for co-polarized field components. On the other hand, for $M\eta=0$ and $M\eta \rightarrow \pm\infty$, the cr-polarized field components vanish. At $M\eta=\pm 1$, it is observed from comparison that cr-polarized component of field intensity assume maximum value whereas co-polarized component of field intensity decreases to minimum value. It is observed from comparison that cr-polarized field intensity decreases as $M\eta$ increases. Also with the increase in admittance parameter, both main and side lobe start vanishing, whereas co-polarized component of field intensity increases as $M\eta$ increases till it approaches the results of two dimensional PEC Cassegrain antenna.

It may be noted that with the increase in admittance parameter, increases the amplitude more of main lobe than the amplitude of the side lobes. There is a little

change in amplitude of side lobes as compared to the main lobe. It may be noted that change in the admittance parameter does not affect number of side lobes. A comparison of field distribution of a PEMC Cassegrain dual reflector antenna having admittance parameter $M\eta \rightarrow \pm\infty$ with the field pattern of a PEC Cassegrain dual reflector system is as shown in Fig. 4.18.

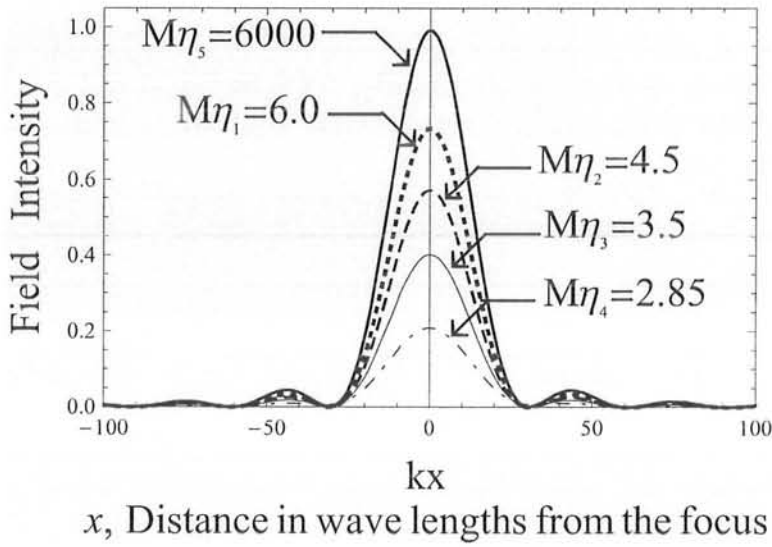


Fig. 4.14. Comparison of co-polarized field intensity distribution along x -axis in the caustic region of a PEMC Cassegrain system having PEMC parameter of $M\eta_1 = 6$ (zero field intensity), $M\eta_2 = 4.5$, $M\eta_3 = 3.5$, $M\eta_4 = 2.85$ and $M\eta_5 = 6000$.

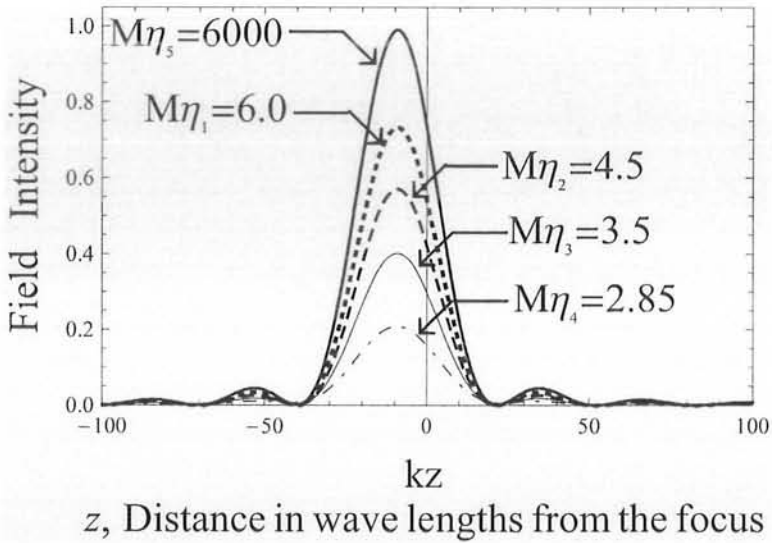


Fig. 4.15. Comparison of co-polarized field intensity distribution along z -axis in the caustic region of a PEMC Cassegrain system having PEMC parameter of $M\eta_1 = 6$, $M\eta_2 = 4.5$, $M\eta_3 = 3.5$, $M\eta_4 = 2.85$ and $M\eta_5 = 6000$.

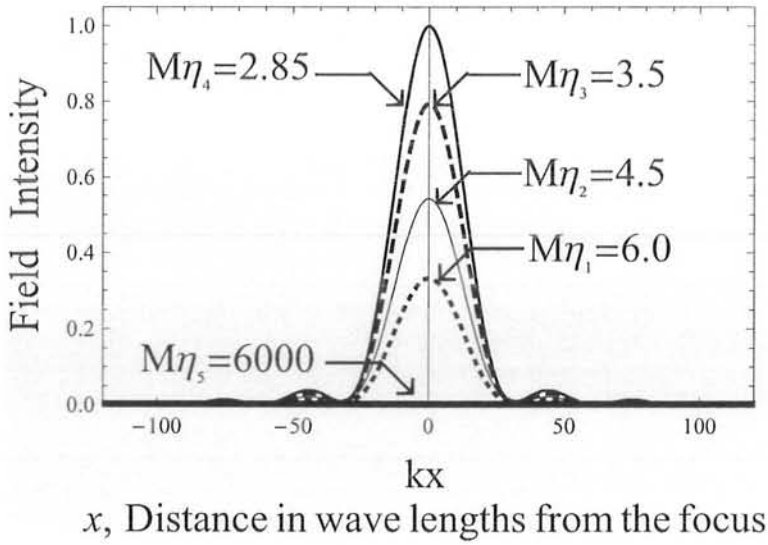


Fig. 4.16. Comparison of *cr*-polarized field intensity distribution along *x*-axis in the caustic region of a PEMC Cassegrain system having PEMC parameter of $M\eta_1 = 6$, $M\eta_2 = 4.5$, $M\eta_3 = 3.5$, $M\eta_4 = 2.85$ and $M\eta_5 = 6000$.

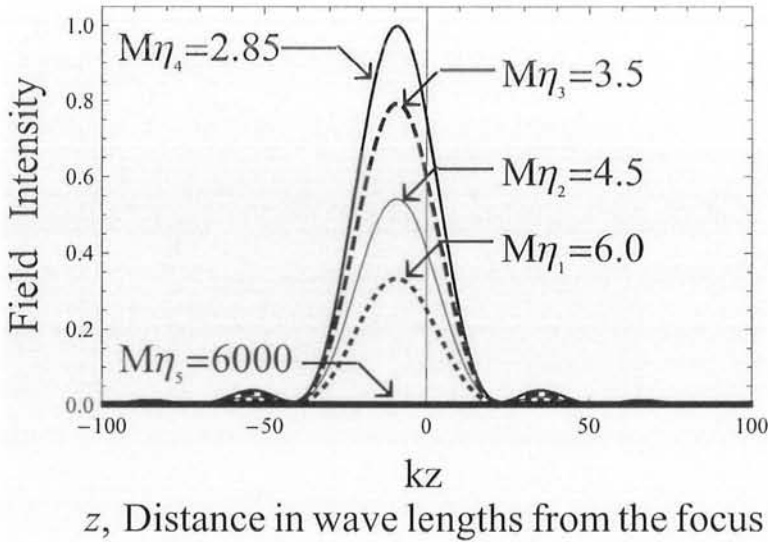


Fig. 4.17. Comparison of *cr*-polarized field intensity distribution along *z*-axis in the caustic region of a PEMC Cassegrain system having PEMC parameter of $M\eta_1 = 6$, $M\eta_2 = 4.5$, $M\eta_3 = 3.5$, $M\eta_4 = 2.85$ and $M\eta_5 = 6000$ (zero field intensity)

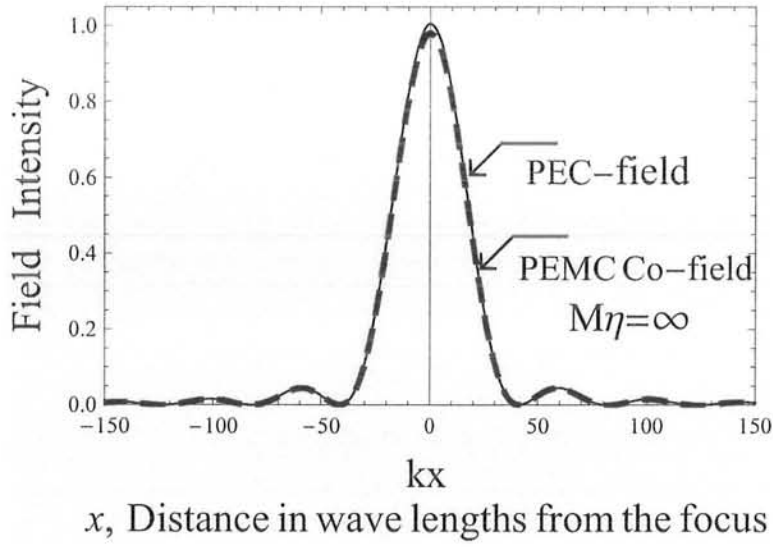


Fig. 4.18. Comparison of co and cr-polarized field intensity distribution along x -axis in the caustic region of PEC and PEMC Cassegrain system with PEMC parameter $M\eta \rightarrow \pm\infty$.

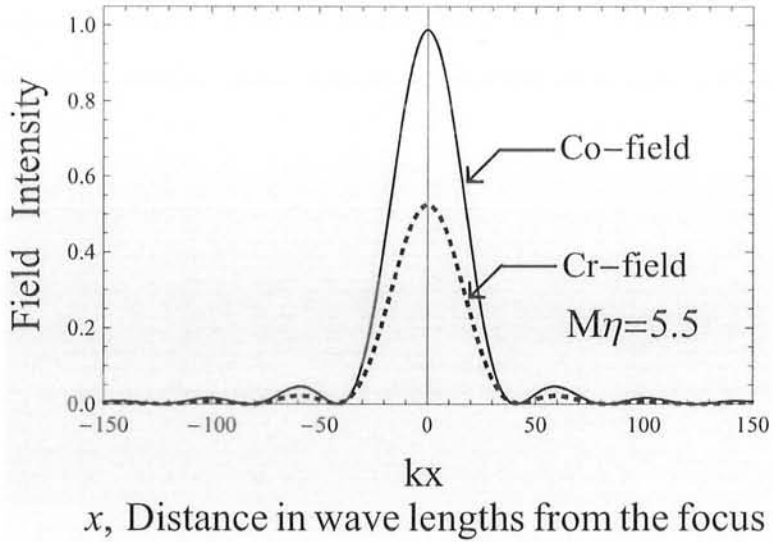


Fig. 4.19. Comparison of co and cr-polarized field intensity distribution along x -axis in the caustic region of a PEMC Cassegrain system with $M\eta = 5.5$.

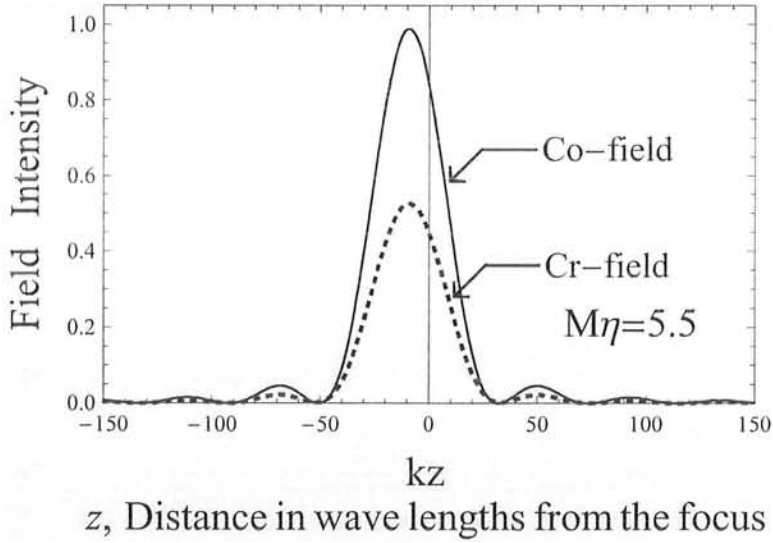


Fig. 4.20. Comparison of co and cr-polarized field intensity distribution along z-axis in the caustic region of a PEMC Cassegrain system with $M\eta = 5.5$.

4.4. PEMC Backed Chiral Nihility Dual Reflector Systems

In the present discussion, our interest is to study the field reflected around caustic region of PEMC Cassegrain and Gregorian dual reflector systems in which parabolic cylindrical reflector has been coated with chiral nihility material. Chiral nihility is a special kind of chiral medium for which the constitutive parameters, at certain frequency known as nihility frequency [49] become $\epsilon=0, \mu=0$, such that $\kappa \neq 0$, where κ is the chirality of the medium. In the next section, expression for the field reflected from interface of chiral nihility slab backed by PEMC material is derived.

4.4.1. Chiral Nihility Slab Backed by PEMC Boundary.

Consider a slab of chiral nihility metamaterial of infinite length and is backed by perfect electromagnetic conductor. Front face of the chiral nihility slab is located at $z = d_1$ while perfect electromagnetic conductor is located at $z = d_2$, where $d_2 > d_1$ as shown in Fig. 4.22.

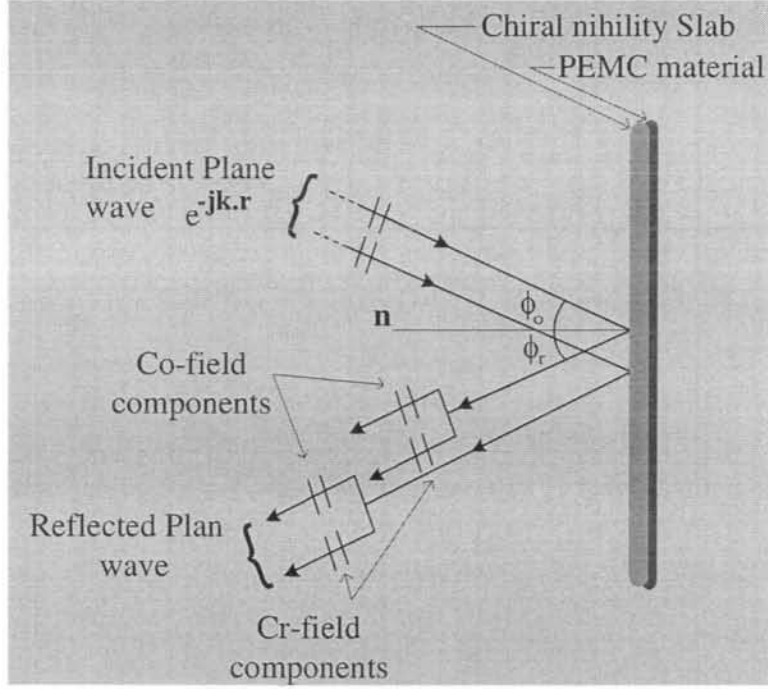


Fig. 4.22. A chiral nihility slab backed by PEC medium. When the slab is excited by a plane wave field, creates both co and cross-field components upon reflection.

A linearly polarized uniform plane wave, is obliquely incident on the chiral nihility slab backed by PEC. The electric and magnetic fields inside and outside the grounded chiral nihility slab may be written in terms of unknown coefficients as [51, 53]

$$\mathbf{E}_0 = \exp(jk_y y) \left[\mathbf{x} \exp(jk_z z) + A^- \mathbf{N}_R^- \exp(-jk_z z) + B^- \mathbf{N}_L^- \exp(-jk_z z) \right], \quad z < d_1 \quad (4.4.1)$$

$$\mathbf{E}_1 = \exp(jk_y y) \left[E^+ \mathbf{M}_R^+ \exp(jk_{1z}^+ z) + F^+ \mathbf{M}_L^+ \exp(jk_{1z}^- z) + E^- \mathbf{M}_R^- \exp(-jk_{1z}^+ z) + F^- \mathbf{M}_L^- \exp(-jk_{1z}^- z) \right], \quad d_1 < z < d_2 \quad (4.4.2)$$

$$\mathbf{H}_0 = \exp(jk_y y) \left[\frac{1}{k\eta} \{ \mathbf{y} \exp(jk_z z) - \mathbf{z} k_y \exp(jk_z z) \} - \frac{j}{\eta} \{ A^- \mathbf{N}_R^- \exp(-jk_z z) + B^- \mathbf{N}_L^- \exp(-jk_z z) \} \right], \quad z < d_1 \quad (4.4.3)$$

$$\mathbf{H}_1 = \exp(jk_y y) \frac{-j}{\eta_1} \left[E^+ \mathbf{M}_R^+ \exp(jk_{1z}^+ z) - F^+ \mathbf{M}_L^+ \exp(jk_{1z}^- z) + E^- \mathbf{M}_R^- \exp(-jk_{1z}^+ z) - F^- \mathbf{M}_L^- \exp(-jk_{1z}^- z) \right], \quad d_1 < z < d_2 \quad (4.4.4)$$

where

$$\begin{aligned}
 \mathbf{N}_R^\pm &= \mathbf{x} \pm \frac{jk_z}{k} \mathbf{y} - \frac{jk_y}{k} \mathbf{z} \\
 \mathbf{N}_L^\pm &= \mathbf{x} \mp \frac{jk_z}{k} \mathbf{y} + \frac{jk_y}{k} \mathbf{z} \\
 \mathbf{M}_R^\pm &= \mathbf{x} \pm \frac{jk_{1z}^+}{k_1^+} \mathbf{y} - \frac{jk_y}{k_1^+} \mathbf{z} \\
 &= \mathbf{x} \pm \frac{jk_{1z}^+}{k_1^\pm} \mathbf{y} - \frac{jk_y}{k_1^\pm} \mathbf{z} \\
 \mathbf{M}_L^\pm &= \mathbf{x} \mp \frac{jk_{1z}^+}{k_1^+} \mathbf{y} - \frac{jk_y}{k_1^+} \mathbf{z} \\
 &= \mathbf{x} \mp \frac{jk_{1z}^\mp}{k_1^\mp} \mathbf{y} - \frac{jk_y}{k_1^\mp} \mathbf{z}
 \end{aligned}$$

Superscript \pm in above relations represent the eigenwaves propagating in the $\pm z$ direction. The superscript R and L refer to RCP and LCP eigenwaves satisfying the dispersion relations as

$$k_y^2 + (k_{1z}^\pm)^2 = (k_1^\pm)^2$$

where $k_1^\pm = \pm\omega\kappa$, at the nihility frequency and κ is chirality parameter. Also for free space medium assuming $k = \omega\sqrt{\mu_0\epsilon_0}$ and $\eta = \sqrt{\frac{\mu_0}{\epsilon_0}}$ such that k_z, k_y satisfy the following dispersion relation

$$k_y^2 + k_z^2 = k^2$$

It may be noted that relation $k_{1z}^+ = -k_{1z}^-$ holds for all modes propagating inside the slab. Substituting \mathbf{N}_R^- and \mathbf{N}_L^- in (4.4.1) gives

$$\begin{aligned}
 \mathbf{E}_0 &= \exp(jk_y y) \left[\mathbf{x} \exp(jk_z z) + A_{co} \mathbf{x} \exp(-jk_z z) + A_{cr} \right. \\
 &\quad \left. \times \left(\frac{jk_z}{k} \mathbf{y} + \frac{jk_y}{k} \mathbf{z} \right) \exp(-jk_z z) \right], z < d_1 \quad (4.4.5)
 \end{aligned}$$

where A_{co} and A_{cr} are values of the co-polarized and cr-polarized reflected fields. Unknown coefficients A_{co} and A_{cr} in field expression (4.4.5) may be obtained using the continuity of tangential components of electric and magnetic fields across the

dielectric interface located at $z = d_1$. Continuity of tangential components of electric and magnetic field yields [53]

$$\exp(jk_z d_1) + A_{co} \exp(-jk_z d_1) = \left(\frac{2j}{M\eta + j} \right) \times \left[E^+ \exp(jk_{1z} d_1) + E^- \exp(-jk_{1z} d_1) \right] \quad (4.4.6)$$

$$A_{cr} \exp(-jk_z d_1) = \frac{k_{1z} k}{k_1 k_z} \left(\frac{2j}{M\eta + j} \right) \times \left[E^+ \exp(jk_{1z} d_1) - E^- \exp(-jk_{1z} d_1) \right] \quad (4.4.7)$$

where it is assumed that $\eta = \eta_1 = \sqrt{\frac{\mu_0}{\epsilon_0}}$. Solving (4.4.6) and (4.4.7) simultaneously, gives

$$A_{co} = -\exp(-2jk_z d_1) + \left(\frac{2j}{M\eta + j} \right) \exp(jk_z d_1) \times \left[E^+ \exp(jk_{1z} d_1) + E^- \exp(-jk_{1z} d_1) \right] \quad (4.4.8)$$

$$A_{cr} = \frac{k_{1z} k}{k_1 k_z} \left(\frac{2j}{M\eta + j} \right) \exp(jk_z d_1) \times \left[E^+ \exp(jk_{1z} d_1) - E^- \exp(-jk_{1z} d_1) \right] \quad (4.4.9)$$

where

$$\begin{aligned} E^- &= -E^+ \left(\frac{jR_f + M\eta}{-jR_f + M\eta} \right) \exp(2jk_{1z} d_1) \\ E^+ &= \frac{2 \exp(jk_z d_1 - jk_{1z} d_1)}{P - QL} \\ P &= 2 \frac{j + M\eta R_f}{M\eta + j} \\ Q &= \left(\frac{jR_f + M\eta}{-jR_f + M\eta} \right) \\ L &= 2 \frac{j - M\eta R_f}{M\eta + j} \\ R_f &= \frac{k k_{1z}}{k_1 k_z} \end{aligned}$$

4.4.2. PEMC backed Chiral Nihility Parabolic Cylinder

Consider a parabolic cylindrical reflector coated with chiral nihility material and defined by $\zeta = \frac{f-\xi^2}{4}$ where f is the focal length of the parabola as shown in the Fig. 4.23. The field of oblique incident plane wave may be defined as

$$\mathbf{E}^i = \mathbf{x} \exp(jk_y y + jk_z z)$$

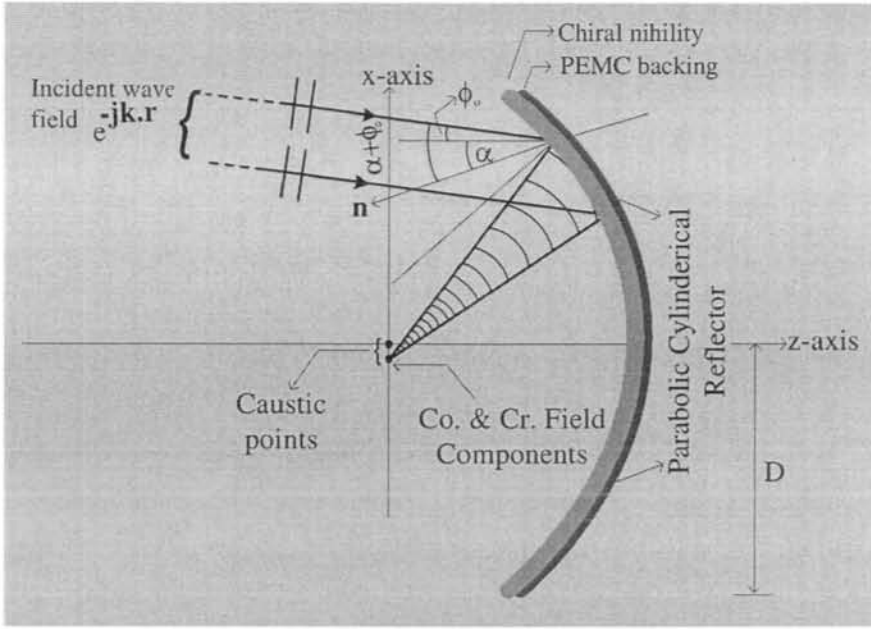


Fig. 4.23. The schematic diagram shows a parabolic cylindrical reflector having PEMC backed chiral nihility coating being excited by oblique incident plane wave. The surface field of parabolic reflector using (4.4.5) is given as

$$\begin{aligned} \mathbf{E}_0 = \exp(jk_y y) & \left[\mathbf{x} \exp(jk_z z) + A_{co} \mathbf{x} \exp(-jk_z z) + A_{cr} \right. \\ & \left. \times \left(\frac{jk_z}{k} \mathbf{y} + \frac{jk_y}{k} \mathbf{z} \right) \exp(-jk_z z) \right], \quad z < d_1 \end{aligned} \quad (4.4.10)$$

The reflection coefficients A_{co} and A_{cr} are given by (4.4.8) and (4.4.9) respectively as

$$A_{co} = -\exp(-2jk_z d_1) + \left(\frac{2j}{M\eta + j} \right) \exp(jk_z d_1)$$

$$\times [E^+ \exp(jk_{1z}d_1) + E^- \exp(-jk_{1z}d_1)] \quad (4.4.11)$$

$$A_{cr} = \frac{k_{1z}k}{k_1k_z} \left(\frac{2j}{M\eta + j} \right) \exp(jk_z d_1) \times [E^+ \exp(jk_{1z}d_1) - E^- \exp(-jk_{1z}d_1)] \quad (4.4.12)$$

where E^- , E^+ , P , Q , L and R_f have been defined in the previous section. When the plane wave is obliquely incident at an angle ϕ_0 on the interface of parabolic cylinder, k_z and k_y in (4.4.10), (4.4.11) and (4.4.12) are defined by

$$k_z = k \cos(2\alpha + \phi_0)$$

$$k_y = k \sin(2\alpha + \phi_0)$$

where α is the angle made with the z -axis by a unit normal \mathbf{n} on the surface of parabolic cylinder. For normal incident plane wave, the incident angle becomes $\phi_0 = 0$, so that

$$k_z = k \cos 2\alpha$$

$$k_y = k \sin 2\alpha$$

4.4.3. Gregorian Dual Reflector System

Gregorian system consists of two reflectors. These two reflectors may be of any material. It is assumed that the main reflector of Gregorian system is of PEMC while sub-reflector is of PEC. The main reflector is coated with chiral nihility material as shown in schematic diagram of Fig. 4.24. If someone is interested in the field distribution around the focus (caustic) F_2 of the system through geometrical optics (GO), he will fail to do so, because GO explodes at caustic. Our interest is to study the effect of these metamaterials on the field patterns around caustic region. So, a high frequency expression for the field around caustic region of chiral nihility coated PEMC Gregorian system is derived using Maslov's method.

where

$$\begin{aligned}\xi_2 &= b\sqrt{\frac{1 - \cos^2 \psi}{\cos^2(\psi - 2\alpha)}} \\ \zeta_2 &= \frac{a \cos \psi}{\cos(\psi - 2\alpha)} \\ \xi_1 &= -2f \tan \alpha \\ \zeta_1 &= \frac{f \cos 2\alpha}{\cos^2 \alpha} - c \\ \tan \psi &= -\frac{a^2 \xi_2}{b^2 \zeta_2} \\ \tan \phi &= \frac{y}{z}\end{aligned}$$

Now, substituting $\mathbf{E}_0^r(\xi_2, \zeta_2)$ from (4.4.10) and $J(\tau)\frac{\partial p_{z2}}{\partial z}$ from (4.2.9) in (4.4.14), co and cr-polarized field components reflected by PEMC backed chiral nihility Gregorian system are given by

$$\begin{aligned}\mathbf{E}_{co}(y, z) &= \sqrt{\frac{k}{j2\pi}} \left[\int_{A_1}^{A_2} + \int_{-A_2}^{-A_1} \right] [A_{co} \mathbf{x} \exp(-jk_z z)] \sqrt{R_1} \\ &\quad \times \exp[-jk(S_0 + \tau_1 + S_{ex})] d(2\alpha)\end{aligned}\quad (4.4.15)$$

$$\begin{aligned}\mathbf{E}_{cr}(y, z) &= \sqrt{\frac{k}{j2\pi}} \left[\int_{A_1}^{A_2} + \int_{-A_2}^{-A_1} \right] \left[A_{cr} \left(\frac{jk_z}{k} \mathbf{y} + \frac{jk_y}{k} \mathbf{z} \right) \right] \sqrt{R_1} \\ &\quad \times \exp[-jk(S_0 + \tau_1 + S_{ex})] d(2\alpha)\end{aligned}\quad (4.4.16)$$

where $A_{co}(\alpha)$ and $A_{cr}(\alpha)$ have been given in (4.4.11) and (4.4.12) respectively. In these equations, $k_z = k \cos 2\alpha$ and $k_y = k \sin 2\alpha$ have been used. It may be noted that in the limit $M\eta \rightarrow \pm\infty$ the backing is PEC, and co scattering coefficient reduces to PEC Gregorian system i.e., $A_{co}(\alpha) = -\exp(-2jk_z d_1)$ while the cross polarization coefficient reduces to zero i.e., $A_{cr} = 0$, the relation (4.4.15) reduces to the relation (3.3.13) of PEC Gregorian system

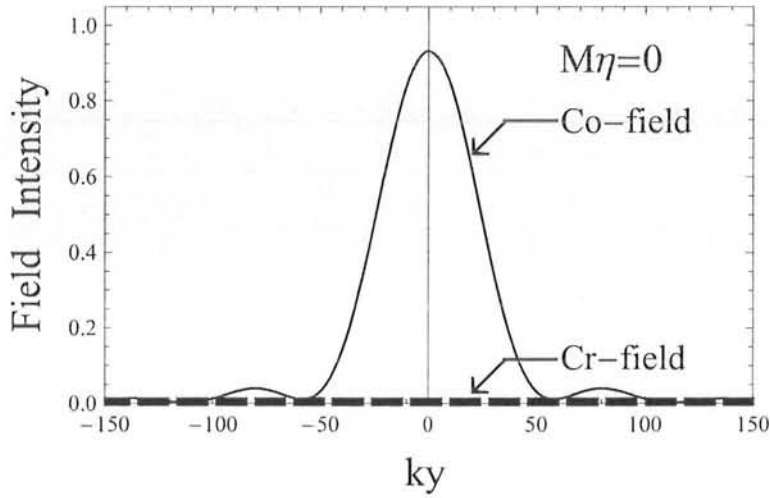
$$E^r(y, z)_{co} = \sqrt{\frac{k}{j2\pi}} \left[\int_{A_1}^{A_2} + \int_{-A_2}^{-A_1} \right] \sqrt{R_1} \exp[-jk(S_0 + \tau_1 + S_{ex})] d(2\alpha)\quad (4.4.17)$$

Similarly, in case of PMC backing, $M\eta = 0$, and the cross polarization co-efficient $A_{cr}(\alpha)$ again vanishes and co-polarization co-efficient $A_{co}(\alpha)$ independent of parameter $M\eta$

4.4.5. Results and Discussion

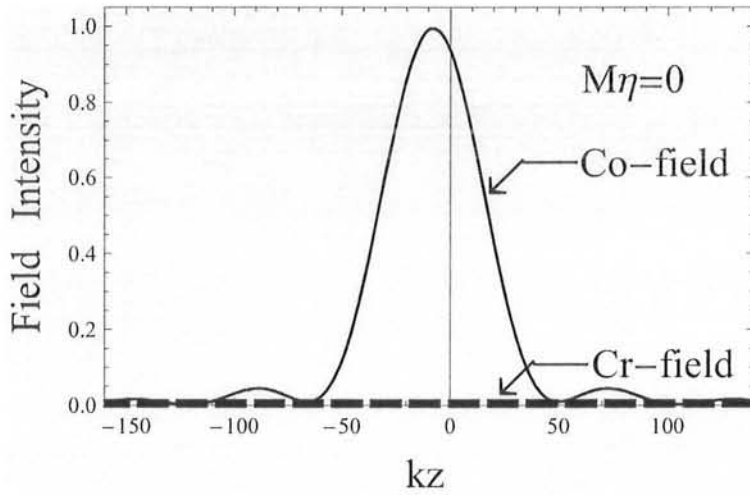
Plots of co-polarized and cr-polarized components of the reflected field along the reflector axes are shown in Fig. 4.25 to Fig. 4.31. The Gregorian system having parameters as $kf = 60$, $ka = 25$, $kb = 23.7$, $kd = 12.5$ and $kD = 40$, is chosen for the study of field behavior around caustic region. It has been observed that admittance parameter $M\eta$ affects the amplitude of the reflected field whereas field distribution pattern remains unchanged. Field intensity Plots have been obtained for different values of $M\eta$. It has been observed that for $M\eta = \pm 1$, cr component of the reflected field is maximum, while co-polarized field component reduces to zero. For $M\eta = 2$, the field amplitude of cross polarized component is greater than the co polarized field component and the behavior is reversed for $M\eta = 3$. For $M\eta > 3$, the field amplitude of the cr component decreases and finally vanishes for large values of $M\eta$. It can also be seen that for $M\eta = 0$ and $M\eta \rightarrow \pm\infty$ cr-polarized components of the reflected field disappear showing the behavior of the chiral nihility reflector backed by PMC and PEC material respectively, which agrees with our analytical formulation. In Fig. 4.29. The results of PEMC backed chiral nihility reflector are compared with the results of PEC backed chiral nihility reflector. The results are in good agreement. It has been observed starting from $M\eta = 0$ (PMC) boundary that field is rotated giving rise to increase and decrease in field intensity of co and cr components for different values of $M\eta$. Finally, observation comes to $M\eta \rightarrow \pm\infty$ (PEC boundary). The field intensity variation behavior of co and cr-polarised components has also been studied for different values of admittance parameter $M\eta_1 = 5$, $M\eta_2 = 3$, $M\eta_3 = 2$, $M\eta_4 = 1.5$ and $M\eta_5 = 1$. The behavior may be observed in the plots of Fig. 4.30. and Fig. 4.31. respectively. These findings may find potential use in some applications where controlled intensity of co and cr-polarized field is required. Another striking feature can be seen that the factor thickness didn't appear in the expression of the reflected field. It means that the thickness of nihility material coating on the reflector, is irrelevant.

It is perhaps due to the fact that in chiral nihility material, the two eigen-waves are circularly polarized but one of them is a backward wave.



y, Distance in wave lengths from the focus

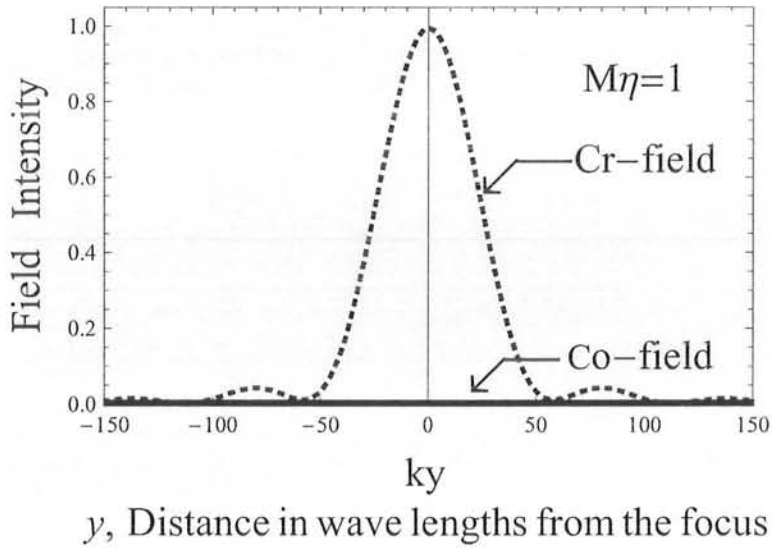
(a)



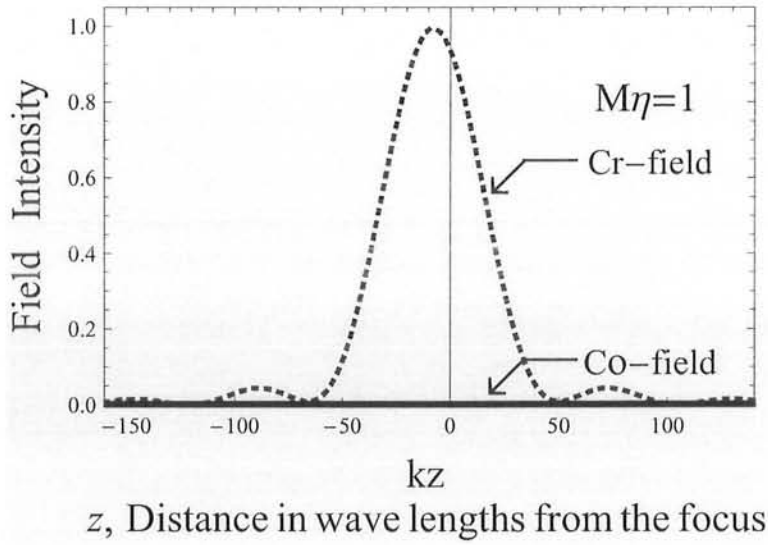
z, Distance in wave lengths from the focus

(b)

Fig. 4.25. Comparison of co and cr-polarized field intensity distribution (a) along y-axis and (b) along z-axis, around the caustic region of a PEMC backed chiral nihility Gregorian system for $M\eta = 0$.

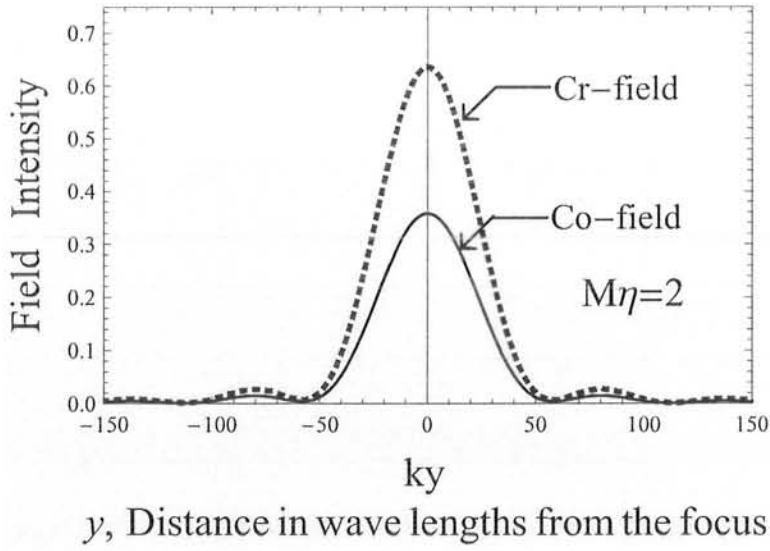


(a)

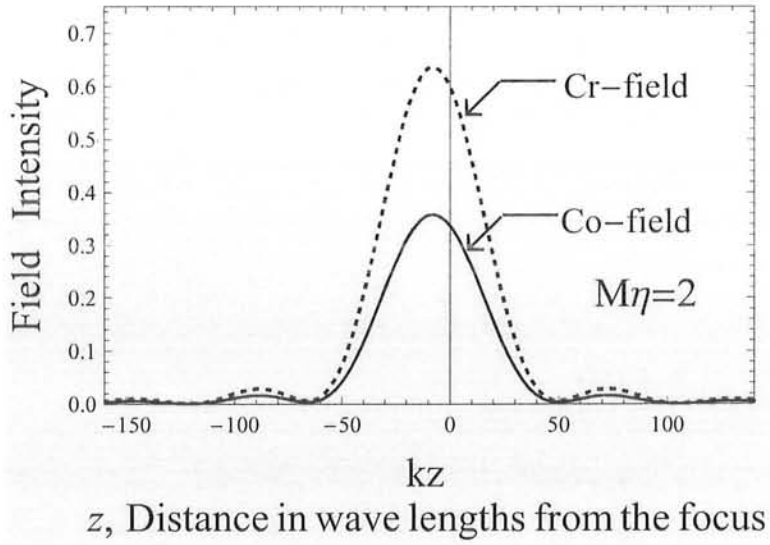


(b)

Fig. 4.26. Comparison of co and cr-polarized field intensity distribution (a) along y -axis and (b) along z -axis, around the caustic region of a PEMC backed chiral nihility Gregorian system for $M\eta = 1$.

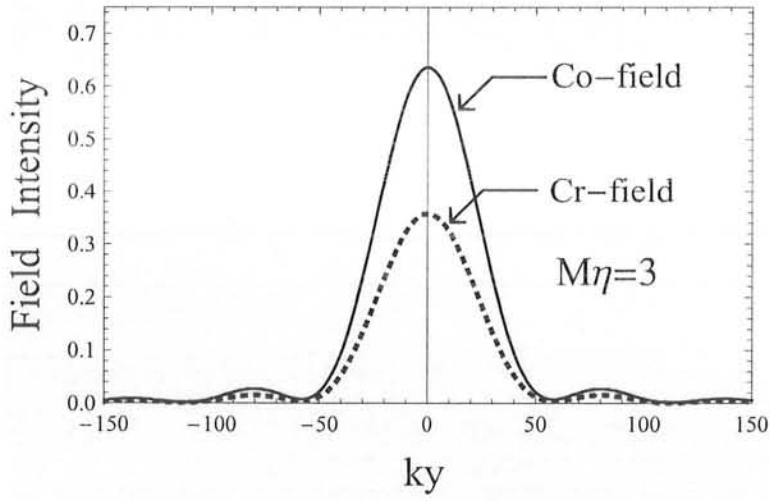


(a)



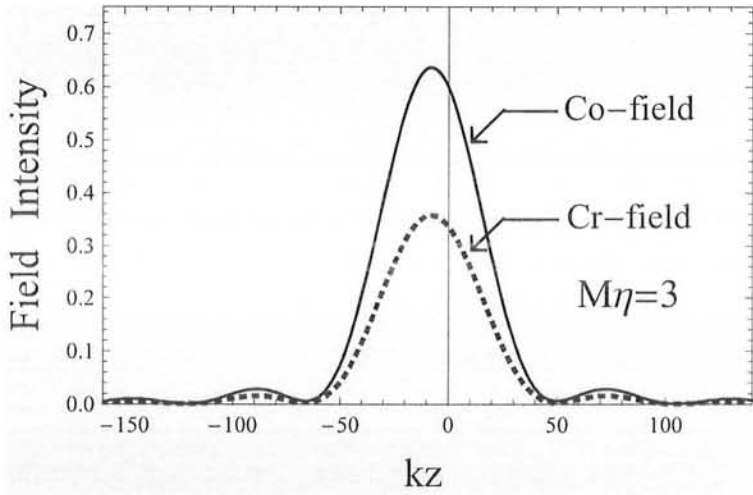
(b)

Fig. 4.27. Comparison of co and cr-polarized field intensity distribution (a) along y -axis and (b) along z -axis, around the caustic region of a PEMC backed chiral nihility Gregorian system for $M\eta = 2$.



y , Distance in wave lengths from the focus

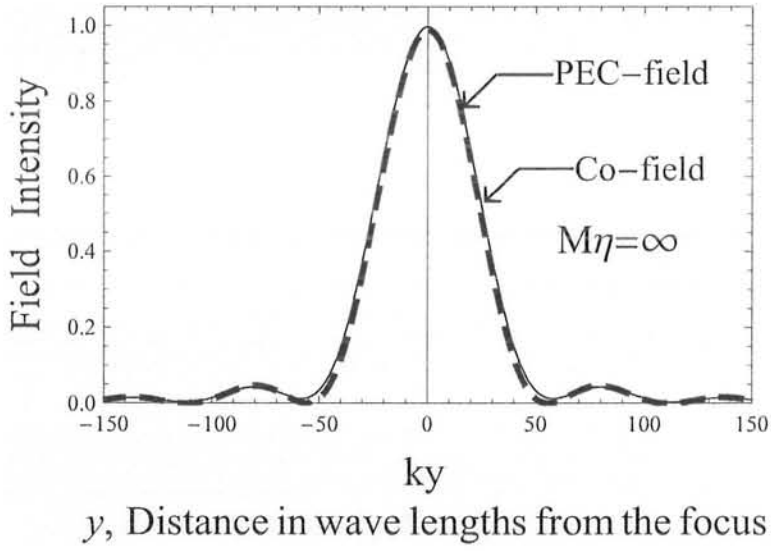
(a)



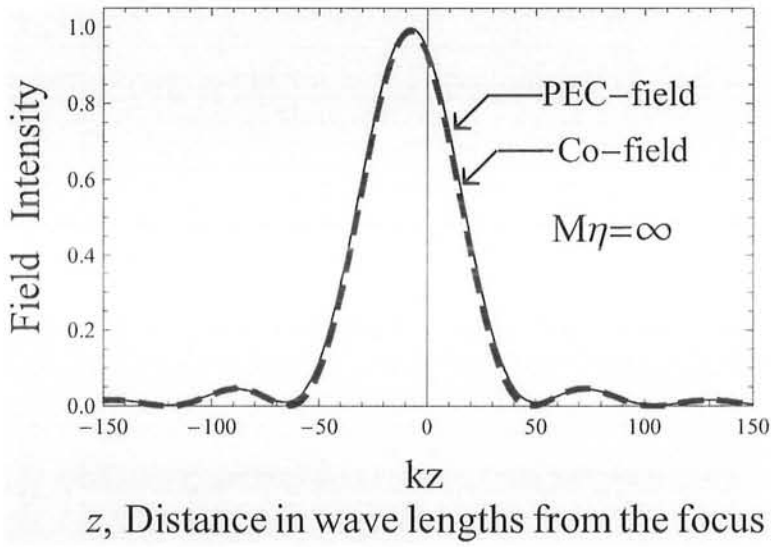
z , Distance in wave lengths from the focus

(b)

Fig. 4.28. Comparison of co and cr-polarized field intensity distribution (a) along y -axis and (b) along z -axis, around the caustic region of a PEMC backed chiral nihility Gregorian system for $M\eta = 3$.



(a)



(b)

Fig. 4.29. Comparison of field intensity distribution (a) along y -axis (b), along z -axis around the caustic region of PEC and PEMC backed chiral nihility Gregorian dual reflector antenna with $M\eta \rightarrow \pm\infty$.

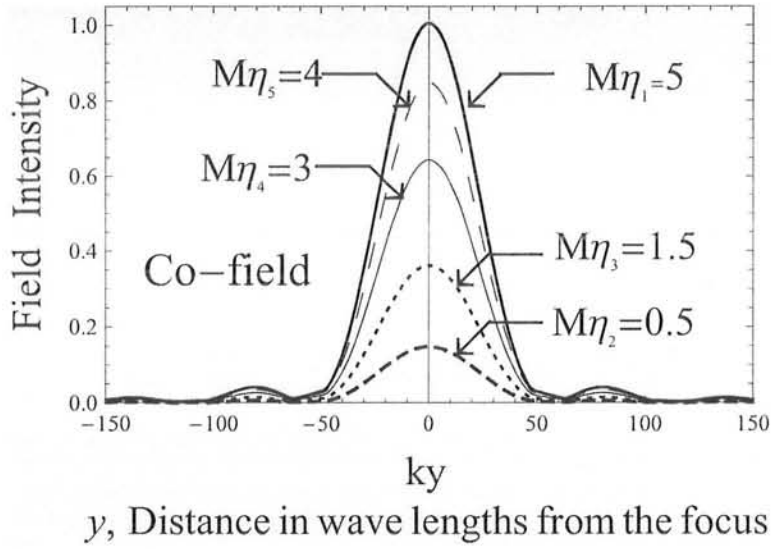


Fig. 4.30. Variations of co-polarized component of field intensity along y -axis, around the caustic region of chiral nihility coated PEMC Gregorian dual reflector system for different values of $M\eta$.

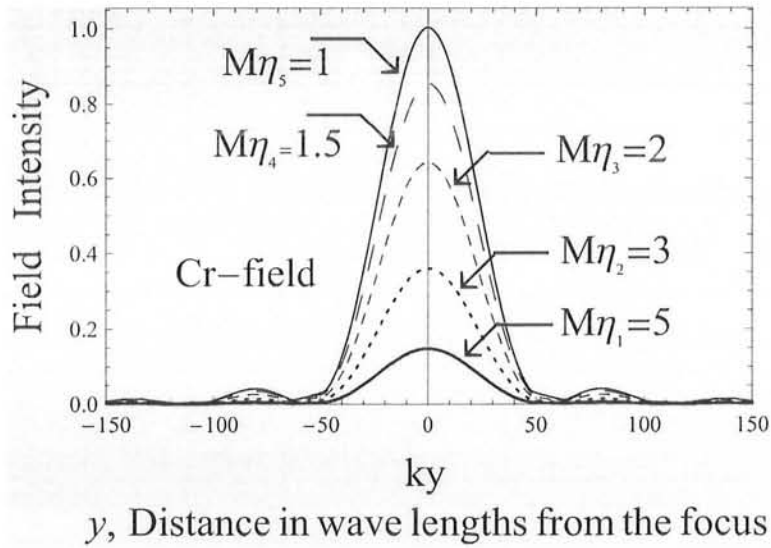


Fig. 4.31. Variations of cr-polarized component of field intensity along y -axis, around the caustic region of chiral nihility coated PEMC Gregorian dual reflector system for different values of $M\eta$.

4.5. Cassegrain Dual Reflector System

Geometry of Cassegrain system composed of two reflectors. In the present discussion, it is assumed that main-reflector is a chiral nihility coated PEMC cylinder whereas sub-reflector is PEC hyperbolic cylinder as shown in Fig. 4.32. The system is being used as high frequency receiving antenna. The main objective here is to determine the field expression based on Maslov's method, which should remain valid around the feed point of the system. This is accomplished by first determining GO field for the system in space coordinates which does contain singularity around focal region and then expressing GO field from spatial domain into spectral or wave vector domain. This gives finite field value at all points including the caustic region.

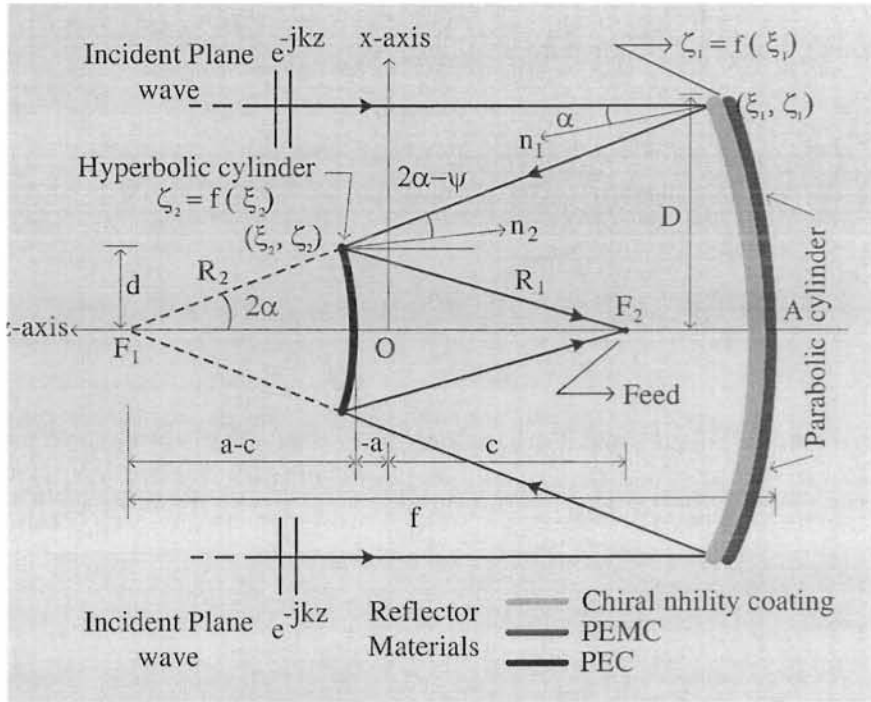


Fig. 4.32. PEMC backed chiral nihility dual reflector microwave antenna.

4.5.1. GO Field

Let the surface of main-reflector be excited by normal incident field of a uniform plane wave as shown in Fig. 4.32. The field is propagating from left to right along z -axis and is defined by

$$\mathbf{E}^i = \mathbf{u}_x \exp(-jkz) \quad (4.5.1)$$

The GO ray expression for the field reflected from the sub-reflector may be given using (3.1.20) as

$$E^r(y, z) = E_0^r(\xi_2, \zeta_2) [J(\tau)]^{-\frac{1}{2}} \exp[-jk\{S_0(\xi_1) + \tau_1 + \tau\}] \quad (4.5.2)$$

where $S_0(\xi_1)$, τ_1 and τ are given by (3.1.20), (3.1.6) and (3.1.5) respectively. Now, substituting the values of $J(\tau)$ and $E_0^r(\xi_2, \zeta_2)$ from (3.1.25) and (4.4.10) respectively in (4.5.2), yields the GO field expression for the Cassegrain system under discussion. It is readily seen that at caustic i.e., $\tau=R_1$ and consequently $J = 0$. Hence GO field expression shows singularity at caustic of Cassegrain microwave antenna. But the main interest here is to study the impact of these metamaterials on the behavior of the field around caustic region. So Maslov's method is used to transform GO field expression (4.5.2) into caustic field expression.

4.5.2. Field Computation Near Caustic

High frequency expression based on Maslov's method for the field around caustic region of Cassegrain system under consideration is given from (3.2.1) as

$$\mathbf{E}^r(y, z) = \sqrt{\frac{k}{j2\pi}} \int_{-\infty}^{\infty} \mathbf{E}_0^r(\xi_2, \zeta_2) \left[J(\tau) \frac{\partial p_{z2}}{\partial z} \right]^{\frac{-1}{2}} \exp[-jk\{S_0 + \tau_1 + S_{ex}\}] d(2\alpha) \quad (4.5.3)$$

where S_0 and τ_1 are given by (3.1.20) and (3.1.6), respectively and $\mathbf{E}_0^r(\xi_2, \zeta_2)$ is the initial field value on sub-reflector. The extra phase term S_{ex} is given by

$$S_{ex} = -\rho \cos(2\psi - 2\alpha + \phi) - \xi_2 \sin(2\psi - 2\alpha) + \zeta_2 \cos(2\psi - 2\alpha)$$

where

$$\begin{aligned}\xi_2 &= \frac{b^2 \sin \psi}{\sqrt{a^2 \cos^2 \psi + b^2 \sin^2 \psi}} \\ \zeta_2 &= \frac{a^2 \cos \psi}{\sqrt{a^2 \cos^2 \psi + b^2 \sin^2 \psi}} \\ \xi_1 &= -2f \tan \alpha \\ \zeta_1 &= \frac{f \cos 2\alpha}{\cos^2 \alpha} - c \\ \tan \psi &= -\frac{a^2 \xi_2}{b^2 \zeta_2} \\ \tan \phi &= \frac{y}{z} \\ \rho &= \sqrt{y^2 + z^2}\end{aligned}$$

The Cassegrain system under study in which main-reflector is of PEMC and is coated with chiral nihility medium, the surface field $\mathbf{E}_0^r(\xi_2, \zeta_2)$ is given by (4.4.10) with A_{co} and A_{cr} obtained from (4.4.11) and (4.4.12) respectively. Now substituting surface field $\mathbf{E}_0^r(\xi_2, \zeta_2)$ and Jacobian of the field $\left[J(\tau) \frac{\partial p_{zz}}{\partial z} \right]^{-\frac{1}{2}}$ from (4.4.10) and (3.2.5) respectively in (4.5.3), yields both co and cr-polarized field components. Therefore, co and cr-polarized fields reflected by PEMC backed chiral nihility Cassegrain system are given by

$$\begin{aligned}\mathbf{E}^r(y, z) &= \sqrt{\frac{k}{j2\pi}} \left[\int_{A_1}^{A_2} + \int_{-A_2}^{-A_1} \right] \left\{ A_{co} \mathbf{x} \exp(-jk_z z) + A_{cr} \left(\frac{jk_z}{k} \mathbf{y} + \frac{jk_y}{k} \mathbf{z} \right) \right\} \\ &\quad \times \sqrt{R_1} \exp[-jk(S_0 + \tau_1 + S_{ex})] d(2\alpha) \quad (4.5.4)\end{aligned}$$

where $A_{co}(\alpha)$ and $A_{cr}(\alpha)$ have been given in (4.4.11) and (4.4.12) respectively. In these relations, $k_z = k \cos 2\alpha$ and $k_y = k \sin 2\alpha$. When $M\eta \rightarrow \pm\infty$ (PEC), $A_{cr} = 0$, $A_{co} = -1$, therefore (4.5.4) becomes as

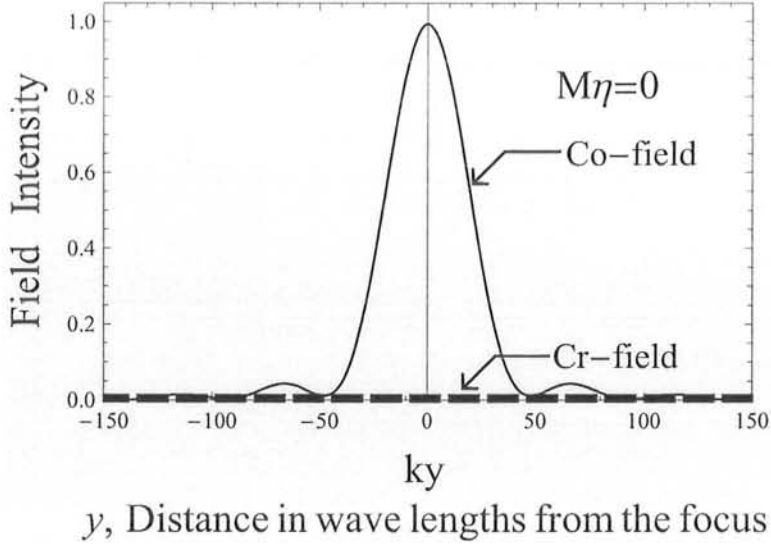
$$E^r(y, z) = \sqrt{\frac{k}{j2\pi}} \left[\int_{A_1}^{A_2} + \int_{-A_2}^{-A_1} \right] \sqrt{R_1} \exp[-jk(S_0 + \tau_1 + S_{ex})] d(2\alpha) \quad (4.5.5)$$

In the above equation R_1 , S_0 , τ_1 and S_{ex} are expressed in terms of α and A_1 , A_2 are the angles subtended at the feed point F_1 and F_2 by the parabolic and hyperbolic cylinders respectively.

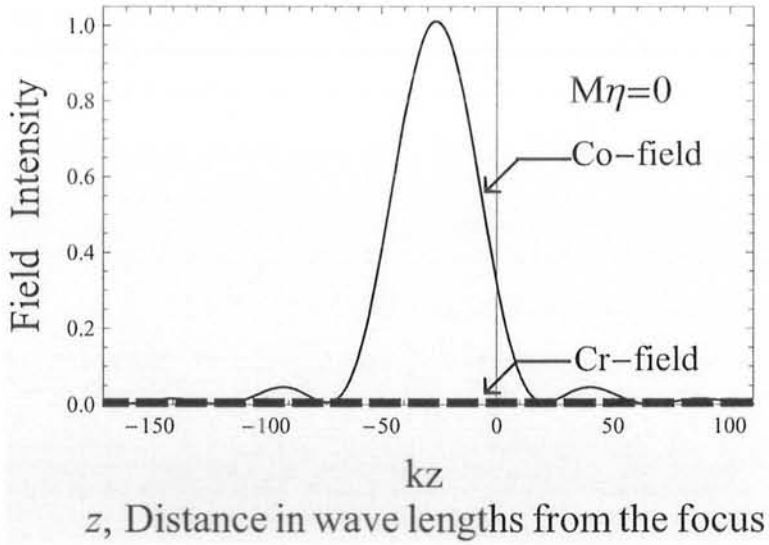
4.5.3. Results and Discussion

Plots of co-polarized and cr-polarized components of the reflected field along the reflector axes are shown in Fig. 4.33. to Fig. 4.39. PEMC backed chiral nihility Cassegrain system with parameters $kf = 60$, $ka = 8$, $kb = 25$, $kd = 8$ and $kD = 40$ is considered for the study of field behavior around caustic region. It has been observed that admittance parameter $M\eta$ affects the amplitude of the reflected field whereas field distribution pattern remains unchanged. Field intensity Plots have been obtained for different values of $M\eta$. It has been observed that for $M\eta = \pm 1$, cr component of the reflected field is maximum, while co polarized field component reduces to zero. For $M\eta = 2$, the field amplitude of cr component is greater than the co-polarized field component and the behavior is reversed for $M\eta = 3$. For $M\eta > 3$, the field amplitude of the cross component decreases and finally vanishes for large values of $M\eta$. It can also be seen that for $M\eta = 0$ and $M\eta \rightarrow \pm\infty$ cr-polarized components of the reflected field disappear showing the behavior of the chiral nihility reflector backed by PMC and PEC material respectively, which agrees with our analytical formulation. In Fig. 4.37., the results of PEMC backed chiral nihility Cassegrain system are compared with that of PEC backed chiral nihility Cassegrain system. The results are in good agreement. The study of field behavior is started from $M\eta = 0$ (PMC) boundary and observed that field is rotated giving rise to increase and decrease in field intensity of co and cr components for different values of $M\eta$. Finally, it reaches $M\eta \rightarrow \pm\infty$ (PEC boundary). The study also includes comparison of field intensity variation of co-polarized and cr-polarized components along y-axis for different values of admittance parameter $M\eta_1 = 5$, $M\eta_2 = 3$, $M\eta_3 = 2$, $M\eta_4 = 1.5$ and $M\eta_5 = 1$. The variation behavior of co and cr-polarized field components may be observed in the plots of Fig. 4.38. and Fig. 4.39. respectively. These findings may find potential use in some applications where controlled intensity of co and cross polarized field is required. Another striking feature can be seen that the factor thickness didn't appear in the

expression of the reflected field. It means that the thickness of the reflector coating, is irrelevant. It is perhaps due to the fact that in chiral nihility material, the two eigenwaves are circularly polarized but one of them is a backward wave.

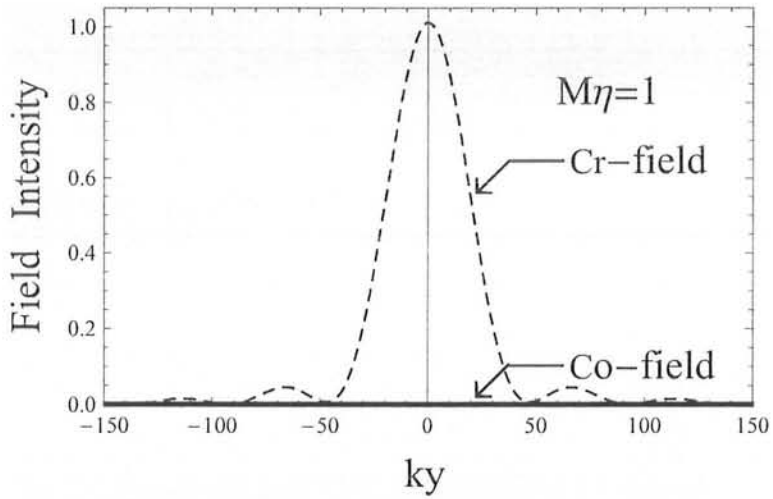


(a)



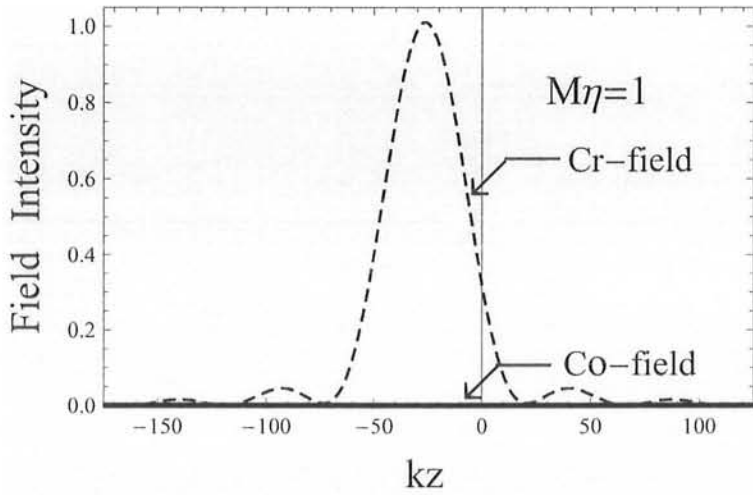
(b)

Fig. 4.33. Distribution of co and cr-polarized components of field intensity (a) along y -axis and (b) along z -axis, around caustic region of PEMC backed chiral nihility Cassegrain system for $M\eta = 0$. Here cr-polarized field component reduces to zero.



y , Distance in wave lengths from the focus

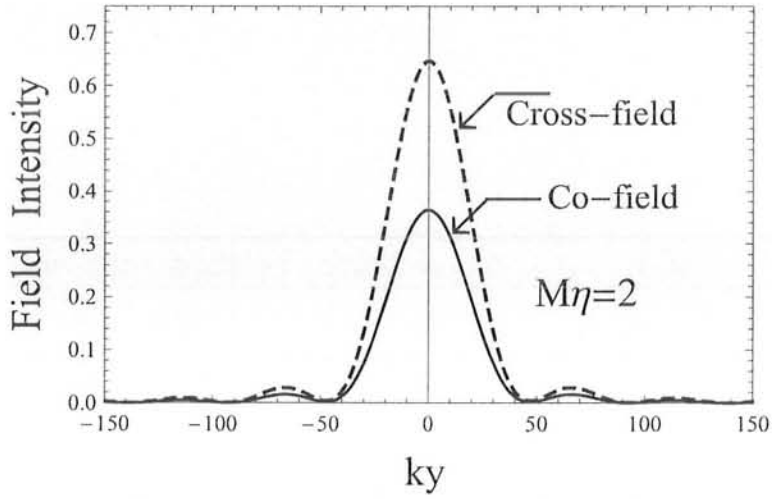
(a)



z , Distance in wave lengths from the focus

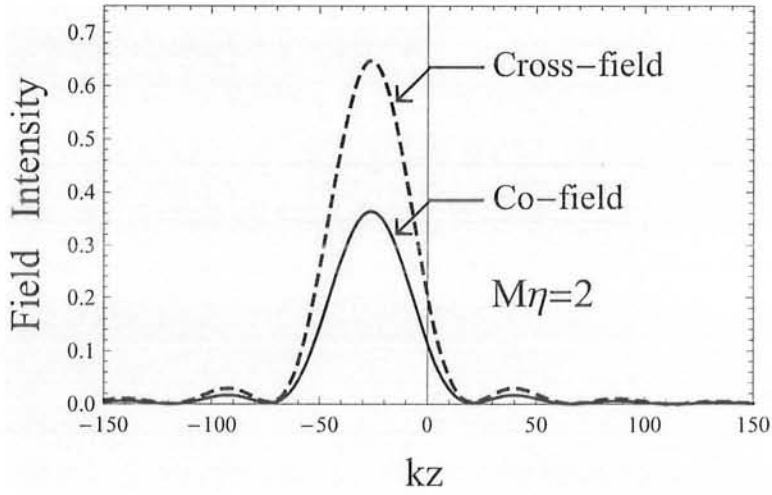
(b)

Fig. 4.34. Distribution of co and cr-polarized components of field intensity (a) along y -axis and (b) along z -axis, around the caustic region of PEMC backed chiral nihility Cassegrain dual reflector system for $M\eta = 1$. Here co-polarized field component reduces to zero



y , Distance in wave lengths from the focus

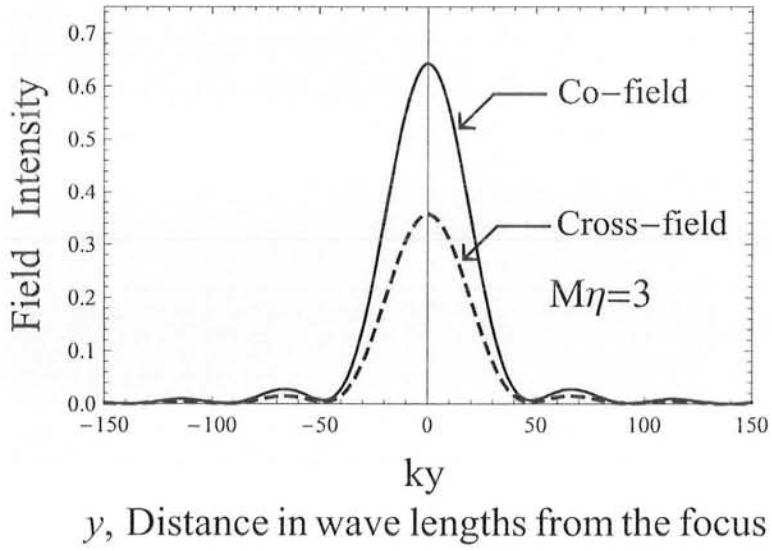
(a)



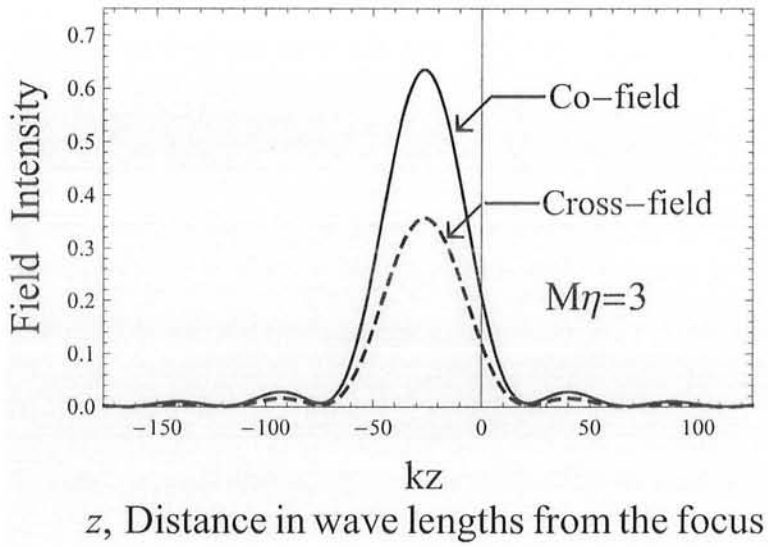
z , Distance in wave lengths from the focus

(b)

Fig. 4.35. Distribution of co and cr-polarized components of field intensity (a) along y -axis and (b) along z -axis, around the caustic region of chiral nihility coated PEMC Cassegrain dual reflector system for $M\eta = 2$.

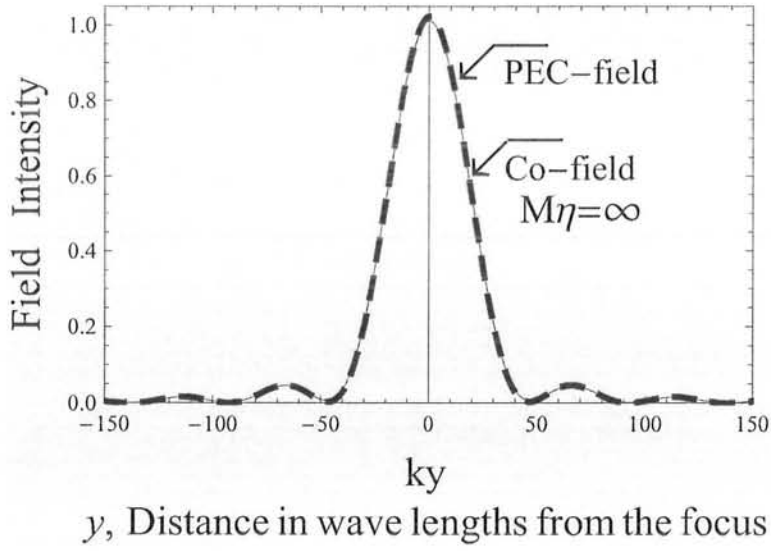


(a)

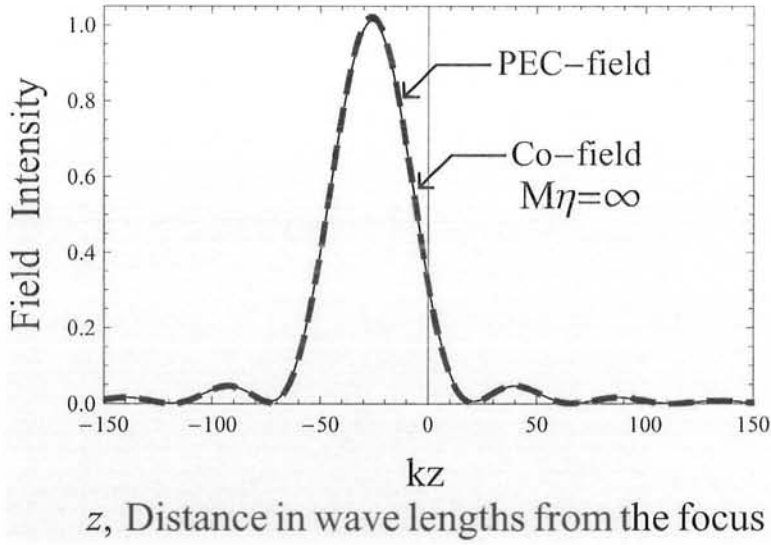


(b)

Fig. 4.36. Distribution of co and cr-polarized components of field intensity (a) along y -axis and (b) along z -axis, around caustic region of chiral nihility coated PEMC Cassegrain dual reflector system for $M\eta = 3$



(a)



(b)

Fig. 4.37. Comparison of field intensity distribution (a) along y -axis and (b) along z -axis, around the caustic region of PEC and PEMC backed chiral nihility Cassegrain dual reflector antenna with $M\eta \rightarrow \pm\infty$.

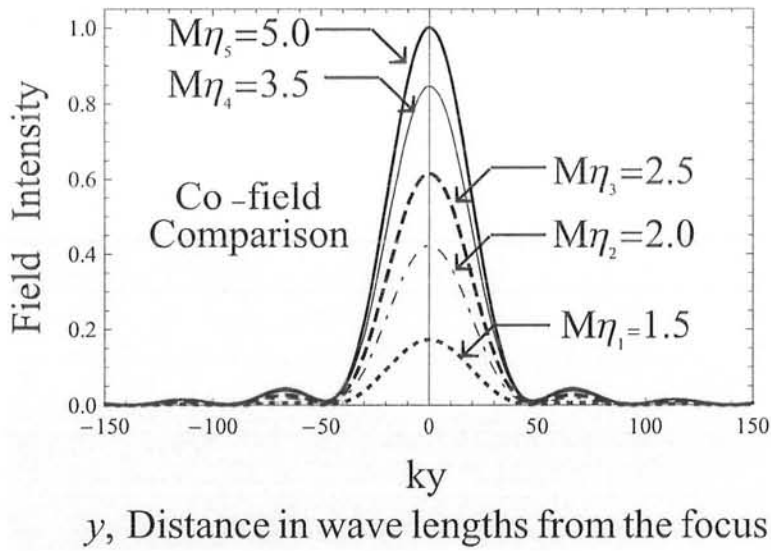


Fig. 4.38. Variations of co-polarized component of field intensity along y -axis, around the caustic region of chiral nihility coated PEMC Cassegrain dual reflector system for different values of $M\eta$.

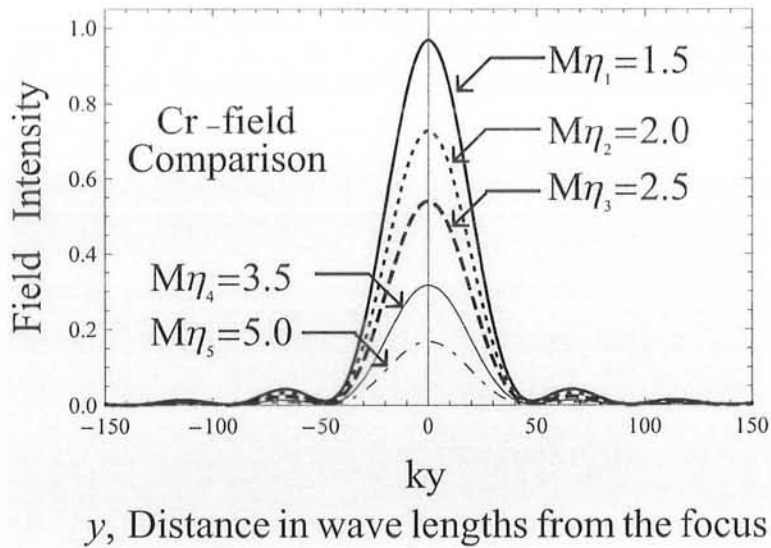


Fig. 4.39. Variations of cross-polarized component of field intensity along y -axis, around the caustic region of chiral nihility coated PEMC Cassegrain dual reflector system for different values of $M\eta$.

Chapter 5

Summary and Conclusion

GO approximation is a powerful tool for dealing with problems of high frequency fields in homogenous and in-homogenous media. However, it fails to quantify the fields in the vicinity of caustic of focussing systems. On the other hand, focussed electromagnetic fields have applications in various areas such as microwave antennas, and integrated optical systems. Field distribution in focal region of focusing systems is studied for synthesizing feed arrays in image field and designing of multiple beam antennas. Usually the conventional Huygens-Kirchhoff's integral is used to evaluate the field around the focal region of focusing systems. Maslov proposed another method to predict the field in the caustic region. Maslov's method is based on the idea that combines the simplicity of GO and generality of Fourier transform. Maslov's method makes use of the fact that appearance of caustic depends on domain formulation of the ray field. It means that appearance of caustic in field formulation cannot take place both in spatial domain and wave vector domain simultaneously. According to Maslov's method the conventional GO field expression in space coordinates is expressed in terms of wave vector domain through the use of Fourier transform to avoid the singularity that exists in spatial domain. The field expression obtained in this way, is valid at all points including the caustic region. When the observation point is far away from caustic, the field expression based on Maslov's method, reduces to GO field expression by applying stationary phase method of integration. The high frequency field expressions for arbitrary reflector, Cassegrain and Gregorian dual reflector systems consisting of PEC, PEMC and PEMC backed chiral nihility reflectors, are derived using Maslov's method, when a plane wave is incident. The field expression based on Maslov's method is obtained for a parabolic reflector from the field expression derived for arbitrary reflector. The corresponding expression for the field reflected from a parabolic reflector,

is also derived using Huygens-Kirchhoff's integral. Both expressions agree completely near caustics whereas they differ slightly in phase and amplitude away from the caustic.

Theoretically derived field expressions for a parabolic reflector, are evaluated through numerical computations so as to determine the field patterns around the caustic region for both oblique and normal incident plane wave. The results are compared with those obtained by Huygens-Kirchhoff's integral. The agreement is fairly good. The results of field pattern around the caustic region of PEC Cassegrain and Gregorian systems are compared with the results of their equivalent parabolas obtained by applying Huygens-Kirchhoff's integral. The results are found in close agreement. This yet again testifies the validity of Maslov's method for both Cassegrain and Gregorian dual reflector systems. For PEMC Cassegrain and Gregorian dual reflector systems, the field behavior around caustic regions is different from corresponding PEC dual reflector systems in that the field reflected from PEMC interface has both co-polarized and cr-polarized field components. The behavior of co and cr-polarized fields around caustic region of PEMC dual reflector systems has been studied for different values of admittance parameter $M\eta$. For the PMC and PEC special cases, i.e., $M\eta = 0$ and $M\eta \rightarrow \pm\infty$ respectively, the cr-polarized field component vanishes in either case whereas co-polarized field component exists in both cases. For $M\eta \rightarrow \pm\infty$, the co-polarized field component approaches the results of two dimensional PEC dual reflector system and is verified through comparison of the two field plots. For PEMC backed chiral nihility Cassegrain and Gregorian dual reflector systems, the field behavior at caustics of these systems has been studied for different values of admittance parameter $M\eta$. It is observed that for $M\eta = 0$ and $M\eta \rightarrow \pm\infty$, cr-polarized components of the reflected field disappear which represents chiral nihility reflector backed by PMC and PEC material respectively which is in accordance to our analytical formulation. The results of co-polarized field components of PEMC backed chiral nihility reflector are also compared with those of PEC backed chiral nihility reflector. The results are

found in good agreement. For the special PEMC case when $M = \frac{1}{\eta}$, the reflected field appears totally cross-polarized. So it acts like twist polarizer which is a non-reciprocal device. It has been observed that value of admittance parameter $M\eta$ affects only the amplitude of the reflected field whereas field pattern remains unchanged. It may be noted that the reflected field is independent of parameter d_2 , the layer thickness of chiral nihility material. This is perhaps due to the fact that in chiral nihility, the two eigenwaves are circularly polarized but one of them is a backward wave. The field reflected from PEMC or PEMC backed chiral nihility reflectors of focussing systems include the variation of co and cross-polarized field components for different values of admittance parameter $M\eta$. These findings may find potential use in Military and other applications where controlled intensity of co and cross-polarized field is required.

The results presented demonstrate that the Maslov's method is straightforward and provides an alternate tool to conventional induced current method or Huygens-Kirchhoff's principle for evaluating diffraction field in the caustic region of focussing systems. It might be an important result of this work to conclude that the two methods are equivalent but Maslov's method is easier to compute than Huygens-Kirchhoff's integral. Maslov's method can be used to solve various focussing problems. It is suggested that the work presented in the thesis may further be extended to apply to more complex practical problem of tri-reflector system being used in Space Technology.

Appendix A Evaluation of $F = J\left(\frac{\partial p_z}{\partial z}\right)$

First evaluate $\frac{\partial p_z}{\partial z}$ as

$$z = f(\xi) + \cot(2\theta - \phi_0)(x - \xi) \quad (A1)$$

On differentiating (A1) with respect to θ , gives

$$\begin{aligned} \frac{\partial z}{\partial \theta} &= f'(\xi) \frac{\partial \xi}{\partial \theta} - \frac{2(x - \xi)}{\sin^2(2\theta - \phi_0)} - \cot(2\theta - \phi_0) \frac{\partial \xi}{\partial \theta} \\ &= - \left[\tan \theta + \cot(2\theta - \phi_0) \right] \frac{\partial \xi}{\partial \theta} + \frac{2\tau}{\sin(2\theta - \phi_0)} \\ &= - \frac{\cos(\theta - \phi_0)}{\sin(2\theta - \phi_0)} \frac{1}{\cos \theta} \frac{\partial \xi}{\partial \theta} \left[1 - \frac{2 \cos \theta}{\cos(\theta - \phi_0)} \frac{\partial \theta}{\partial \xi} \tau \right] \end{aligned} \quad (A2)$$

Hence the differential $\frac{\partial z}{\partial p_z}$ can be derived as follows.

$$\begin{aligned} \frac{\partial z}{\partial p_z} &= \frac{\partial z}{\partial \theta} \frac{\partial \theta}{\partial p_z} = \frac{1}{2 \sin(2\theta - \phi_0)} \frac{\partial z}{\partial \theta} \\ &= - \frac{\cos(\theta - \phi_0)}{2 \sin^2(2\theta - \phi_0) \cos \theta} \frac{\partial \xi}{\partial \theta} \left[1 + \frac{2f''(\xi) \cos^3 \theta}{\cos(\theta - \phi_0)} \tau \right] \end{aligned} \quad (A3)$$

Using (A3) and (2.1.16) yields the final result

$$\begin{aligned} F = J(\tau) \frac{\partial p_z}{\partial z} &= \left[1 + \frac{2f''(\xi) \cos^3 \theta}{\cos(\theta - \phi_0)} \tau \right] \left[\frac{2 \cos^3 \theta \sin^2(2\theta - \phi_0)}{\cos(\theta - \phi_0)} f''(\xi) \right] \\ &\quad \left[1 + \frac{2f''(\xi) \cos^3 \theta}{\cos(\theta - \phi_0)} \tau \right]^{-1} \\ &= \frac{2 \cos^3 \theta \sin^2(2\theta - \phi_0)}{\cos(\theta - \phi_0)} f''(\xi) \end{aligned} \quad (A4)$$

Appendix B Derivation of the Jacobian

Evaluating the Jacobian of coordinate transformation (x, z) to (ξ_1, τ) with (x, z) given by (3.1.19).

$$\begin{aligned} D(\tau) &= \frac{\partial(x, z)}{\partial(\xi_1, \tau)} = \begin{vmatrix} \frac{\partial \xi_2}{\partial \xi_1} + \frac{\partial p_{x2}}{\partial \xi_1} \tau & \frac{\partial \xi_2}{\partial \xi_1} + \frac{\partial p_{z2}}{\partial \xi_1} \tau \\ p_{x2} & p_{z2} \end{vmatrix} \\ &= 2 \frac{\partial(\alpha - \psi)}{\partial \xi_1} \tau - \frac{\cos(2\alpha - \psi)}{\cos \psi} \frac{\partial \xi_2}{\partial \xi_1} \end{aligned} \quad (B1)$$

where the relation used is $\frac{\partial \zeta_2}{\partial \xi_1} = \frac{\partial \zeta_2}{\partial \xi_2} \frac{\partial \xi_2}{\partial \xi_1} = \tan \psi \frac{\partial \xi_2}{\partial \xi_1}$. The relation between (ξ_1, ζ_1) and (ξ_2, ζ_2) is given by

$$\xi_2 - \xi_1 = -\tan 2\alpha(\zeta_2 - \zeta_1) \quad (B2)$$

and differentiating both sides with respect to ξ_1 , yields

$$\frac{\partial \xi_2}{\partial \xi_1} = \frac{\cos \psi}{\cos(2\alpha - \psi)} \left[1 - \frac{\zeta_2 - \zeta_1}{f} \frac{\cos^2 \alpha}{\cos 2\alpha} \right] = \frac{\cos \psi}{\cos(2\alpha - \psi)} \frac{R_2 \cos^2 \alpha}{f} \quad (B3)$$

Furthermore,

$$\frac{\partial \alpha}{\partial \xi_1} = \frac{1}{2f} \cos^2 \alpha, \quad \frac{\partial \psi}{\partial \xi_1} = \frac{\partial \psi}{\partial \xi_2} \frac{\partial \xi_2}{\partial \xi_1} = \cos^2 \psi \frac{a^4}{b^2 \zeta_2^3} \frac{1}{\zeta_2^3} \frac{\partial \xi_2}{\partial \xi_1} \quad (B4)$$

Substituting (B3) and (B4) in (B1) yields

$$D(\tau) = 2t \left\{ \frac{\cos^2 \alpha}{2f} - \frac{\cos^3 \psi}{\cos(2\alpha - \psi)} \frac{a^4}{b^2 \zeta_2^3} \left[1 - \frac{\zeta_2 - \zeta_1}{f} \frac{\cos^2 \alpha}{\cos 2\alpha} \right] \right\} - \left[1 - \frac{\zeta_2 - \zeta_1}{f} \frac{\cos^2 \alpha}{\cos 2\alpha} \right] \quad (B5)$$

From Fig. 3.1. and with simple calculation it can be readily found that the following relations hold

$$\zeta_2 = c - R_2 \cos 2\alpha, \quad \zeta_1 = \frac{\xi_1^2}{4f} - f + c = -f \frac{\cos 2\alpha}{\cos^2 \alpha} + c, \quad 1 - \frac{\zeta_2 - \zeta_1}{f} \frac{\cos^2 \alpha}{\cos 2\alpha} = \frac{R_2}{f} \cos^2 \alpha \quad (B6)$$

Hence $D(\tau)$ can be written as

$$D(\tau) = \frac{\cos^2 \alpha}{f} \left\{ \left[1 - \frac{2 \cos^3 \psi}{\cos(2\alpha - \psi)} \frac{a^4}{b^2 \zeta_2^3} R_2 \right] \tau - R_2 \right\} \quad (B7)$$

By using the relations

$$\cos 2\alpha = \frac{c - \zeta_2}{R_2}, \quad \sin 2\alpha = \frac{\xi_2}{R_2} \quad (B8)$$

$\cos(2\alpha - \psi)$ in (B7) can be expressed by

$$\begin{aligned} \cos(2\alpha - \psi) &= \frac{c - \zeta_2}{R_2} \cos \psi + \frac{\xi_2}{R_2} \sin \psi \\ &= \frac{1}{R_2 \sqrt{R_1 R_2}} \left[\frac{b}{a} \zeta_2 (c - \zeta_2) + \frac{a}{b} \xi_2^2 \right] \\ &= \frac{1}{R_2 \sqrt{R_1 R_2}} \left[\frac{b}{a} c \zeta_2 - ab \left(\frac{\zeta_2^2}{a^2} - \frac{\xi_2^2}{b^2} \right) \right] \\ &= \frac{1}{R_2 \sqrt{R_1 R_2}} \frac{b}{a} (c \zeta_2 - a^2) = \frac{b}{\sqrt{R_1 R_2}} \end{aligned} \quad (B9)$$

where the relation used is $R_2 = \sqrt{(c - \zeta_2)^2 + \xi_2^2} = \frac{c\zeta_2 - a^2}{a}$. Then the coefficient of τ in (B7) is simplified to

$$U = 1 - \frac{2 \cos^3 \psi}{\cos(2\alpha - \psi)} \frac{a^4}{b^2 \zeta_2^3} R_2 = 1 - \frac{2abR_2}{(R_1 R_2)^{\frac{3}{2}}} \frac{aR_2 \sqrt{R_1 R_2}}{b(c\zeta_2 - a^2)} = 1 - \frac{2a}{R_1} = \frac{R_2}{R_1} \quad (B10)$$

Hence $D(\tau)$ in (B7) becomes

$$D(\tau) = \frac{\cos^2 \alpha}{f} R_2 \left[1 - \frac{\tau}{R_1} \right] \quad (B11)$$

This shows that the ray is focused at point F_2 .

Appendix C Evaluation of $F = J(\tau) \frac{\partial p_{z2}}{\partial z}$

The integrand of (3.2.1) is used to derive the expression which is valid at the focal point F_2 . From the relation

$$z = \zeta_2 + \frac{p_{z2}}{p_{x2}}(x - \xi_2) = \zeta_2 + \cot(2\alpha - 2\psi)(x - \xi_2) \quad (C1)$$

one can obtain

$$\begin{aligned} \frac{\partial z}{\partial \xi_2} &= \frac{\partial \zeta_2}{\partial \xi_2} - \frac{2(x - \xi_2)}{\sin^2(2\alpha - 2\psi)} \frac{\partial(\alpha - \psi)}{\partial \xi_2} - \cot(2\alpha - 2\psi) \\ &= -\frac{\cos(2\alpha - \psi)}{\cos \psi \sin(2\alpha - 2\psi)} + \frac{2\tau}{\sin(2\alpha - 2\psi)} \frac{\partial(\alpha - \psi)}{\partial \xi_2} \\ &= \frac{1}{\sin(2\alpha - 2\psi)} \frac{\partial \xi_1}{\partial \xi_2} \left[2\tau \frac{\partial(\alpha - \psi)}{\partial \xi_1} - \frac{\cos(2\alpha - \psi)}{\cos \psi} \frac{\partial \xi_2}{\partial \xi_1} \right] \end{aligned} \quad (C2)$$

By using the relations

$$\begin{aligned} \frac{\partial z}{\partial p_{z2}} &= \frac{\partial z}{\partial \xi_2} \frac{\partial \xi_2}{\partial p_{z2}}, & \frac{\partial p_{z2}}{\partial z} &= \frac{\partial \xi_2}{\partial z} \frac{\partial p_{z2}}{\partial \xi_2}, \\ \frac{\partial p_{z2}}{\partial \xi_2} &= 2 \sin(2\alpha - 2\psi) \frac{\partial(\alpha - \psi)}{\partial \xi_2} = 2 \sin(2\alpha - 2\psi) \frac{\partial \xi_1}{\partial \xi_2} \frac{\partial(\alpha - \psi)}{\partial \xi_1} \end{aligned} \quad (C3)$$

it gives

$$\begin{aligned} \frac{\partial p_{z2}}{\partial z} &= \frac{\partial \xi_2}{\partial z} \frac{\partial p_{z2}}{\partial \xi_2} = 2 \sin(2\alpha - 2\psi) \frac{\partial \xi_1}{\partial \xi_2} \frac{\partial(\alpha - \psi)}{\partial \xi_1} \sin(2\alpha - 2\psi) \frac{\partial \xi_2}{\partial \xi_1} \\ &\times \left[2\tau \frac{\partial(\alpha - \psi)}{\partial \xi_1} - \frac{\cos(2\alpha - \psi)}{\cos \psi} \frac{\partial \xi_2}{\partial \xi_1} \right]^{-1} \end{aligned} \quad (C4)$$

There we have

$$\begin{aligned} \frac{D(\tau)}{D(0)} \frac{\partial p_{z2}}{\partial z} &= \left[2t \frac{\partial(\alpha - \psi)}{\partial \xi_1} - \frac{\cos(2\alpha - \psi)}{\cos \psi} \frac{\partial \xi_2}{\partial \xi_1} \right] \left[\frac{\cos \psi}{\cos(2\alpha - \psi)} \frac{\partial \xi_2}{\partial \xi_2} \right] \frac{\partial p_{z2}}{\partial z} \\ &= 2 \sin^2(2\alpha - 2\psi) \frac{\partial(\alpha - \psi)}{\partial \xi_1} \frac{\cos \psi}{\cos(2\alpha - \psi)} \frac{\partial \xi_1}{\partial \xi_2} \end{aligned} \quad (C5)$$

From the results of Appendix B we have

$$\begin{aligned} \frac{D(\tau)}{D(0)} \frac{\partial p_{z2}}{\partial z} &= 2 \sin^2(2\alpha - 2\psi) \frac{\cos^2 \alpha R_2}{2f R_1} \frac{\cos \psi}{\cos(2\alpha - \psi)} \frac{\cos(2\alpha - \psi)}{\cos \psi} \frac{f}{R_2 \cos^2 \alpha} \\ &= \frac{\sin^2(2\alpha - 2\psi)}{R_1} \end{aligned} \quad (C6)$$

where

$$\begin{aligned} R_1 &= \frac{c\zeta_2 + a^2}{a} = a \frac{c \cos \psi + \sqrt{a^2 \cos^2 \psi - b^2 \sin^2 \psi}}{\sqrt{a^2 \cos^2 \psi - b^2 \sin^2 \psi}}, & \cos \psi &= \frac{c + a \cos 2\alpha}{\sqrt{a^2 + c^2 + 2ac \cos 2\alpha}}, \\ \sin \psi &= \frac{a \sin 2\alpha}{\sqrt{a^2 + c^2 + 2ac \cos 2\alpha}}, & \xi_1 &= 2f \tan \alpha, & \zeta_1 &= c - \frac{2f \cos 2\alpha}{1 + \cos 2\alpha} \\ \xi_2 &= \frac{b^2 \sin \psi}{\sqrt{a^2 \cos^2 \psi - b^2 \sin^2 \psi}}, & \zeta_2 &= \frac{a^2 \cos \psi}{\sqrt{a^2 \cos^2 \psi - b^2 \sin^2 \psi}} \end{aligned} \quad (C7)$$

Appendix D Parameters of Cassegrain Antenna

$$(D1) \quad \tan \frac{\phi_v}{2} = \frac{D}{2f} \quad \text{and} \quad \tan \frac{\phi_r}{2} = \frac{D}{2f_e}$$

The equation of the parabolic cylinder is given by (3.1.1). Hence, it produces

$$OA = -f + c, \quad AH = \frac{D^2}{4f}, \quad FH = f - \frac{D^2}{4f} \quad (D1)$$

and

$$\tan \phi_v = \frac{D}{f - \frac{D^2}{4f}} = \frac{2 \cdot \frac{D}{2f}}{1 - \left(\frac{D}{2f}\right)^2} = \frac{2 \tan \frac{\phi_v}{2}}{1 - \tan^2 \frac{\phi_v}{2}} \quad (D2)$$

From (D2) we have $\tan \frac{\phi_v}{2} = \frac{D}{2f}$. It may be noted that D is height of the edge of the parabolic cylinder from horizontal axis.

Similarly, it gives

$$\tan \frac{\phi_r}{2} = \frac{D}{2f_e} \quad (D3)$$

where f_e is the focal length of the equivalent parabola.

$$(D2) \quad e = \frac{\sin \frac{1}{2}(\phi_v + \phi_r)}{\sin \frac{1}{2}(\phi_v - \phi_r)}$$

From the similarities of the triangles, one can obtain

$$\frac{f_e}{f} = \frac{L_r}{L_v} = \frac{c+a}{c-a} = \frac{e+1}{e-1} = \frac{\tan \frac{1}{2}\phi_v}{\tan \frac{1}{2}\phi_r} \quad (D4)$$

The last term is obtained from the results in (D1). From the above equation e is obtained as

$$e = \frac{\tan \frac{1}{2}\phi_v + \tan \frac{1}{2}\phi_r}{\tan \frac{1}{2}\phi_v - \tan \frac{1}{2}\phi_r} = \frac{\sin \frac{1}{2}(\phi_v + \phi_r)}{\sin \frac{1}{2}(\phi_v - \phi_r)} = \frac{L_r + L_v}{L_r - L_v} \quad (D5)$$

and

$$1 - \frac{1}{e} = \frac{2L_v}{L_r + L_v} = 1 - \frac{\sin \frac{1}{2}(\phi_v + \phi_r)}{\sin \frac{1}{2}(\phi_v - \phi_r)} \quad (D6)$$

Appendix E

The surface contour of elliptical cylinder is defined as

$$\frac{\zeta_2^2}{a^2} + \frac{\xi_2^2}{b^2} = 1 \quad (E1)$$

with

$$c^2 = a^2 - b^2$$

Let the foci of (E_1) be $F_1(0, -c)$, $F_2(0, c)$ and (ξ_2, ζ_2) be the point on the surface.

Then

$$R_1 = \sqrt{(\zeta_2 + c)^2 + \xi_2^2}, \quad R_2 = \sqrt{(\zeta_2 - c)^2 + \xi_2^2}$$

so that

$$\begin{aligned}
 (R_1 R_2)^2 &= \left[\sqrt{(\zeta_2 + c)^2 + \xi_2^2} \right] \left[\sqrt{(\zeta_2 + c)^2 + \xi_2^2} \right] \\
 &= (c^2 + \zeta^2 + \xi^2 + 2c\zeta) (c^2 + \zeta^2 + \xi^2 - 2c\zeta) \\
 &= (c^2 + \zeta^2 + \xi^2) - 4\zeta^2 c^2 \\
 &= \left[a^2 - b^2 + \zeta^2 + b^2 \left(1 - \frac{\zeta^2}{a^2} \right) \right] - 4\zeta^2 (a^2 - b^2) \\
 &= \left[a^2 + \left(1 - \frac{b^2}{a^2} \right) \zeta \right]^2 - 4\zeta^2 (a^2 - b^2) \\
 &= a^4 - 2a^2 \left(1 - \frac{b^2}{a^2} \right) \zeta^2 + \left(1 - \frac{b^2}{a^2} \right)^2 \zeta^4 \\
 &= \left[\left(\frac{b^2}{a^2} - 1 \right)^2 \xi + b^2 \right]^2
 \end{aligned}$$

Let the unit normal at point (ξ_2, ζ_2) on the elliptical cylinder by $\zeta_2 = f(\xi_2)$ be \mathbf{n} , then

$$\mathbf{n} = \sin \psi \mathbf{i}_x + \cos \psi \mathbf{i}_z$$

then

$$\begin{aligned}
 \sin \psi &= \frac{a\xi_2}{b\sqrt{R_1 R_2}} \\
 \cos \psi &= \frac{b\zeta_2}{b\sqrt{R_1 R_2}}
 \end{aligned}$$

Therefore

$$\begin{aligned}
 f'(\xi_2) &= \frac{1}{2} a \left(\frac{1 - \xi_2^2}{b^2} \right)^{-\frac{1}{2}} \left(\frac{-2\xi_2}{b^2} \right) \\
 &= -\frac{a^2 \xi_2}{b^2 \zeta_2} \\
 1 + [f'(\xi_2)]^2 &= 1 + \frac{a^4 \xi_2^2}{b^4 \zeta_2^2} \\
 &= 1 + \frac{a^2 \xi_2^2}{b^4 \left(1 - \frac{\xi_2^2}{b^2} \right)} \\
 &= \frac{b^2 (b^2 - \xi_2^2) + a^2 \xi_2^2}{b^2 (b^2 - \xi_2^2)} \\
 &= \frac{b^4 - b^2 \xi_2^2 + a^2 \xi_2^2}{b^2 (b^2 - \xi_2^2)} \\
 &= \frac{R_1 R_2}{b^2 - \xi_2^2}
 \end{aligned}$$

Then

$$\begin{aligned}
 \cos \psi &= \frac{1}{\sqrt{1 + f'^2(\xi_2)}} \\
 \cos \psi &= \frac{1}{\sqrt{\frac{R_1 R_2}{b^2 - \xi_2^2}}} \\
 &= \sqrt{\frac{b^2 - \xi_2^2}{R_1 R_2}} \\
 &= \frac{b\zeta_2}{\sqrt{R_1 R_2}} \\
 &= \frac{b\zeta}{a\sqrt{R_1 R_2}} \tag{E2}
 \end{aligned}$$

$$\begin{aligned}
 \sin \psi &= \frac{-f'(\xi_2)}{\sqrt{1 + f'^2(\xi_2)}} \\
 &= -\frac{b\zeta_2}{a\sqrt{R_1 R_2}} \left(-\frac{a^2 \xi_2}{b^2 \zeta_2} \right) \\
 &= \frac{a\xi_2}{b\sqrt{R_1 R_2}} \tag{E3}
 \end{aligned}$$

Appendix F Perfect Electromagnetic Conductor and Chiral Medium

The perfect electromagnetic conductor (PEMC) is an idealized electromagnetic medium that has been introduced as a non-reciprocal generalization of both perfect electric conductor (PEC) and perfect magnetic conductor (PMC). Possibilities for realization of a PEMC has been suggested by Lindel [35, 36] in terms of a layer of certain non-reciprocal materials resting on a PEC plane. Parameters of a bi-isotropic medium can be chosen so that the interface of the layer acts as a PEMC boundary. The PEMC boundary conditions [35-38] are of more general form as given below.

$$\mathbf{n} \times (\mathbf{H} + M\mathbf{E}) = 0, \quad \mathbf{n} \cdot (\mathbf{D} - M\mathbf{B}) = 0 \quad (PEMC) \tag{F1}$$

The vector boundary condition is given by

$$M\mathbf{E} = -\mathbf{H} + (1 + M^2\eta_0^2)\mathbf{nn} \cdot \mathbf{H}, \quad \eta_0 = \sqrt{\mu_0/\epsilon_0} \tag{F2}$$

where M denotes the admittance of the PEMC boundary (dimension $\frac{1}{\Omega}$). Obviously, PMC corresponds to $M=0$ while PEC is obtained as the limit $M \rightarrow \pm\infty$.

Chiral Medium

A chiral medium [44-46] is macroscopically continuous medium composed of equivalent chiral objects, uniformly distributed and randomly oriented. A chiral object consists of a circular loop of wire whose two ends extend perpendicular to the plane of the loop in opposite direction. When an incident wave falls on the helix, it induces both electric and magnetic dipole moments. Following Maxwell's equations, the constitutive relations for isotropic chiral media, for time harmonic fields $\exp(j\omega t)$ must have the form

$$\begin{aligned} \mathbf{D} &= \epsilon\mathbf{E} + j\kappa\mathbf{H} \\ \mathbf{B} &= \mu\mathbf{H} - j\kappa\mathbf{E} \end{aligned} \tag{F3}$$

so that the dispersive relation for the wave number k is

$$k_{\pm} = \omega(\sqrt{\mu\epsilon} \pm \kappa) \tag{F4}$$

where '+' and '-' represent different eigenwaves in the above expression and κ is the chirality of the medium which is assumed to be positive for this study. Such media are characterized by two intrinsic eigenwaves with left-handed and right-handed circular polarization and both of them have different phase velocities and refraction indices. Recent researches show that the refraction index for one of the eigenwaves will even be negative [47, 48] for strong chirality (κ) chiral nihility is a special kind of chiral medium for which the constitutive parameters, at certain frequency known as nihility frequency [49] will become $\epsilon=0$, $\mu=0$, such that $\kappa \neq 0$, where κ is the chirality of the

medium. Hence the constitutive relations (F6) for an isotropic chiral nihility medium will become

$$\begin{aligned}\mathbf{D} &= +j\kappa\mathbf{H} \\ \mathbf{B} &= -j\kappa\mathbf{E}\end{aligned}\tag{F5}$$

$$k_{\pm} = \pm\omega(\kappa)\tag{F6}$$

In chiral nihility, the two eigenwaves are still circularly polarized. But one of them is a backward wave whose phase velocity has an anti-parallel direction with corresponding Poynting vector. Phenomena of negative refraction occurs when a plane wave enters from vacuum into chiral nihility medium. That is when a plane wave obliquely hits the interface of vacuum and chiral nihility. One refracted eigenwave propagates on one side of the normal at certain angle while other eigenwave propagates at same angle on the other side of normal to the interface.

References

- [1] Kravtsov, Y. A., “Two new asymptotic methods in the theory of wave propagation in inhomogeneous media (review),” *Sov. Phys. Acoust.*, 14(1), 1–17, 1968.
- [2] Felson, L. B., “Hybrid formulation of wave propagation and scattering,” *Nato ASI Series*, Martinus Nijhoff, Dordrecht, The Netherland, 1984.
- [3] Dechamps, G. A., “Ray techniques in electromagnetics,” *Proc. IEEE*, 60, 1022–1035, 1972.
- [4] Chapman, C. H., and R. Drummond, “Body wave seismograms in inhomogeneous media using Maslov asymptotic theory,” *Bull. Seismol., Soc. Am.*, 72, 277–317, 1982.
- [5] Ziolkowski, R. W., and G. A. Deschamps, “Asymptotic evolution of high-frequency field near a caustic,” *An introduction to Maslov’s Method*, *Radio Science*, 19, 1001–1025, 1984
- [6] Gorman, A.D., “Vector field near caustics,” *Journal of Electromagnetic Waves and Applications*, Vol. 26, 1404–1407, 1985.
- [7] Kravtsov, Y. A., and Y.I. Orlov, “Geometrical optics in engineering Physics,” *Alpha Science, International Ltd.*, UK., 2005.
- [8] Maslov, V. P., “Perturbation theory and asymptotic methods,” *Moskov., Gos., Univ., Moscow*, 1965. (Translated into Japanese by Ouchi et al. *Iwanami, Tokyo*, 1976.)
- [9] Maslov, V. P., and M.V. Fedoriuk, “Semi-classical approximation in quantum mechanics,” translated from Russian by J. Mieder and J. Talor, *D. Riedel, Hingham, Mass*, 1981.

- [10] Dechamps, G. A., “Electromagnetics and differential forms,” *Proc. IEEE*, 69, 676–696, 1981.
- [11] Ziolkowski, R. W., and G. A. Deschamps, “Maslov’s Method and asymptotic Fourier transform,” paper presented at URSI symposium, Quebec, Canada, 1988.
- [12] Arnold, J. M., “Spectral synthesis of uniform wave functions, *Wave Motion*, no. 8, pp. 135–150, 1986.
- [13] Kay, I., and J.B. Keller, “Asymptotic evaluation of the field at caustic,” *Journal of Applied Physics*, 23, 876–883, 1954.
- [14] Kravtsov, Y. A., and Y.I. Orlov, *Caustics catastrophes and wave fields*, Springer Verlag, Berlin, 1993.
- [15] Gorman, A.D., S.P. Anderson, and R.B. Mohindra, “On caustic related to several common indices of refraction,” *Radio Science*, 21, 434–436, 1986.
- [16] Stannnes, J.J., “Waves in focal regions,” Adam Hilger, Bristol Boston, 1986, section 16.2
- [17] Hongo, K., Yu Ji, and E. Nakajima, “High-frequency expression for the field in the caustic region of a reflector using Maslov’s method,” *Radio Science*, Vol. 21, No. 6, 911–919, 1986.
- [18] Hongo, K., and Yu Ji., “High-frequency expression for the field in the caustic region of a cylindrical reflector using Maslov’s method,” *Radio Science*, 22, 3, 357–366, 1987.
- [19] Hongo, K., and Yu Ji., “Study of the field around the focal region of spherical reflector antenna by Maslov’s method,” *IEEE Transactions on Antennas and Propagation*, vol. 36, 592–598, May 1988

- [20] Yu Ji and K. Hongo., “Field in the focal region of a dielectric spherical by Maslov’s method,” *Journal of optical society of America A*, 8, 1721–1728, 1991
- [21] Yu Ji and K. Hongo., “Analysis of electromagnetic waves refracted by a spherical dielectric interface by Maslov’s method,” *Journal of optical society of America A*, 8, 541–548, 1991
- [22] Hongo, K., and H. Kobayashi, “Radiation characteristics of a plano convex lens antenna, *Radio Science*, Vol. 31, No. 5, 1025–1035, 1987.
- [23] Aziz, A., Q. A. Naqvi and K. Hongo, “Analysis of the fields in two dimensional Cassegrain system,” *Progress In Electromagnetics Research*, PIER 71, 227–241, 2007.
- [24] Aziz, A., A. Ghaffar, Q. A. Naqvi and K. Hongo, “Analysis of the fields in two dimensional Gregorian system,” *Journal of Electromagnetic Waves and Applications*, 22, no.1, 85–97, 2008.
- par
- [25] Ghaffar, A., Q. A. Naqvi and K. Hongo, “Analysis of the fields in three dimensional Cassegrain system,” *Progress In Electromagnetics Research*, PIER 72, 215–240, 2007.
- [26] Ghaffar, A., A. Hussain, Q. A. Naqvi and K. Hongo, “Radiation characteristics of an inhomogeneous slab,” *Journal of Electromagnetic Waves and Applications*, Vol. 22, No. 2, 301–312, 2008.
- [27] Ghaffar, A., Q. A. Naqvi and K. Hongo, “Study of focusing of field refracted by a cylindrical plano-convex lens into a uniaxial crystal by using Maslov’s method,” *Journal of Electromagnetic Waves and Applications*, Vol. 22, 665–679, 2008.
- [28] Ghaffar, A., Q. A. Naqvi and K. Hongo, “Focal region fields of three dimensional Gregorian system,” *Optics Communications* 281, 1343–1353, 2008.

- [29] Ghaffar, A., and Q. A. Naqvi, “Focusing of electromagnetic plane wave into uniaxial crystal by a three dimensional plano convex lens,” *Progress In Electromagnetics Research, PIER* 83, 25–42, 2008.
- [30] Ghaffar, A., and Q. A. Naqvi, “Study of focusing of field refracted by an Inhomogeneous Slab into a uniaxial crystal by using Maslov’s method,” *Journal of Modern Optics*, Vol. 55, 21, 3513–3528, 2008.
- [31] Ashraf, M. R., A. Ghaffar and Q. A. Naqvi, “Fields in the focal space of symmetrical hyperbolic focusing lens,” *Journal of Electromagnetic Waves and Applications*, Vol. 22, 815–828, 2008.
- [32] Hussain, A., Q. A. Naqvi and K. Hongo, “Radiation characteristics of the Wood lens using Maslov’s method,” *Progress In Electromagnetics Research, PIER* 73, 107–129, 2007.
- [33] Hehl, F. W. and Y. N. Obukhov, “Linear media in classical electrodynamics and post constraint,” *Phys. Lett. A*, Vol. 334, 249–259, 2005.
- [34] Obukhov, Y. N. and F. W. Hehl, “Measuring a piecewise constant axion field in classical electrodynamics,” *Phys. Lett. A*, Vol. 341, 357–365, 2005.
- [35] Lindell, I. V., and A. H. Sihvola, “Perfect electromagnetic conductor,” *Journal of Electromagnetic Waves and Applications*, Vol. 19, No. 7, 861–869, 2005.
- [36] Lindell, I. V., and A. H. Sihvola, “Realization of the PEMC boundary, *IEEE Transactions on Antennas and Propagation*, Vol. 53, 3012–3018, Sep. 2005.
- [37] Lindell, I. V., “Differential forms in Electromagnetics,” New York Willey IEEE press, 2004.
- [38] Lindell, I. V., and A. H. Sihvola, “The PEMC resonator,” *Journal of Electromagnetic Waves and Applications*, Vol. 20, No. 7, 849–859, 2006.

- [39] Jancewicz, B., “Plane electromagnetic wave in PEMC,” *Journal of Electromagnetic Waves and Applications*, Vol. 20, No. 5, 647–659, 2006.
- [40] Ruppin, R., “Scattering of electromagnetic radiation by a perfect electromagnetic conductor sphere,” *Journal of Electromagnetic Waves and Applications*, Vol. 20, No. 12, 1569–1576, 2006.
- [41] Ruppin, R., “Scattering of electromagnetic radiation by a perfect electromagnetic conductor cylinder,” *Journal of Electromagnetic Waves and Applications*, Vol. 20, No. 13, 1853–1860, 2006.
- [42] Fiaz, M. A., A. Ghaffar and Q. A. Naqvi, “High frequency expressions for the field in the caustic region of a PEMC cylindrical reflector using Maslovs method,” *Journal of Electromagnetic Waves and Applications*, Vol. 22, 358–397, 2008.
- [43] Fiaz, M. A., A. Aziz, A. Ghaffar and Q. A. Naqvi, “High frequency expressions for the field in the caustic region of a PEMC Gregorian system using Maslovs method,” *Progress In Electromagnetics Research*, PIER 81, 135–148, 2008.
- [44] Lindell, I. V., A. H. Sihvola, S. A. Tretyakov, A. J. Viitanen, “*Electromagnetic waves in chiral and bi-Isotropic media*,” Artech House Publisher, 2002.
- [45] Faryad, M., and Q. A. Naqvi, “High frequency expressions for the field in the caustic region of a cylindrical reflector placed in chiral medium,” *Progress In Electromagnetics Research*, PIER 76, 153–182, 2007.
- [46] Faryad, M., and Q. A. Naqvi, “Cylindrical reflector in chiral medium supporting simultaneously positive phase velocity and negative phase velocity,” *Journal of Electromagnetic Waves and Applications*, Vol. 22, 563–572, 2008.
- [47] Lakhtakia, A., “An electromagnetic trinity from negative permittivity and negative permeability.” *Int. J. Infrared and Millimeter Waves*, 22, 1731–1734, 2001.